DEVELOPMENT OF A NANOPARTICLE DNA BASED BIOSENSOR FOR THE SHIGA-LIKE TOXIN 1 DETECTION USING CO-POLYERMIZATION HYBRIDIZATION READOUT AMPLIFICATION

By

Michael Jeffrey Anderson

A DISSERTATION

Submitted to
Michigan State University
in partial fulfillment of the requirements
for the degree of

DOCTOR OF PHILOSOPHY

Biosystems Engineering

2012

ABSTRACT

DEVELOPMENT OF A NANOPARTICLE DNA BASED BIOSENSOR FOR THE SHIGA-LIKE TOXIN 1 DETECTION USING CO-POLYERMIZATION HYBRIDIZATION READOUT AMPLIFICATION

By

Michael Jeffrey Anderson

Approximately 3.4 million deaths occur each year due to lack of clean water. The Shigatoxigenic group of *Escherichia coli* (STEC) bacteria causes approximately 2.2 million of these deaths and nearly a billion cases of illness. Current approved testing methods for *Escherichia coli* require a 12-24 hours growth of the sample in order to test for an indicator species. This indicator species only suggests possible *E. coli* O157:H7 presence, but does not confirm it. Direct culture testing cannot identify the pathogenic STEC bacteria either. Confirmation of toxicity requires molecular methods of identification leading to specialized equipment needs and higher testing costs. Typical molecular methods use polymerase chain reaction (PCR) to amplify a very specific target DNA sequence, indicating the presence of a specific microorganism. PCR requires a thermocycler and a clean laboratory environment. Recent work has been successfully explored using nanomaterial based systems to identify the same genes used in a PCR reaction in a simpler detection system. The nanomaterials are used for both signal amplification and as the detection molecule. In this dissertation work a biosensor utilizing nanoparticles has been developed for the detection of Shiga-like toxin 1 gene that is present in *Escherichia coli* O157:H7. The system has been successfully constructed using a novel carbohydrate coated gold nanoparticle for delivery of the self assembling co-polymerization DNA oligonucleotide reporters. A set of self-assembled single-stranded DNA

(ssDNA) molecules has been developed to amplify a target sequence without the use of enzymes. The full detection system incorporates the gold nanoparticle and a magnetic microparticle into a DNA recognition step. The gold nanoparticle is used for both co-polymerization detection and electrochemical detection. Input material (genomic DNA) is extracted using a modified commercial extraction method to produce PCR quality DNA from whole bacterial cells. When extraction and recognition elements are combined, a limit of detection for *E. coli* O157:H7 of 10^5 cells/mL using co-polymerization and 10^1 cells/mL with electrochemical detection has been achieved. Sample preparation from spiked culture samples until final detection takes a total of 7 hours. Electrochemical detection provides only a presence or absence indicator, where tethered co-polymerization is able to provide quantitative values of the input bacterial concentration. So a combination of co-polymerization amplification and electrochemical detection can provide the potential for more sensitive and quantitative measurement without the need for enzymes as in PCR applications.

ACKNOWLEDGEMENTS

I sincerely thank everyone who has contributed and supported this research over the years. I would like to specially thank Dr. Evangelyn Alocilja for believing in me and making everything possible. As a mentor she has been encouraging, supportive, and very patient in my research and growth as a scientist. Equally important, Dr. Alocilja has been both a friend and taken me into her family. Her support has been crucial in graduate career and shaping me as a responsible scientist. I would like to thank my SMART scholarship sponsor, Dr. Clint Smith and his team, for their support of my educational process and the opportunity to use my research in an applied setting to help people. I would also like to thank the members of my Ph.D guidance committee: Dr. Gary Blanchard, Dr. Xuefei Huang, and Dr. Renfu Lu for their support.

I would also like to extend my sincerest gratitude to my friends and family for all their support, patience, and belief in me during my Ph.D pursuit. Everything I have accomplished has been a combination of the support from all those in my life.

Michael Anderson

TABLE OF CONTENTS

LIST OF TABLES

LIST OF FIGURES

Chapter 1: Introduction

One in ten illnesses worldwide is attributed to water-borne sources, resulting in 3.4 million deaths a year. The main contributors being enterohemorrhagic *Escherichia coli* (EHEC), Shigatoxigenic group of *Escherichia coli* (STEC), and *Salmonella* [1, 2]. Rapid testing of water supplies would help eliminate microorganism-associated illness through better water treatments and awareness programs. The Environmental Protection Agency's (EPA) current standard testing and identification methods for microorganisms are all growth in a selective media [3, 4]. Growth based methods are the standard for identification but are non-rapid, often requiring 18 or more hours, and have a limited selectivity between related species. Culture plating based methods identify bacteria by metabolic pathways, not pathogenic capabilities [5-7]. Antibody detection involves the recognition of antigenic proteins on the cell surface of microorganisms and used in both enzyme-linked immunosorbent assay (ELISA) assays and bio-barcode detection. Antibodies are more rapid than culture techniques, but are limited by cost, cross-reactivities and storage requirements [8]. Much like culture techniques, antibody recognition does not identify pathogenic traits, but rather by binding surface antigens that are commonly found together with pathogenic traits. More recent techniques have used DNA gene sequences for microorganism detection and identification. DNA techniques currently require an amplification step for detection, and polymerase chain reaction (PCR), isothermal amplification, and the bio-barcode method have been explored for DNA detection [9-11]. PCR is an extremely sensitive technique, but is often limited for laboratory use due to equipment and storage needs. Isothermal amplification is less expensive to operate because of simplified equipment needs, but is still limited to temperature sensitive enzyme storage. The bio-barcode technique has been used for

enzyme free detection and amplification of DNA, but DNA input and detection times are less rapid.

This dissertation describes the generation of a fluorescence based biosensor for Shiga-like Toxin 1 (*stx1*) detection using gold nanoparticles and self assembling co-polymerization hybridization amplification. Chapter 2 presents a review of the literature pertaining to technologies relevant to this research project including gold nanoparticle generation, construction of a co-polymerization hybridization DNA set, gold nanoparticle based detection, and detection of the *stx1* gene from bacterial culture. Chapter 3 describes the generation and size control of a carbohydrate gold nanoparticle under alkaline reduction conditions. Chapter 4 describes the generation of a DNA hybridization system and its use as a detection technology from a DNA hybridization assay. The combination of an improved DNA extraction protocol, gold nanoparticle functionalized assay particles and hybridization co-polymerization readout into a working biosensor is presented in Chapter 5. Chapter 6 contains recommendations for future work and research extending from this dissertation. The following section of this introduction describes the research hypothesis, objectives, and novelty of the work performed.

1.1 Hypothesis

The research presented in this dissertation is based on the following hypotheses:

Gold nanoparticles can be synthesized with ‘green’ methodologies using a single step reaction, under alkaline conditions, and a carbohydrate reduction and capping agent.

A set of short oligonucleotides can be engineered to self-assemble into longer double-stranded DNA sequences detectable using fluorescence detection and intercalating DNA dyes.

A rapid DNA extraction method can be developed to provide quality genomic DNA input for hybridization detection.

A biosensor platform can be developed using co-polymerizing DNA for readout in a hybridization sandwich assay targeting the *stx1* gene with increased detection compared to end labeled oligonucleotides DNAs.

1.2 Research objectives

The overall objective of this dissertation research is to develop a rapid fluorescent detection biosensor to detect the Shiga-like toxin 1 (*stx1*) gene.

The detailed objectives of this project are:

- To synthesize gold nanoparticles under alkaline conditions using a carbohydrate capping agent as an alternative to acidic citrate particle methodologies.
- To develop a single-strand DNA detection system using a self assembly method called co-polymerization hybridization.
- To develop *stx1* specific DNA probes and functionalize the carbohydrate generated gold nanoparticles with the DNA probes.
- To develop a fluorescent and electrochemical biosensor with the carbohydrate functionalized gold nanoparticles based on co-polymerization hybridization.

1.3 Research significance and novelty

The novelty of the presented research in this dissertation relies on the use of a self-assembling DNA system in conjunction with carbohydrate capped gold nanoparticles for use with genomic DNA target and rapid fluorescence detection. Gold nanoparticles have been used as a carrier for signal amplification previously, and most recently used for electrochemical detection through

reduction/oxidation potentiometry. Traditional DNA targets are enzymatically amplified sequences utilizing multiple hybridization events or DNA reporters labeled with fluorescent molecules. To the best of our knowledge, this is the first report of successful detection of a DNA target from genomic input using carbohydrate generated gold nanoparticles with fluorescent co-polymerization.

Detection of specific DNA sequences commonly requires extraction, purification and PCR amplification of the target sequence. These steps often require the use of frozen enzymes, expensive thermocyclers, or larger centrifuges limiting the range of physical locations the detection can be accomplished. This approach is also more costly. Detection of fluorescently labeled DNA systems has the ability to have high sensitivity but also requires larger equipment needs with higher associated equipment costs. To the best of our knowledge, the techniques described in this dissertation are the first time fluorescence detection has been accomplished using extracted genomic DNA for the *stx1* gene target using self assembling co-polymerization. The following techniques require no special storage, no temperature requirements, and all equipment can be portable. A summary of the presented research is listed in Table 1-1 and comparison with current literature illustrates the novelty and scientific contribution [11-15].

Table 1-1. Research contribution of this dissertation project to the literature.

Subject	References		
DNA hybridization detection	[16]	[17]	[10]
Self-assembling DNA for fluorescent ssDNA detection	[13]		
One step alkaline generated glyco-nanoparticles	[12]		
Biogenic AuNP DNA functionalization	[12]		
Sandwich assay detection	[11]	[18]	[10]
Direct fluorescence genomic AuNP detection	[15]	[13]	
Fluorescent detection of genomic DNA by self-assembling DNA amplification	This work		

Chapter 2: Literature review

2.1 *Escherichia coli* and coliform detection

It has been argued that clean water is the most important resource for modern civilization. Each year an estimated 3.4 million people die from water-borne diseases. Of these deaths, approximately 2.2 million are due to diarrheal disease [19]. The main victims of diarrheal disease are children five years and younger and the elderly. The causative agents of this disease include viruses, protozoa, and bacteria [20]. The most common viral species include Adenovirus, Enterovirus, *Hepatitus*, Norovirus and *Rotaviruses* with Adenovirus and *Rotaviruses* causing more severe disease symptoms. Common Protozoa responsible for water-borne disease include *Cryptosporidium*, *Cyclospora*, and *Giardia*. These two classes of water-borne disease agents are resistant to disinfectants, have less severe effects than the bacterial agents, and are more stable in water.

Bacterial causative agents include but are not limited to *Escherichia*, *Legionella*, *Salmonella*, *Shigellla*, *Vibrio* and *Yersinia* geneses. Bacterial infections cause more severe diarrhea, dehydration, and are life-threatening if left untreated. Hydration is an important part of treatment, but without clean water, hydrating often reinforces the infection. Within the bacterial agents two classes are most studied, as they are the major contributors to disease. The classes are the enterohemorrhagic *Escherichia coli* (EHEC) and the Shigatoxigenic group of *Escherichia coli* (STEC). The STEC group contains the Shiga toxin and Shiga-like toxin producing organisms that include *Escherichia coli* (*E. coli*) O157:H7, *Shigella dysenteriae*, and various other non-

O157:H7 *E. coli*. Table 2-1 lists selected water related disease data, with diarrheal related cases being the largest agent of death [21].

Table 2-1. Estimated infection from water related agents are taken from Gleick (2002).

Disease	Yearly Estimated Morbidity	Yearly Estimated Mortality	Relationship to water
Diarrheal diseases	1,000,000,000	2,200,000	Unsafe drinking water
Intestinal helminths	1,500,000,000	100,000	Unsafe drinking water
Schistosomiasis	200,000,000	200,000	Unsafe drinking water
Other	150,000,000	130,000	Unsanitary washing conditions

Water quality is often determined by measuring indicator organisms, since monitoring every possible microbe is impractical and nearly impossible. Historically, the detection of a low number of organisms has not been accurate. Water assessment is based on the detection of bacteria that are normally found in high numbers along with the infectious targets. These indicator organisms become detectable when individuals are infected and contagious, indicating contamination and presence of the infectious agent. The currently measured bacterial indicators are called coliform, coli-aerogens, or fecal coliforms [2]. Coliforms are a broad class of microorganisms found naturally in water, soil, and warm-blooded animals and include *Escherichia*, *Enterobacter*, *Klebsiella*, *Citrobacter*, *Shigella* and *Salmonella*. Many coliforms are harmless to humans, but the presence of fecal coliforms in water often indicates contamination

through water run-off, improper sanitation, or insufficient treatment methods. The most common fecal coliform group is *Escherichia* [22].

Within the coliform class, EHEC, STEC, and *Salmonella* groups are good indicator species for water contamination. Both *E. coli* groups (EHEC and STEC) contain a conserved gene encoding a Shiga-like toxin, which is also found in *Shigella*. The Shiga toxin is responsible for severe diarrhea, abdominal pain, vomiting, bloody urine, and can cause death in children, the elderly and immuno-compromised individuals through dehydration, hemolytic uremia, or renal failure [23]. Each year, approximately 73,000 cases of illness specific to *E. coli* O157:H7 are reported in the United States, with the more publicized cases being the food recalls of hamburger [24], spinach [25] and cookie dough [26]. Domestically about 15% or 11,000 cases are specifically attributed directly to water-borne sources [27].

The Environmental Protection Agency (EPA) has set a limit of zero detection of total coliform, both harmful and harmless, with mandatory reporting when more than 5% of samples test positive [28]. Testing of treated, bottled, and tap water can easily conform to zero tolerance. Irrigation water, produce wash water, ground, and surface waters tend to contain non-fecally derived bacteria that are ubiquitous in the environment. These non-fecal bacteria often pose no risk to human health but will cause false positives in detection systems. Confirmation of coliform presence has been limited to metabolic testing for governmental health monitoring which requires between 18-24 hours for presence/absence determination. Identification of cell surface markers has reduced detection time; molecular recognition methods have attempted to investigate the genes responsible for pathogenicity.

The following sections discuss the accepted, traditional, unconventional, and novel methods of coliform detection used in bacterial monitoring efforts.

2.1.1 Traditional methods of detection

Historically, determination of bacterial identification is based on metabolic differences. Determination is through gas generation or colorimetric change. The EPA approved methods that fall under this category are: multiple tube fermentation, membrane filtration, and presence/absence testing.

Multiple tube fermentation involves growth of a sample in liquid media with an inverted tube placed in the solution. The media used can be either lactose, lauryl tryptose, or lactose bile broth. The coliforms are grown at 35-45°C for 24-48 hours under anaerobic conditions such that gas is produced. The exact conditions determine if total coliform or fecal coliform are the identified target. As a result of the growth conditions, results are reported as a most probable number, which is a statistical estimate of the starting concentration. For example, this corresponds to a 37% likelihood of a positive reading when a sample containing 1 cell/mL is tested. Positive quantification of fecal coliform requires a second fermentation of 24 hours to determine total and fecal coliform amounts. Multiple tube fermentation remains useful for sample matrices that are non-transparent or colored such as milk or environmental samples.

Membrane filtration is a combined concentration and growth assay. A typical detection would filter a liquid sample through a 0.45 μm filter to capture all bacteria as well as larger particulates

on the filter membrane. EPA methods grow the filter on selective media agar, m-Endo-type agar, containing lactose which produces red colonies after 24 hours of growth at 35°C. Other agar media have been used including MacKonkey, MacKonkey-sorbital, ChromAgar, Rainbow agar, and antibiotic augmented agars. These other types of media can be used with membrane filtration, but are not approved currently by the EPA. Membrane filtration allows for sample concentration, but has considerable limits for its use. Concentration on the filter membrane does not provide optimal distribution of bacteria. This can cause over-crowding, uncountable plate growth, and capture of non-target microbes that can out-compete weakened coliforms on the filter. This method is used regularly for drinking water systems as it allows for large volumes of dilute samples to be concentrated for detection.

Metabolic enzyme activity has been recently utilized for differentiation of microbe populations. Two of the most common enzymes targeted in coliform detection are beta-D-glucuronidase and beta-D-galactosidase. Detection is accomplished by conjugating a reporter molecule to a metabolizable sugar. Upon proper metabolism, the reporter is released causing a change to the system that is measured. It was found that the enzyme beta-D-glucuronidase was specific to *Enterobacteriaceae* and contained in 95% of *E. coli* that were tested [29]. The enzyme beta-D-galactosidase is contained by mainly *E. coli*, and conjugation of a reporter can give the probable presence of *E. coli* when metabolized. Even though these enzyme systems are specific to the organisms they target, false signals are possible. *Shigella*, *Salmonella*, and *Yersinia* are all pathogenic *Enterobacteriaceae* which do not contain either enzyme. This would give a negative result while still being capable of infection. False positives for *E. coli* can be generated by *Bacillus* spp. and *Aerococcus viridans* when present [30]. A major advantage to enzyme linked

assays is multiple detections in a single sample. The commercial product, Colilert by IDEXX, uses a dual substrate system. Coliform detection is accomplished by a yellow color change upon metabolism of ortho-Nitrophenyl-β-galactoside, and *E. coli* determination is accomplished by having a yellow color and also by a fluorescence signal after metabolism of 4-Methylumbelliferyl-beta-D-glucuronide. This is just an example of a metabolic enzyme test that has been approved by the EPA and is commercially available.

Various combinations of detection methods have been tried and include: enzymatic substrates, selective growth media with membrane filtration, culture plating, and multiple tube fermentation. Each of the possible pairings combines the various advantages and disadvantages of the different methods involved. The combination of methods with light absorbency or fluorescence measurements allows for detection of total coliforms in as little as 12 hours.

These EPA-approved and other metabolic methods have drawbacks however; the most apparent is the required time from sample to detection. Common methods take 24-48 hours, and rapid methods taking as little as 12 hours. Another issue is that these growth systems are subject to contamination with other microorganisms. A high number of non-target microorganisms can slow or retard growth of the target thus giving false negatives. When metabolic pathways are shared among a large family of closely-related species, selective media may lack the specificity needed for identification and give a false positive. Lastly, selective media do not always provide optimal growth conditions thereby limiting growth of the target organisms. This can lead to false negatives when there is low or stressed target present.

2.1.2 Antibody detection

Antibodies are proteins that have the ability to specifically bind to other molecules with a high degree of specificity. The specificity of the antibody to the target can vary based on the species of host used for generation, individual host differences, and the type of antibody. Antibody recognition of bacteria uses surface antigens (features) such as the terminal sugars (O) on the cell surface lipopolysaccharide (LPS), the capsule component (K) and the flagella antigens (H) as common targets. When monoclonal antibodies are produced, each antibody is a clone and targets the same antigen. Polyclonal antibodies are purified from blood serum and contain a mixture of antibodies that can recognize different portions of the target antigen. Many antibodies available for research use are uncharacterized, meaning the manufacturer does not know the exact target antigen. These uncharacterized antibodies can lead to cross-reactivity, such as *Klebsiella pneumoniae*, *Klebsiella. oxytoca*, *Enterobacter cloacae*, *Enterobacter aerogenes*, *Citrobacter amalonaticus*, *Citrobacter koseri*, and some species of the *Citrobacter freundii* being reported as *E. coli* O157:H7. Antibodies common to O157 have been reported to cross-react with O7 and O116 LPS components [31] resulting in false positive identification of non-harmful microorganisms.

To avoid the cross-reactivity of a single antibody binding event, two different antibodies can be used in conjunction in a sandwich structure to increase specificity. The enzyme-linked immunosorbent assay (ELISA) uses an antibody anchored to a surface. The target is allowed to bind, and then a second antibody is challenged in the system. The second antibody is then detected through an attached enzyme or by recognition with a third antibody attached to a reporter. In an ELISA, two different antibodies are used for recognition. The double recognition

reduces non-specific binding and increases the specificity of the assay. Attachment of fluorescent reporters to the antibodies allows for multiplex detection. Horseradish peroxidase and luciferase are commonly used chemiluminescent reporters.

One downside of antibody recognition (capture) is that the target must come in close proximity to be captured. For dilute solutions or large sample volumes the time for sample capture can be on the scale of hours, providing bound target the chance to disassociate. To address this issue, larger amount of antibody can be used to increase the chance of binding the target. A technique called immunomagnetic separation (IMS) has been developed, combining antibodies and magnetic particles. The antibodies are attached to the magnetic particle, allowed to mix in a sample, and a magnetic field is applied and collects the magnetic particles. The magnetic separation allows for good mixing of the sample and antibodies followed by a concentration step on the magnet. IMS separation only provides the initial antibody recognition and requires culturing, second antibody bonding, or other form of reporter for detection [32-34].

Antibody detection is rapid and can be specific with appropriate product selection, but it does not measure pathogenicity. The use of surface antigens for detection is successful in many cases for antibody binding, but surface antigens are not perfect. As mentioned before, cross-reactivities can lead to false positive and false negatives, even with a two antibody system. The quick assay times with higher antibodies or target concentrations, large target selection, and compatibility with multiple reporter system make antibodies extremely useful tools for rapid screening, but not always for identification of the pathogenicity of an organism.

2.1.3 Molecular DNA methods of detection

Molecular techniques of detection utilize the hybridization properties of DNA and RNA. DNA is a more commonly used molecular species than RNA owing to the increased stability and ease of amplification. Recognition is accomplished using Watson-Crick base pairing to bind to a known DNA sequence. The DNA sequences targeted genetically encode for genes in the host organism. Unlike antibodies, DNA hybridization can be used to look for genes targeting internal cellular components such as toxins, enzymes, and proteins.

Identification of specific DNA sequences provides a detection technique with ~95% specificity when properly designed primers and probes are used. Table 2-2 lists some common gene targets for identification of waterborne coliforms.

Table 2-2. Commonly used gene targets for coliform and *Escherichia coli* detection.

Gene / Target	Target Type	Coliform Target	Source
stx1	Toxin	O157 - Shiga Toxin	[9, 35, 36]
stx2	Toxin	O157 - Shiga Toxin	[9, 35, 36]
O157 LPS antigen	Surface Feature	O157:H7, O55:H7	[37]
fliC	Surface Feature	*E. coli* - H antigen	[38]
rfb	Surface Feature	*E. coli* - O antigen	[37]
lamB	Surface Feature	STEC - binding protein	[39]
eae	Surface Feature	*E. coli* - attachment protein	[40]
espB	Surface Feature	E .coli - attachment protein	[40]
phoE	Surface Feature	STEC - membrane protein	[41]
lacI	Enzyme	Total coliform – beta-galactosidase	[42]
uidA	Enzyme	STEC - beta-glucuronidase	[43, 44]
uidR	Enzyme	STEC - beta-glucuronidase regulation	[45]
lacZ	Enzyme	Total coliform - lactose metabolism	[39, 46]

The use of pathogenic gene targets is a common method with molecular techniques, especially in water and food safety. This safety concern arises when other detection methods give false

negatives and positives based on antigen recognition. Identification of a pathogenic gene, such as Shiga toxin production, can be determined independently of the organism using DNA hybridization. This becomes important when an antibody based assay is looking for *E. coli* but misses *Shigella*. A Shiga toxin molecular assay would show positive and prevent possible illness for both *E. coli* O157:H7 and *Shigella*.

When the above gene targets are in sufficient concentration, detection can be accomplished in a number of hybridization based formats which include: polymerase chain reaction (PCR) [37], real-time PCR [36], microarray hybridization [47], fluorescent labeled-DNA probes [48], enzyme labeled DNA probes [49], Förster resonance energy transfer (FRET) [50], fluorescence *in situ* hybridization (FISH) [51], colorimetric change [52], and change of mass systems [53]. The common requirement for most of the hybridization detection methods is sufficiently high number of target for capture and/or relatively clean DNA input. Additional steps are required to meet both of these input requirements. Commercially ready non-laboratory DNA testing methods are limited and usually include enzymatic amplification [54].

2.2 Enzymatic amplification

Successful detection of any target requires a signal with sufficient strength for measurement. Detection of STEC, *E. coli*, or *stx1* containing organisms is currently accomplished through an amplification reaction. Many novel methods have been developed for gene target amplification, and have future potential use in microorganism detection. This section describes the enzyme based amplification methods.

2.2.1 Polymerase chain reaction (PCR)

PCR is by far the most common enzyme based amplification method for DNA in use today. Since its discovery in 1983, the use of PCR is now ubiquitous as a biological detection or identification technique. The PCR method is described briefly, and is the basis for most of the other enzyme-based methods. Figure 2-1 is a schematic representation of the PCR process.

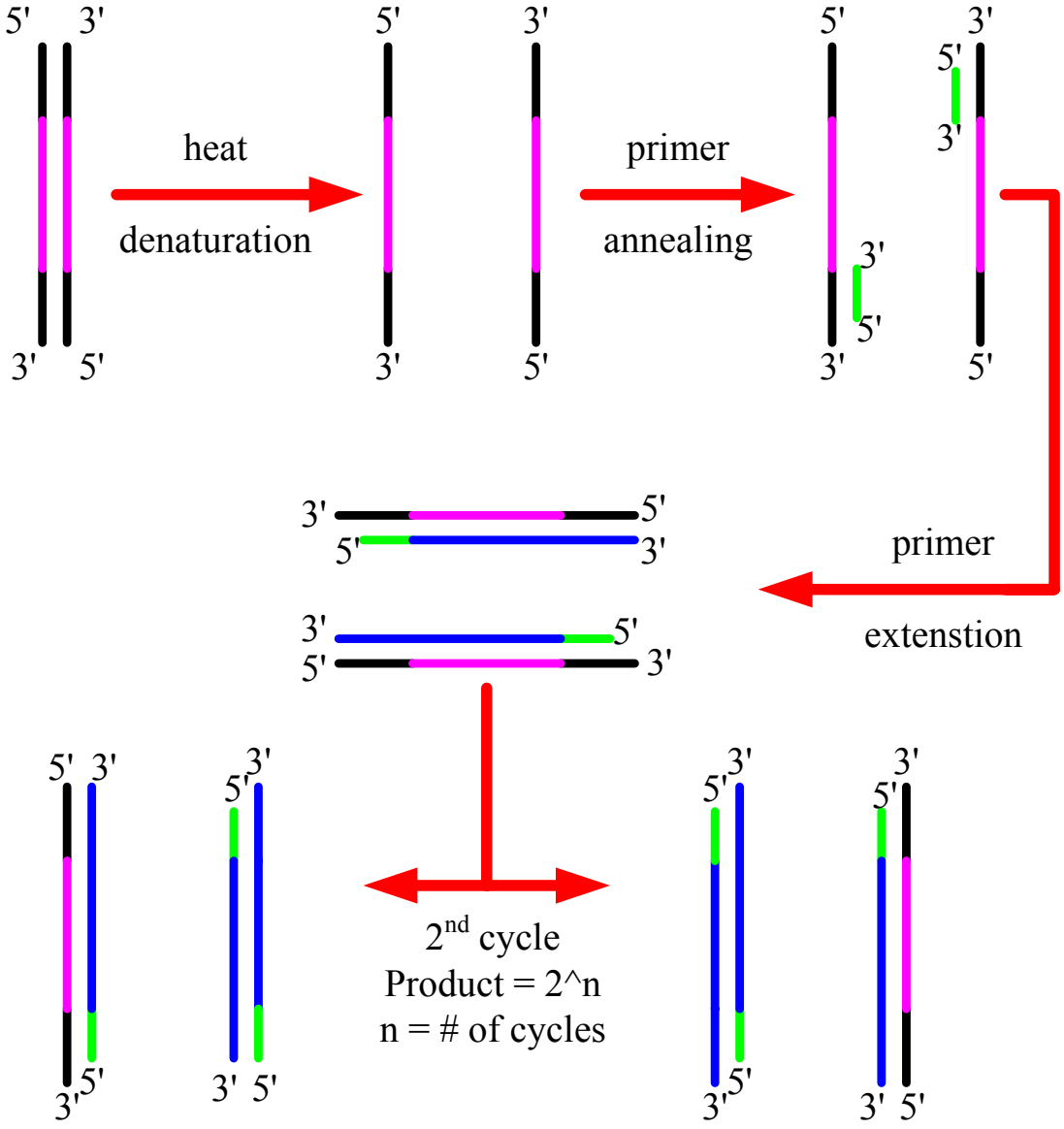

Figure 2-1. Schematic representation of a polymerase chain reaction. A double-strand target is heated to create two single-stranded species. Primers hybridize to each strand creating double-stranded regions for enzyme binding. The polymerase enzyme binds and builds on the primer creating a copy of the initial strand. (For interpretation of the references to color in this and all other figures, the reader is referred to the electronic version of this dissertation.)

The target is first heated to denature the DNA in to single-strands. Primers bind to each strand, and the enzyme polymerase binds to the primer-target double-strand DNA region formed. The polymerase polymerizes the primer in a 5' to 3' fashion completing new double-stranded DNA, which is a copy of the original target. The process repeats between 20-30 cycles creating more target exponentially.

PCR reaction conditions vary based on the target DNA sequence being amplified, the DNA sequence of the primers used, and matrix interference. This highly sensitive amplification system requires expensive amplification equipment and refrigerated reagents preventing the portability of the system outside the laboratory environment.

2.2.2 Rolling circle amplification (RCA)

More advanced methods of primer design have been developed to reduce the complexity of the amplification process. Rolling circle amplification utilizes a circular primer to bind to the target DNA section. The polymerase enzyme then begins creating a copy of the bound section. Upon exhausting the target sequence-circular primer region, the enzyme continues using the circularized primer as the template. Once the entire circular primer is duplicated, the enzyme displaces the recently generated double-stranded portion and continues replication and strand displacement [55-57]. Strand displacement polymerases maintain attachment to the guide strand, while removing the bound DNA in front of the polymerization direction. The product generated from this style of amplification is a single-long single-stranded DNA sequence with a continually repeated internal structure. Three methods of executing RCA are shown in Figure 2-2 [58].

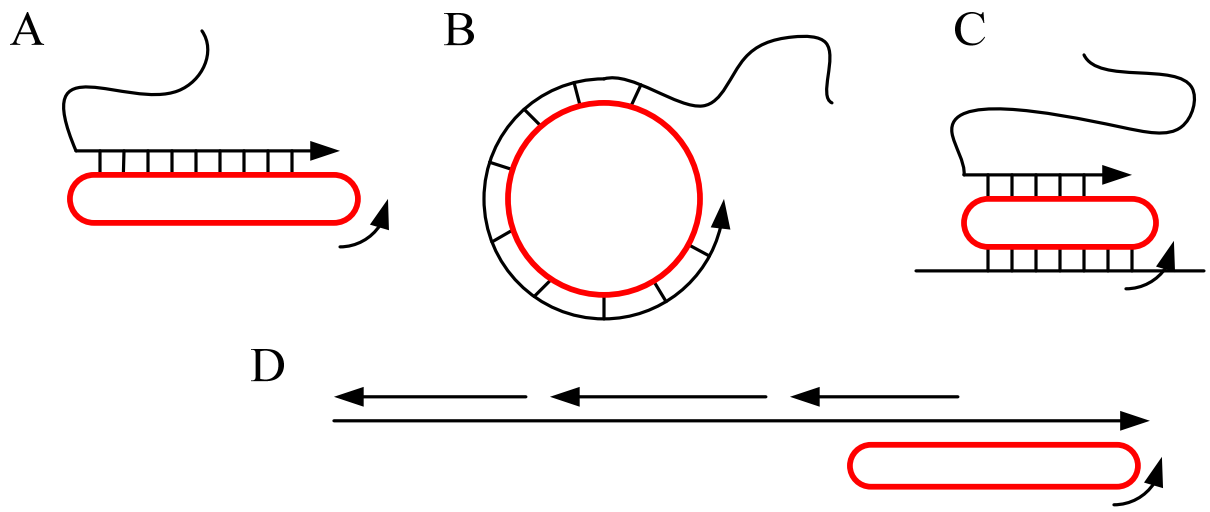

Figure 2-2. Common RCA modes of reaction. (a) Initial binding; (b) Reaction product; (c) Binding of internal DNA sequence; (d) Double RCA, a second primer is added to create a traditional double-stranded product (adapted and modified from Demidov, 2002).

RCA benefits from simplified reaction conditions and equipment needs. Once the primer is initially bound, only a single temperature is required for continuous amplification. Detection of RCA product is common via electrophoresis or fluorescence measurement. Addition of labeled primers is not well suited to RCA as the primer is not actually consumed in the reaction. Further hybridization detection is also not well suited as the number of target molecules is not amplified [59].

2.2.3 Loop-mediated isothermal amplification (LAMP)

Loop-mediated isothermal amplification is a novel method of using structure switching primers to create a single long double-strand DNA output comprised of the target DNA sequence [60]. LAMP amplification is accomplished using a set of six primers and a strand displacement

polymerase enzyme. A set of primers initially binds to each of the single-strand targets in the region of interest. Amplification is allowed to occur as it would in PCR for one cycle, Figure 2-3,b-1. A second primer set is then introduced into the solution and allowed to separate the previously generated DNA, Figure 2-3,b-2. At this step, the first primer set has increased the target size by introducing a possible loop structure. A third set of primers is added that upon another round of amplification introduces a second possible loop structure into the target strand, also increasing the product length, Figure 2-3, b2-5. When the second primer set is then added to the double loop structure, the primer changes the loop structure opening up free DNA for a polymerase to polymerize a new DNA strands, but unlike normal PCR, when the enzyme reaches the loop structure, it continues back towards the point of origin. The strand displacement polymerase pulls apart the structure until it reaches the point of origin, where a loop structure exists also. This polymerase will continue along this cyclic amplification until the reactants are exhausted.

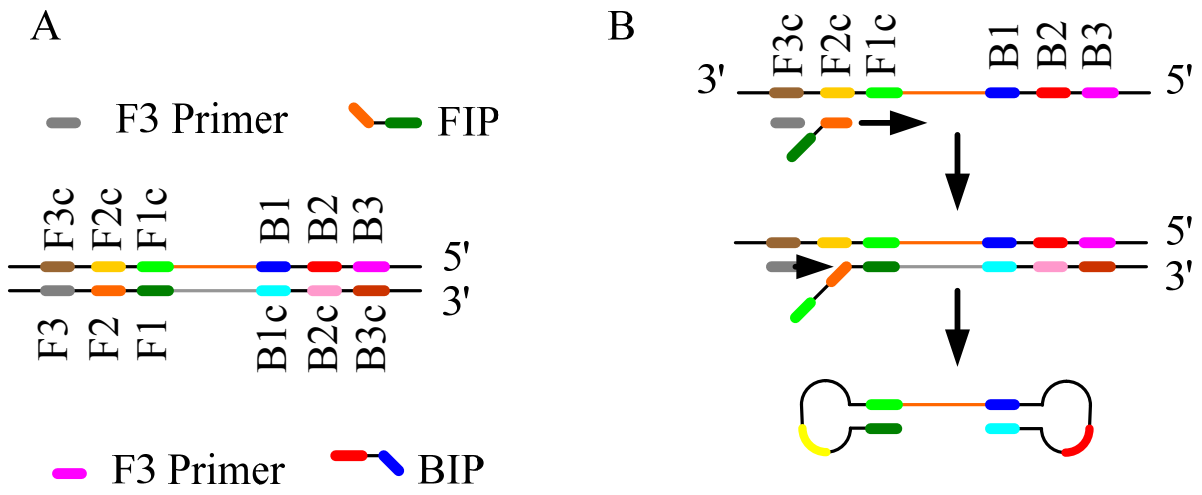

Figure 2-3: Cartoon illustration of the LAMP method. (a) Primer design location. Six primer sites are required and noted as F1-F3 for forward primer and B1-B3 for reverse primer. Primers notes with 'c' are complimentary to the associated sites; (b) The first primer to bind (FIP) adds a region during the first amplification, step 1. Step 2 uses an external primer (F3) to free the newly created DNA strand. Step 3 uses a new primer (BIP) to add a second region to the other end of the new DNA strand. A second external primer (B3) is used to free the strand. Now is step 5, the added DNA and then end of the target self-hairpin creating a self primed sequence (adapted and modified from Notomi *et al.*, 2000).

The LAMP reaction creates a single long double-stranded output. Once the initial primer set creates the hair pinning target structure, the enzyme amplification reaction proceeds isothermally until the reactants are exhausted or the polymerase degrades. For example, the system produces a highly detectable target with fluorescent staining, but suffers from design constraints. The six primer set is not compatible with all gene sequences, requires a large initial target (>200 bp), and entails multiple steps with manual addition of the primers in a precise sequence. LAMP demonstrates what careful primer design can accomplish though enzymatic polymerization.

2.3 Non-enzymatic amplification methods

Novel methods have been developed to remove the need for enzymatic amplification. The move to create more stable assays based on DNA hybridization has provided some basic tools for potential field-based methods. This section describes hybridization-based amplification methods.

2.3.1 Hybridization chain reaction

Hybridization chain reaction utilizes a dual hairpin DNA system that upon target binding causes a chain reaction of hybridization. The system is based on the stored energy in the hairpin-loop DNA reactant [17]. A single-stranded target binds to a free portion of the first hairpin structure (H1). The target causes H1 to open, and the target continues to hybridize stabilizing H1 into a linear structure. The newly exposed section on H1 then binds in the same fashion to the second hairpin (H2). H1 and H2 then hybridize exposing a binding area on H2 that will then bind to H1. This series of alternating hairpin opening and hybridization continues until the reactants are exhausted. Figure 2-4 shows the hybridization scheme.

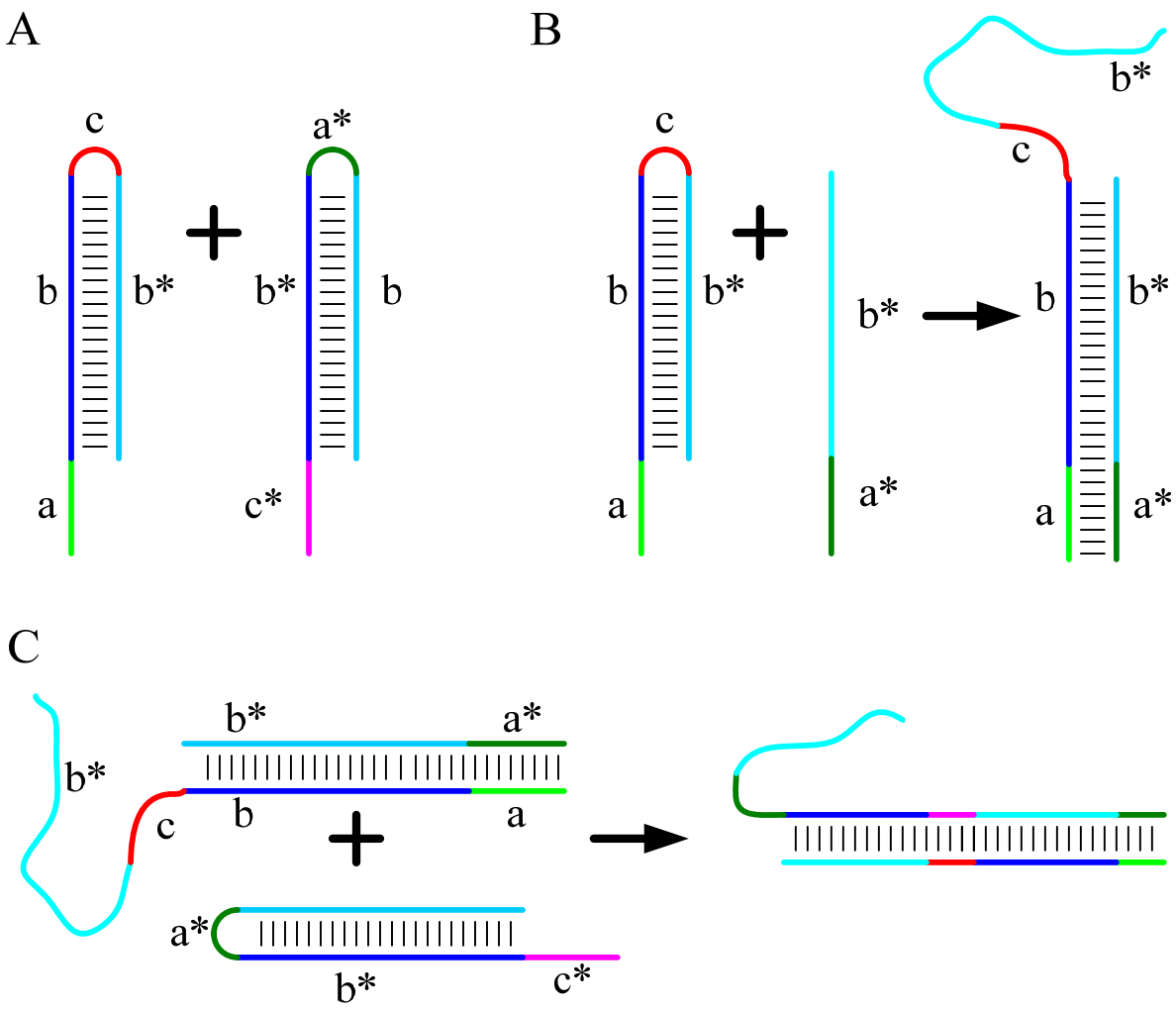

Figure 2-4: Hybridization chain reaction mechanism. (a) The two hairpin system at start of reaction; (b) Addition of the target (initiator) and initial hairpin opening; (c) Exposed sites on first hairpin cause the second hairpin to open and hybridize (adapted and modified from Dirks and Pierce, 2004).

This system is enzyme free and produces large double-stranded DNA sequences. The hairpin structure of the reagents provides for an inexpensive system of oligonucleotides that can produce a large increase in size of the target. Detection in this system currently requires electrophoresis readout. DNA intercalating dyes in solution used with this system do not show change in total

signal strength, as both the starting and end products are double-stranded. Even a single hairpin opening could cause false negative detection. This opening event would be a thermodynamic possibility leading to the same response as if the target were present. Readout would be possible with a molecular beacon approach for fluorescence, but this would not alleviate the spontaneous hairpin openings.

2.3.2 Isothermal chain elongation

Isothermal chain elongation is based on the concept of capturing a target single-strand DNA sequence on a plate surface. The surface is decorated with a capture strand that hybridizes to the target partially. The un-hybridized portion of the target is used to hybridize with a second strand that is labeled with biotin. This second hybridization is also a partial hybridization, leaving a portion of the strand open for binding to another target molecule [61]. Repeated hybridizations of target generate a long double-stranded DNA sequence tethered to the plate surface. Detection is achieved by binding of a quantum dot-streptavadin conjugate to the biotin attached to the second hybridization molecule. Upon washing off the unbound quantum dots, the solution is fluorescently detected. Figure 2-5 schematically details this method.

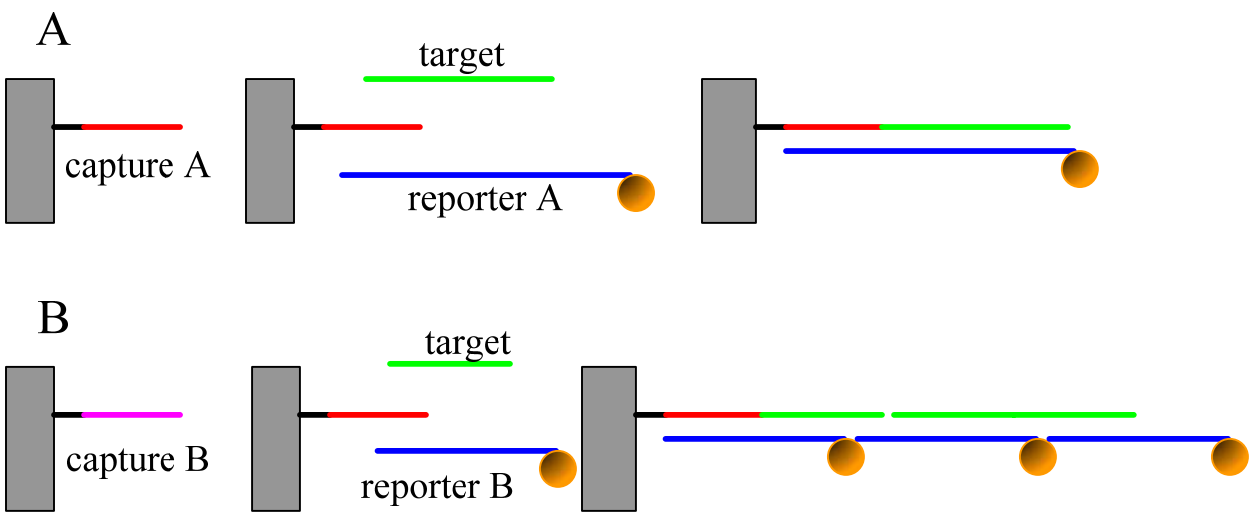

Figure 2-5. Isothermal chain elongation. (a) Single round of hybridization; (b) Target is linked to the tethering molecule via reporter B. Additional reporter B hybridizes and allows for additional target binding and subsequent reporter B binding. Addition of a quantum dot-streptavidin complex binds to biotin on the reporter B molecule (adapted and modified from Song, Lau and Lu, 2012).

This method has the advantage of being an enzyme free method capable of being conducted without heating or temperature sensitive reactants. The quantum dot reporter system allows for multiple different emission wavelengths, with possible use multiplexing in a microarray format. The final sensitivity of this system is no better than microarray hybridization using a quantum dot labeled probe. Since the target is half of the double-stranded product, at a 1:1 ratio with the reporter, no increase in signal is observed over standard microarrays.

2.3.3 Triplex signal enhancement

Triplex signal enhancement is the process of electrostatic binding of a cationic polymer to a single-strand DNA reporter. The thiopene polymer is quenched upon binding to a single-stranded DNA molecule. Hybridization of the complimentary DNA sequence forms a triplex complex creating a resonance energy transfer system with fluorescent properties. When each DNA-cationic polymer duplex is labeled with green emitting fluorophore, a process of 'super lighting' can occur [62]. Super lighting happens when a single triplex structure is formed and acts as the donor to multiple acceptors in close proximity. This process yields great sensitivity, but requires equally sensitive photodetection equipment. The cationic polymer is not sequence specific in duplex formation. Close proximity of non-target single-strand DNA and off-target hybridization pose the possibility of a false positive in this system.

2.3.4 Branched DNA amplification

Branched DNA amplification is the technique of hybridizing a single-stranded target to an array surface and through subsequent hybridizations, bind additional DNA reporter molecules. In Figure 2-6, the method is shown in an abbreviated format [63]. A target hybridizes to multiple bound surface probes. The multi-probe attachment creates a strong target-surface structure. A preamplifier is then hybridized to the free portion of the target and stabilized though accessory DNA strands (label extenders). The preamplifier DNA is then loaded by hybridizing labeled probes.

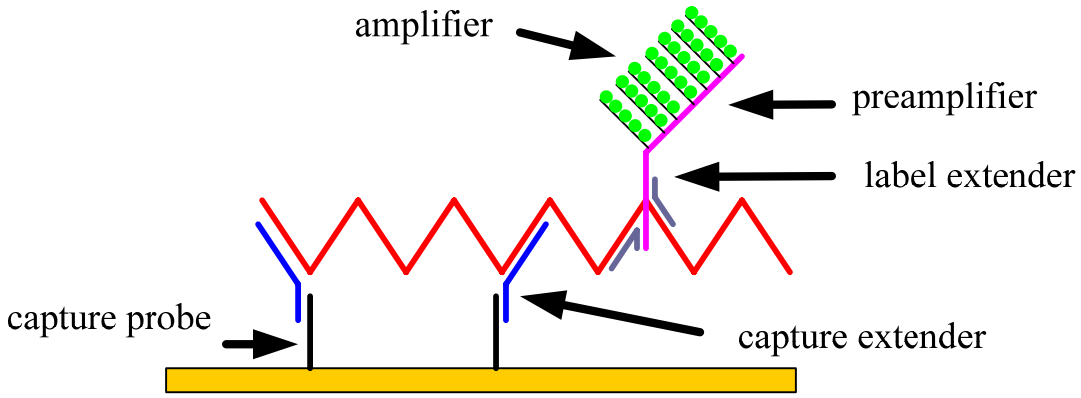

Figure 2-6. End product of branched DNA amplification. Target nucleic acid is captured and hybridized to a second ssDNA to allow for additional labeled probe binding (adapted and modified from Tsongalis, 2006).

This enzyme free system provides a good deal of amplification, but at the cost of increasing system complexity and material costs. The target DNA or RNA sequence must be sufficiently long to bind both to the surface and for loading of the preamplifier sequence. Additionally, the input DNA or RNA must be relatively pure so as to avoid off target binding from the many different stabilizing, amplifying, and extension DNA sequences required for this system.

2.4 Nanoparticle based biosensor platforms

Biosensors are defined as sensing devices which integrate a biological recognition element and a transducer to quantify a biochemical interaction. The biological recognition element is responsible for capturing the signal. Once captured, the transducer changes the signal into another form of energy that can be detected. Common recognition elements can be grouped broadly into immunosensors, DNA hybridization sensors, enzyme based sensors, and combinations of each. Transduction of the signal can be into many forms, with the most common

being light, electrical, and chemical change. Figure 2-7 shows a representative schematic of the biosensor.

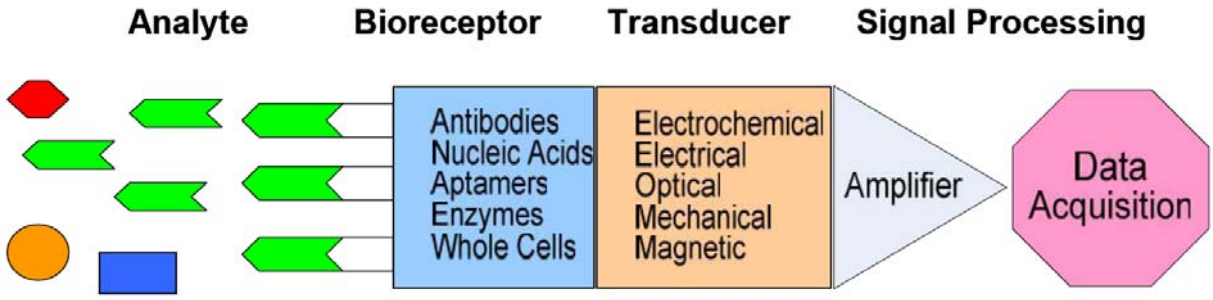

Figure 2-7. Schematic diagram of the components in a biosensor system.

DNA biosensor systems typically rely on hybridization to either a surface or a particle for recognition. The hybridization event is then transduced into another form such as light via fluorescent reporters, electrical via metallic particles, change in mass vibration frequency and other physical properties through enzyme mediated events. The signal is then detected and related back to the original binding event. As described in the previous sections, the only governmental approved biosensors are based on metabolic changes via growth of the target organism. Scientific biosensors have focused on antibody immobilization and DNA amplification via PCR. Culture based methods are simple but time consuming and actually produce more of the target organism. PCR techniques are more rapid but have very involved processing steps and require a laboratory environment. The development of a rapid and simple method for DNA detection is needed for public safety and water quality monitoring.

The following methods described show the current technology for a bio-sensing system based on DNA recognition. They employ hybridization techniques which when used with the gene targets in Table 2-2 would make viable bio-sensing systems for *E. coli* O157:H7.

2.4.1 Nanoparticle sensing

The recent use of nanoscale materials for biosensing elements, transducers and reporters have led to a whole group of nanomaterial based sensing systems. The traditional role of nanoparticles has been as reporters, delivery vehicles, and attachments surfaces. Quantum dots are a class of semi-conducting nanoparticles that exhibit fluorescent properties. As previously described in section 2.3.2, isothermal chain elongation uses a quantum dot reporter in lieu of standard organic fluorescent molecules. When nanoparticles were incorporated into a full sensor, a new field of nanodiagnostics was created.

The most widely used of the nanoparticles is the gold nanoparticle. It has been used both for its colorimetric application and its ability to tether a large array of molecules to the surface. Gold nanoparticles exhibit a deep red color when in solution. As gold nanoparticles aggregate, or are linked together in close proximity, the surface plasmon resonance between adjacent particles causes a color change to purple. This change in color is used to report binding events [64-66]. Binding is accomplished by labeling two species of gold particles with different bio-elements that recognize the physical molecule. The successful demonstration of the technique was shown by the Mirkin group with both DNA and antibody probes [67]. When colorimetric detection is used with DNA hybridization, no amplification of signal is seen. There is still a one-to-one relation between target and reporter.

The use of gold nanoparticles for signal amplification has been recently achieved using a technique called the bio-barcode [16, 68]. The bio-barcode (BBC) was the first truly enzyme free DNA amplification assay. Selection and amplification of a DNA signal was accomplished with a two particle system comprised of a magnetic microparticle and a gold nanoparticle. Each particle is labeled with a different single-stranded DNA probe. The probes used are based on the same sequences targeted in PCR amplification. The largest difference in probe design between the BBC assay and PCR is that both particles are engineered to bind the same ssDNA sequence. When a DNA target hybridizes, a bridge is formed linking the gold nanoparticle to the magnetic microparticle. This DNA-bridge allows for magnetic separation of the solution, and only when a target is present, are gold nanoparticles recovered, Figure 2-8.

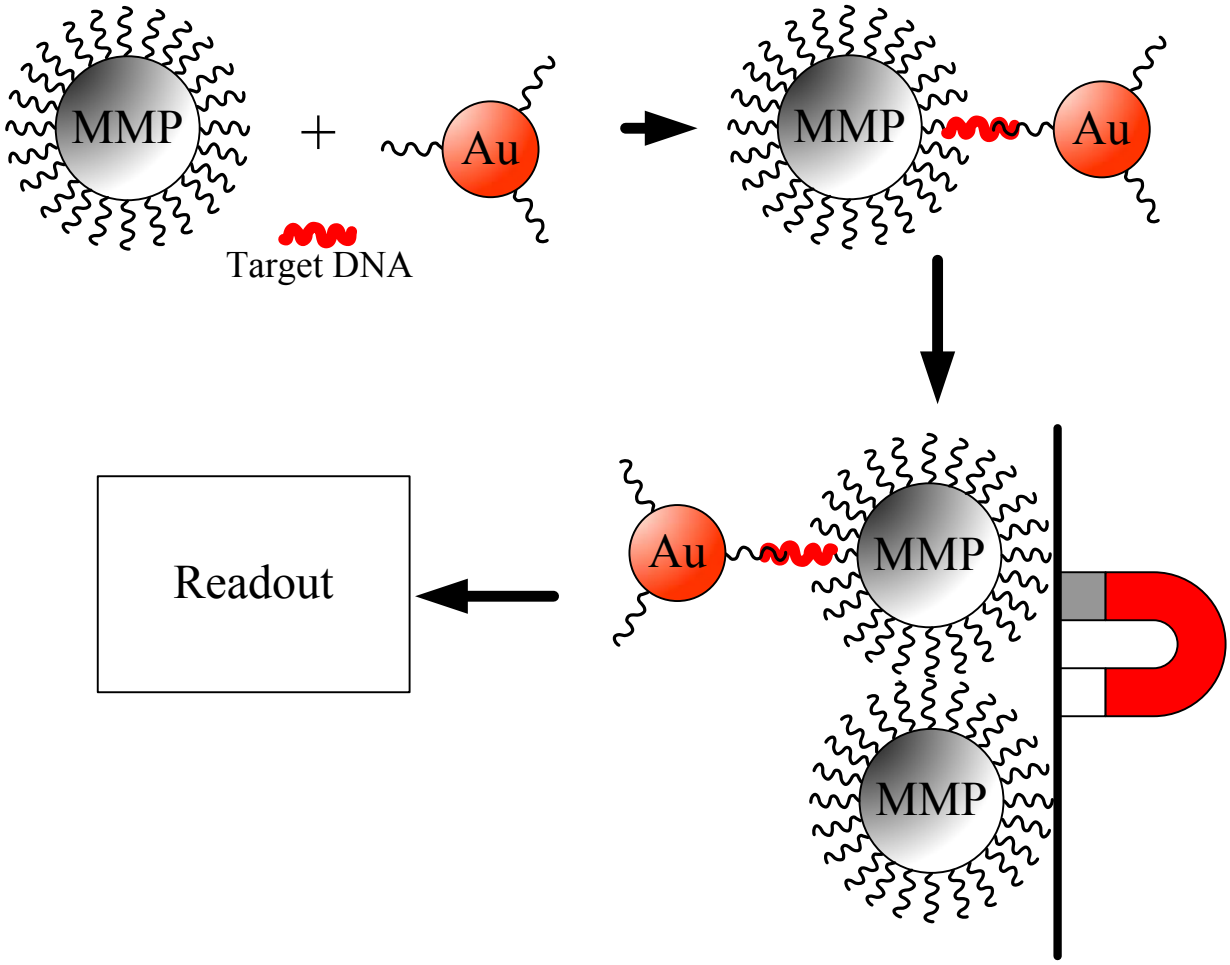

Figure 2-8: DNA detection using the sandwich assay. The magnetic microparticle (MMP) and gold nanoparticle (Au) are mixed with a DNA target. A sandwich is formed between the MMP-DNA-Au which is magnetically separated. The separated product contains Au particles only when DNA target is present. Measurement is then performed based on the reporter used (adapted and modified from Nam, Stoeva, and Mirkin, 2004).

This hybridization method uses the gold nanoparticle as a platform for amplification. Amplification is achieved by attachment of a second molecule to the gold nanoparticle, either through fluorescence or electrochemistry.

2.4.1.1 Bio-barcode detection

The bio-barcode was the first assay to popularize the use of gold nanoparticles in a complete sensing system using enzyme free DNA amplification. Target recognition and recovery of the gold nanoparticle are accomplished as shown in Figure 2-8 [69]. The bio-barcode amplification is achieved by attachment of small single-strand DNAs (bio-barcodes, BBCs) to the gold nanoparticle at a ratio of 100:1 with the probe DNA strand. The reporter BBCs are then recovered by ligand exchange with dithiothreitol (DTT), Figure 2-9.

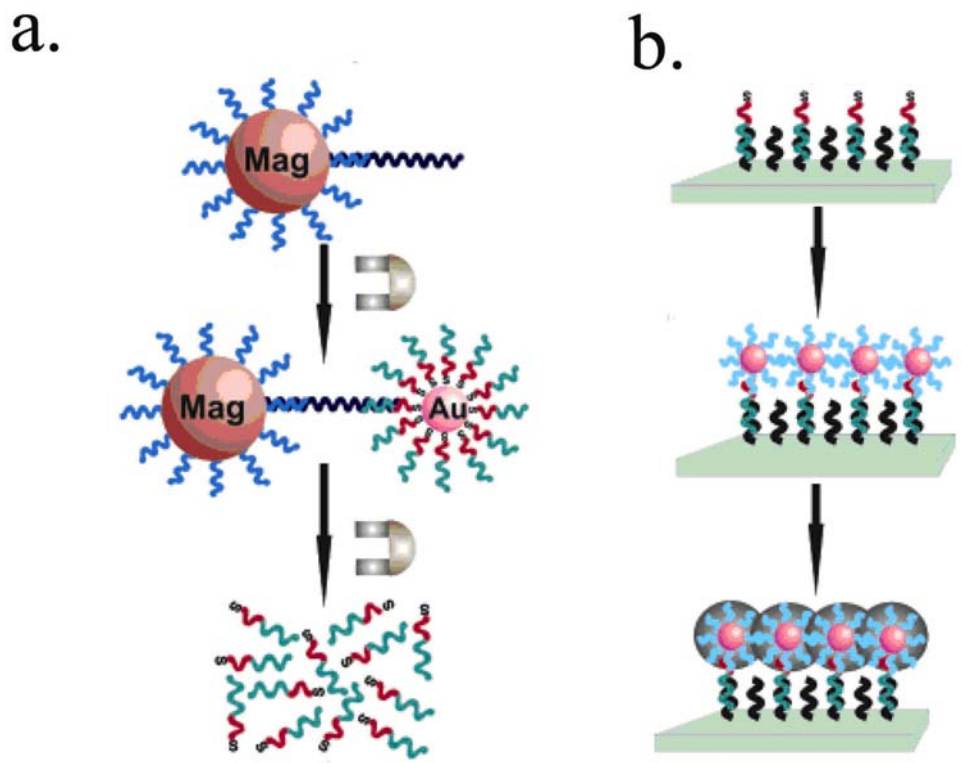

Figure 2-9: Bio-barcode detection overview. (a) Capture and release of the bio-barcode based on target hybridization; (b) Bio-barcode is hybridized to a surface, providing a tethering molecule for a second gold nanoparticle (adapted and modified from Thaxton *et al*., 2005)

Once the BBCs are freed, they are hybridized to a surface (Figure 2-9b.). The immobilized BBCs act as a hybridization point for a further round of hybridization with a second gold nanoparticle. This second gold nanoparticle is used as a growth point for standard silver enhancement and subsequent reflective scanning readout. This platform has been successfully used for detection of the *pagA* gene in *Bacillus anthracis* and viral targets [16, 70, 71]. Despite this assay method being highly successful, it requires a relatively pure DNA input and the assay time after sample is extracted is approximately 8 hours.

2.4.1.2 Gold reduction / oxidation

Electrochemical detection using the sandwich assay structure from the bio-barcode method has been recently accomplished using the gold nanoparticle itself [10]. The same DNA hybridization sandwich structure is used for target recognition and gold nanoparticle recovery. Once the gold nanoparticle is recovered, it then is transferred to an electrode, as in Figure 2-10.

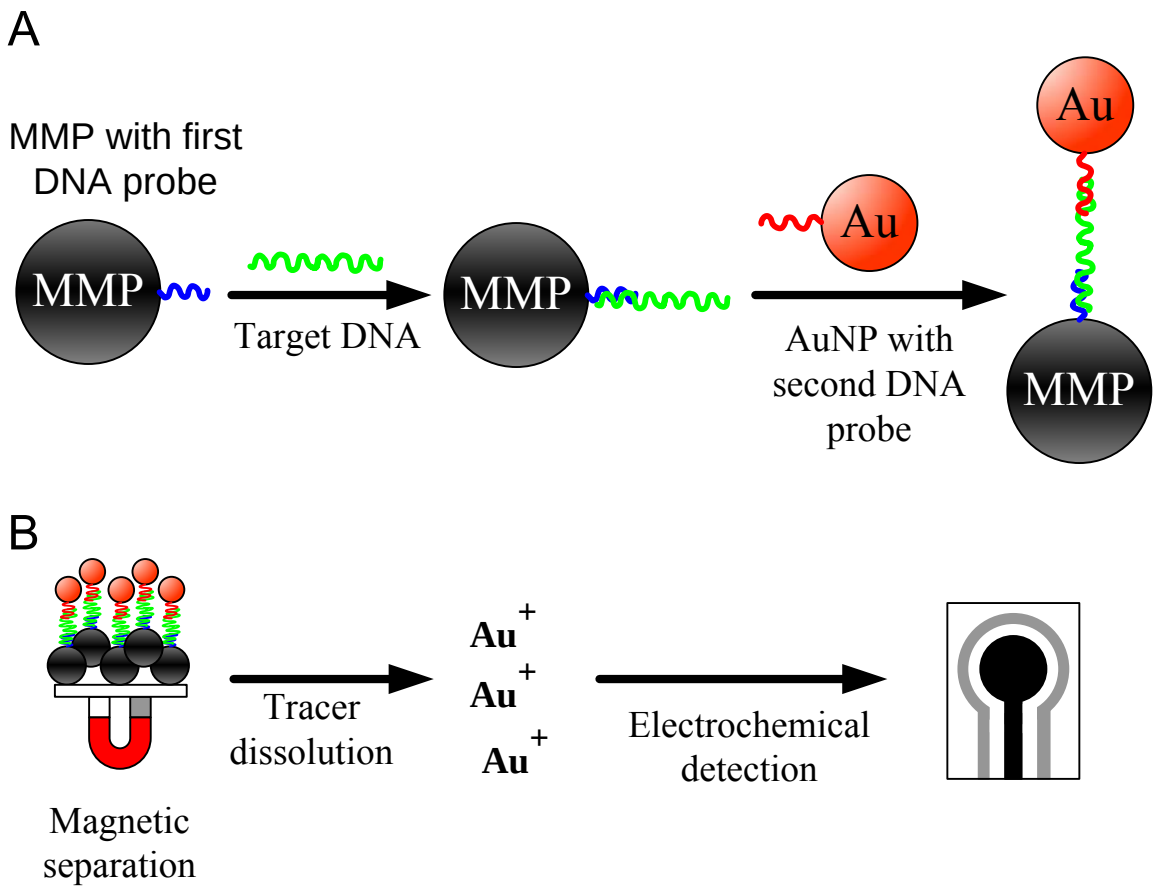

Figure 2-10: Electochemical detection of gold nanoparticles. (a) Formation of the sandwich structure; (b) Gold nanoparticle recovery and detection (adapted and modified from Torres-Chavolla and Alocilja, 2011).

The gold nanoparticles are oxidized under positive potential and acidic conditions to generate a detectable ion species. The gold ions are reduced under differential pulse voltammetry producing a detectable current characteristic to the gold in the electronic system. This form of detection was successfully used to detect target from Mycobacterium tuberculosis from enzymatically amplified target. This detection system was a proof of concept for bacterial detection, but shows great promise as a guide for a future rapid hybridization assays.

2.4.1.3 Other metallic nanoparticle electrochemical detection

An improvement to electrochemical detection is accomplished through the same methodology as the bio-barcode assay. Attachment of nanoscale heavy metal-particles to the BBC produces an amplified metallic system. The recovered gold nanoparticle-heavy metal particle conjugates are oxidized in a similar fashion as the gold nanoparticle. The reduction of heavy metals (cadmium or lead) is then measured as a current peak. Each metal in the system (gold, cadmium, lead) produces a peak at a different reducing voltage. This enhanced nanoparticle system was used successfully to detect PCR amplified target from *Bacillus anthracis* and *Salmonella enteritidis*. Though highly sensitive, pure target from enzymatic amplification is still required for detection from this assay system.

2.4.2 Fluorescence detection

The use of metallic nanoparticles and secondary hybridization structures creates a sensitive detection assay, but adds steps to the process making it more complicated. Fluorescent readout has been used to simplify the process. One approach to fluorescent output is to replace the gold nanoparticle with a polystyrene (PSM) microparticle [72]. This PSM is labeled with approximately 40,000 fluorescent reporter molecules. Other replacements for the gold nanoparticle include DNA dendrimer agglomerates [73]. The dendrimer agglomerates contain multiple biotin binding sites for a reporter molecule. The PSM molecules provide a greater amplification factor than the gold nanoparticles (40,000x v. 100x) but do not suspend well in water and provide higher amounts of non-specific binding. This non-specific binding reduces the specificity of the assay as a whole. DNA dendrimers remain highly water soluble, but require

further conjugation of a reporter molecule to the biotin. This additional step also increases system complexity.

2.4.3 Targets

Nanoparticle based DNA assay systems have been successfully used with short DNA targets often resulting from enzymatic amplification. The steps required to generate a target for the assay are not included in the total assay time. The extraction and preparation of a DNA target requires an additional 2-3 hours to the total assay detection time. Focus is shifting to use of raw genomic inputs [15], but have not included rapid detection methods.

2.5 Gold nanoparticle synthesis

The unique properties of gold nanoparticles make them well-suited for a variety of applications. As described previously, they are used in spectral detection, colorimetrics, electrochemical detection, and as platforms for other reporters. The utility of gold nanoparticles are a result of their size and chemical reactivity. Controlled generation of gold nanoparticles is key to the production of a uniform product for assay reproducibility. Generation of gold nanoparticles is most commonly via citrate reduction. This process uses high temperatures and acidic conditions for particle generation. Particle size is controlled through the surface capping agent (citrate) to gold chloride concentration [74]. Other methods such as non-polar synthesis and biological synthesis have been successful at generating gold nanoparticles [75-79]. Biological methods are becoming more widely used as they provide a gentler or ‘green’ means of particle production. The use of carbohydrate and protein capping agents has the potential for better bio-compatibility in medical diagnostic systems [80, 81].

This chapter is adapted from our recently published work in the Journal of Nanoparticle Research:

Anderson, J. Michael; Torres-Chavolla, Edith; Castro, A. Brian and Alocilja, C. Evangelyn. One step alkaline synthesis of biocompatible gold nanoparticles using dextrin as capping agent. Journal of Nanoparticle Research. 2011. 13(7):2843-2851.
DOI: 10.1007/s11051-010-0172-3

Chapter 3: Synthesis and characterization of dextrin gold nanoparticles

3.1 Introduction

Gold nanoparticles have been widely studied in recent years for their wide range of applications. Gold nanoparticles exhibit surface plasmon resonance and have been used in colorimetric assays and surface enhanced plasmon resonance (SERS) for fluorescent applications [82-84]. Electrochemical detection with gold nanoparticles has been accomplished using reduction/oxidation potentiometry or as conductive elements in electrical circuits [85-87]. Assays involving gold nanoparticles all require attachment of recognition molecules for detection. Surface molecules, or ligands, include but are not limited to DNA, proteins, polymers, peptides and antibodies [11, 18, 88-90]. The attached ligands both aid in target recognition and stabilize the gold nanoparticle cores by providing appropriate hydrophobicities.

Traditional gold nanoparticles synthesis has been achieved by three methods: 1) Brust method in a non-polar media [76], 2) Turkevich method in aqueous media [91], and 3) biological synthesis using microorganisms [78, 92]. Current aqueous generation is under aggressive conditions (pH=3, 95°C), commonly requiring post-processing before biological materials can be attached. Low energy input and milder generation conditions have been a recent focus for synthesis of gold nanoparticles as trends towards ‘green’ processes are becoming more important. A second benefit for milder generation conditions is the possibility for protein and DNA interaction during particle generation. Generation of gold nanoparticles at pH 7.0-9.0, using temperatures between 20-50°C and with biomolecules would allow for exploration of gold nanoparticle generation and surface functionalization with a minimum of processing steps.

Recent work into mild generation conditions has involved glyconanoparticles, or carbohydrate coated particles and amines [93-95]. These particles are being tested in biomedicine, biolabeling, and biosensings applications [10]. Cyclo-dextrins, dextrans, and glucose have been used recently to generate gold nanoparticles [81, 96, 97]. This paper describes a generation process under alkaline conditions using a dextrin, a carbohydrate, as a capping molecule under modest temperatures.

3.2 Materials and methods

3.2.1 Optimization of gold nanoparticle synthesis

Gold nanoparticles were synthesized from a gold chloride (HAuCl4) stock solution of 20 mM [Aldrich #520918-5G]. The gold chloride was prepared fresh weekly using deionized water and stored under refrigeration. A stock solution of dextrin at 25 g/L was prepared in deionized water and autoclave sterilized prior to use [Fluka #31400]. All reaction volumes were 50 mL and carried out in 250 mL Erlenmeyer flasks that were washed and acetone rinsed before synthesis.

A volume of 5 mL of gold chloride was mixed with the stock dextrin to achieve 45 mL of solution to achieve a final dextrin concentration between 2.5 and 20.0 g/L. The solution was pH adjusted to pH 9 using filter sterilized sodium carbonate (Na2CO3). The reaction volume was adjusted to 50 mL using pH 9 adjusted water, yielding a final gold chloride concentration of 2 mM. Each reaction flask was wrapped in aluminum foil to protect from light and continuously agitated at 50°C for 8 hours.

Particle formation was observed visually through the following stages: yellow, clear, purple tint, red tint, and finally red (520 nm), the same sequence reported for standard citrate generation of gold nanoparticles [98]. Reaction temperature (25°C and 50°C) and pH (3 to 11) were varied to explore the effects on gold nanoparticles generation.

3.2.2 Gold nanoparticle characterization

The gold nanoparticles were monitored during and after synthesis. Reaction completion was evaluated using absorbance reading with a UV/Vis spectrometer. Size distribution was evaluated using dynamic light scattering and transmission electron microscopy (TEM) imaging. Reported size information was obtained from TEM images using a JEOL 100CX Transmission Electron Microscope and a Zetasizer Nano series (Malvern Instruments). Samples were diluted 1:4 in distilled water, and a volume of 5 μL was placed on to a formvar/carbon coated copper grid of 300 mesh. The samples were vacuum dried on the grids prior to imaging. TEM samples for specific time points were prepared immediately after sample collection for proper reaction monitoring.

3.2.3 Gold nanoparticle functionalization

Functionalization of the synthesized particles was accomplished using sulfur chemistries and was necessary to evaluate particle compatibility within biosensor systems. Functionalization was performed with a modified DNA molecule containing a three prime (3') reactive thiol group and a five prime (5') fluorescent 6-carboxyfluorescein group (6-FAM, excitation peak = 495 nm, emission peak = 520 nm). Standard DNA notation was used for all sequence and includes: adenine (A), cytosine (C), thymine (T), and guanine (G). The sequence used was 5' – TTA TTC

GTA GCT AAA AAA AAA A - 3' (Integrated DNA Technologies, Coralville, IA). The thiol group was chemically activated in a 1 M solution of dithiothreitol (DTT) for 2 hours and purified through an Illustra NAP-5 desalting column (GE Healthcare #17-0853-02) producing a solution of reactive DNA. The activated DNA was ligand exchanged for the capping dextrin molecules over a 72 hour period before, with salting additions every 8 hours to promote close packing DNA on the gold particle surface. The closed packed DNA creates a stable AuNP for potential assay use. The procedure is the same used for citrate generated gold nanoparticles [11]. Successful functionalization of the particles yielded a product with the same color as the initial dextrin coated gold nanoparticles. Functionalization efficiency was determined by washing the functionalized gold nanoparticles three times in distilled water and resuspension in a 5 M DTT solution at 65°C for 15 minutes followed by a 45°C incubation at 25°C to remove the DNA from the gold nanoparticle. The DTT treated samples were centrifuged at 13,000 x g for 30 minutes and the supernatant was fluorescently excited on a VICTOR3 1420 Multilabel plate counter (Perkin-Elmer) using a 492 ± 4 nm excitation filter and 535 ± 12.5 nm emission filter set for detection.

3.3 Results and discussion

3.3.1 Gold nanoparticle characterization and synthesis

Gold nanoparticles were successfully generated with dextrin as a capping agent under alkaline conditions. The baseline reaction conditions were: 10 g/L dextrin concentration, 2 mM gold chloride, pH 9.0, 50°C and 24 hours for synthesis. The particle generation was monitored through absorbance measurements of the 520 nm peak characteristic of gold nanoparticles of the size range 5 – 100 nm (Figure 3-1). Absorbance at 520 nm was recorded after the visual color of

the solution began changing from a light purple to the light red tint between 4 – 6 hours of reaction (Figure 3-2) [12]. The reactions were monitored for a full 24 hours to assess the degree of completion of the reaction.

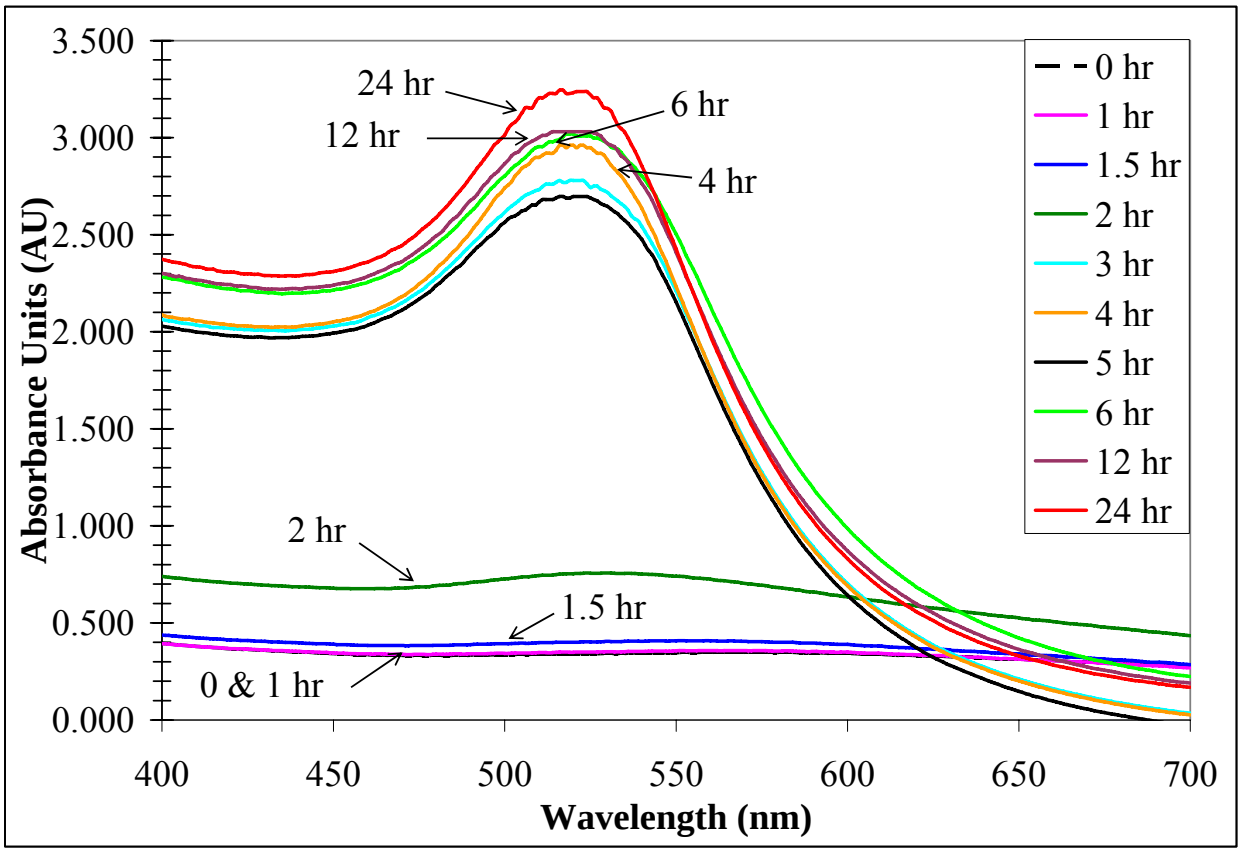

Figure 3-1: UV-Vis spectra time monitoring of gold nanoparticles synthesis. Generation conditions 10 g/L dextrin, pH 9.0, 50°C (adapted and modified from Anderson *et al.*, 2011).

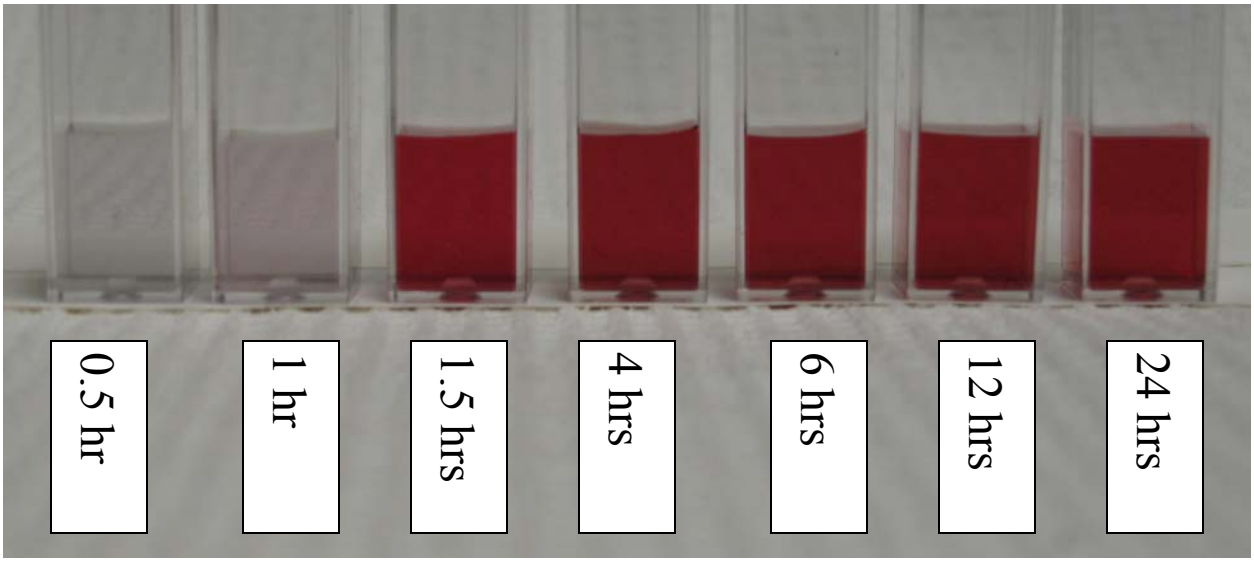

Figure 3-2: Visual time monitoring of gold nanoparticles synthesis. Generation conditions 10 g/L dextrin, pH 9.0, 50°C (adapted and modified from Anderson *et al.*, 2011).

The generation of particles required the presence of dextrin, alkaline pH, sodium carbonate and gold chloride. Reactions lacking any of the mentioned reactants did not form gold nanoparticles. When gold chloride was present in the reactions that either lacked dextrin, alkaline pH or sodium carbonate, the gold would deposit in the neutral metallic state on the flask walls after several days.

3.3.2 Effects of dextrin concentration, pH, and temperature

Successful generation of gold nanoparticles was accomplished under a large set of synthesis conditions. Controlling the ratio of capping agents and reaction rate has been used to manage the final particle size in nanoparticle production. The concentration of the dextrin was varied from 2.5 g/L to 20 g/L final concentration to determine the effect of capping agent on final particle size. Production of 8.6 nm ± 1.2 nm, 10.6 nm ± 1.6 nm, and 12.4 nm ± 1.5 nm was accomplished

for dextrin concentrations of 20.0, 10.0 and 2.5 g/L respectively. Particle size determinations were made from TEM image measurements. Figure 3-3 shows the TEM images of generation conditions. Figure 3-4 shows the resulting data versus generation concentration.

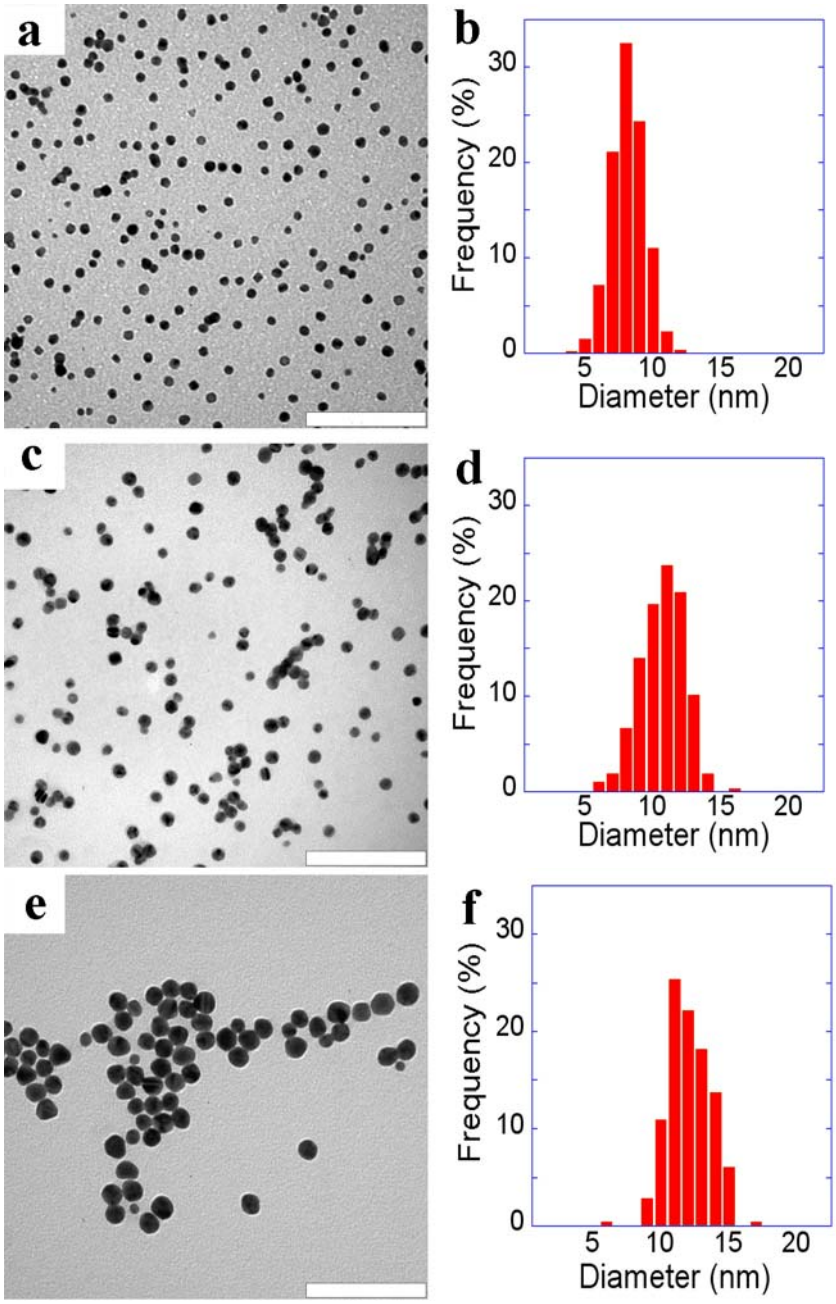

Figure 3-3: Transmission electron micrographs of gold nanoparticle. AuNP synthesis using various dextrin concentrations. (a and b) 20 g/L, (c and d) 10 g/L, and (e and f) 2.5 g/L. Scale bars of a, c, and e are equal to 100 nm (adapted and modified from Anderson *et al.*, 2011).

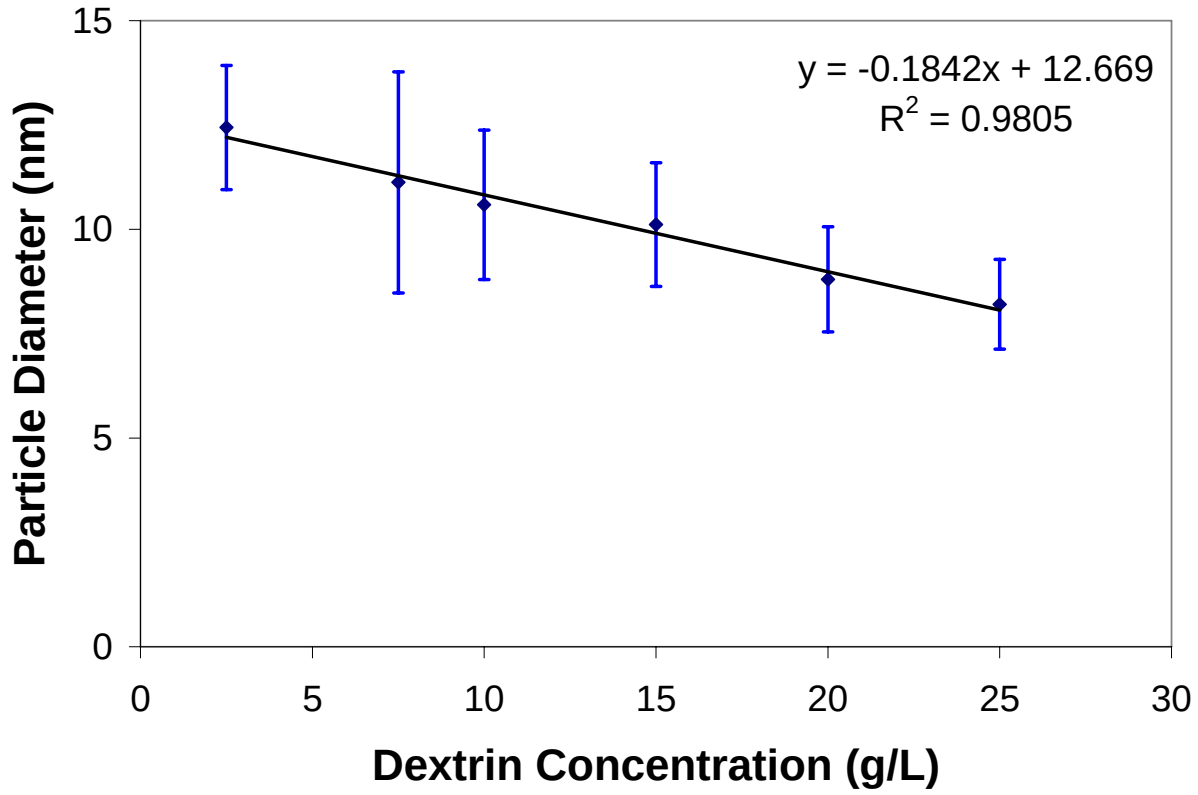

Figure 3-4: Average gold nanoparticles diameter as a function of generation dextrin concentration (adapted and modified from Anderson *et al.*, 2011).

The linear relation between dextrin concentration and particle diameter implies a direct relationship between reaction conditions and size. Observation of the time for the initial red color to form suggests that the dextrin is also responsible for the reduction of the gold chloride. The normal reaction progression is for the yellow gold chloride solution to change to a clear or grey tinted solution prior to particle formation. This same transition occurs when the sodium carbonate is used for pH adjustment. The time for red color to form decreased as the dextrin concentration was increased. Particle formation was observed between 5 and 6 hours for 2.5 g/L and between 1 and 2 hours for 20 g/L dextrin generation conditions.

The generation of ground state gold atoms for nanoparticles production requires a reducing agent. Citrate generated particles use citric acid as the reducing agent at acidic pH values, and recent reports have used a sodium hydroxide pH adjustment and polyvinylpyrrolidone for gold ion reduction [90]. The use of dextrin synthesis conditions was explored between the pH range of 3 and 11 at 10 g/L dextrin concentration, 50°C, and 2 mM gold chloride. Control reactions using sodium hydroxide for pH adjustment, lack of dextrin or lack of gold chloride did not form gold nanoparticles with the common red color. The use of sodium hydroxide for particle formation yielded a dark purple precipitate that was visible to the human eye. These large purple particles that formed were unstable and caused ground state metallic gold deposition on the glassware at the air-liquid interface. Upon 24 hours of generation gold nanoparticles were generated from 7.0 nm ± 1.2 nm to 16.8 nm ± 2.3 nm in diameter. In Figure 3-5 the effect on size resulting from pH and dextrin concentration variation is shown.

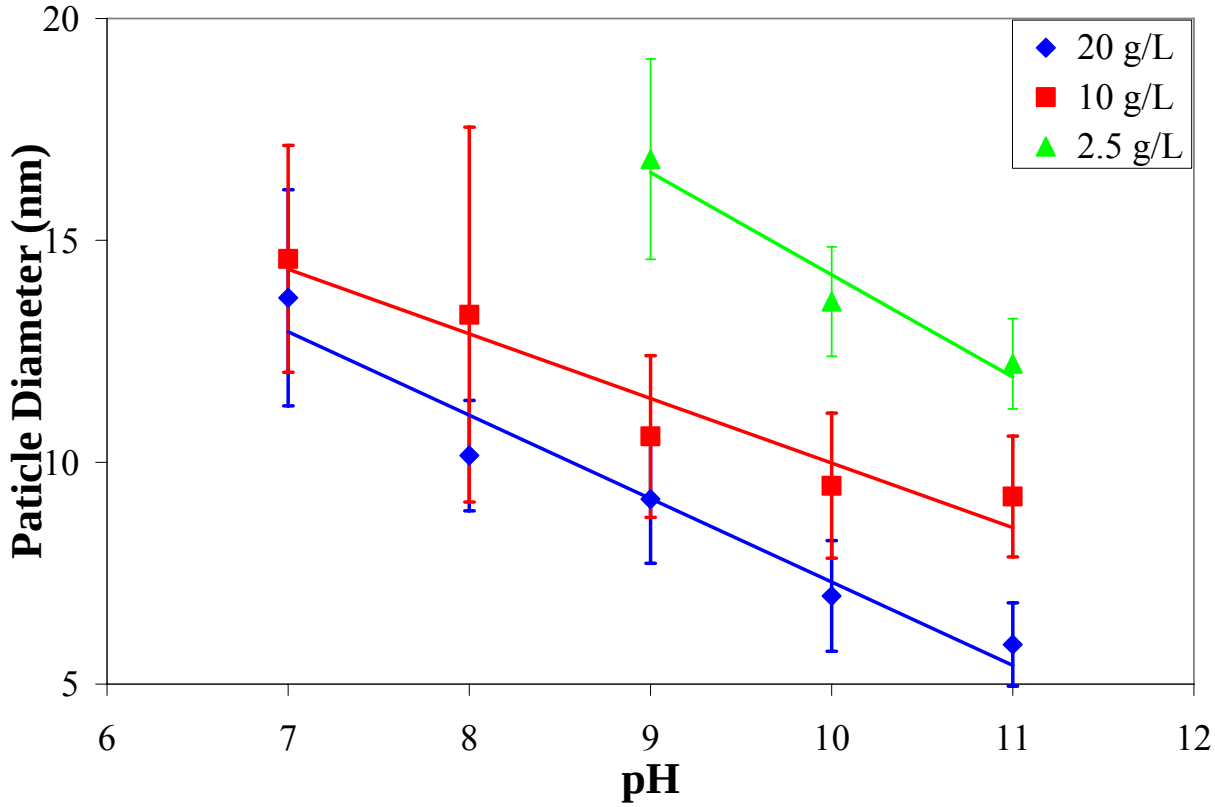

Figure 3-5: Average gold nanoparticle diameter as a function of generation pH, ranging from pH 7.0 – 11.0 (adapted and modified from Anderson *et al.*, 2011).

Successful generation of particle using dextrin was accomplished between the pH range of 7.0 and 11.0. Reaction times were reduced with increasing pH from 1 minute at pH 11 to 24 hours at pH 7.0.

Traditional citrate generated particles are produced at near boiling or boiling temperatures. The effects of generation temperature on the particle size were also explored. Lower generation temperatures required reduced energy input making the particle synthesis less expensive and

more environmentally friendly. Figure 3-6 shows the effects of temperature on the mean particle size generated as a function of dextrin concentration.

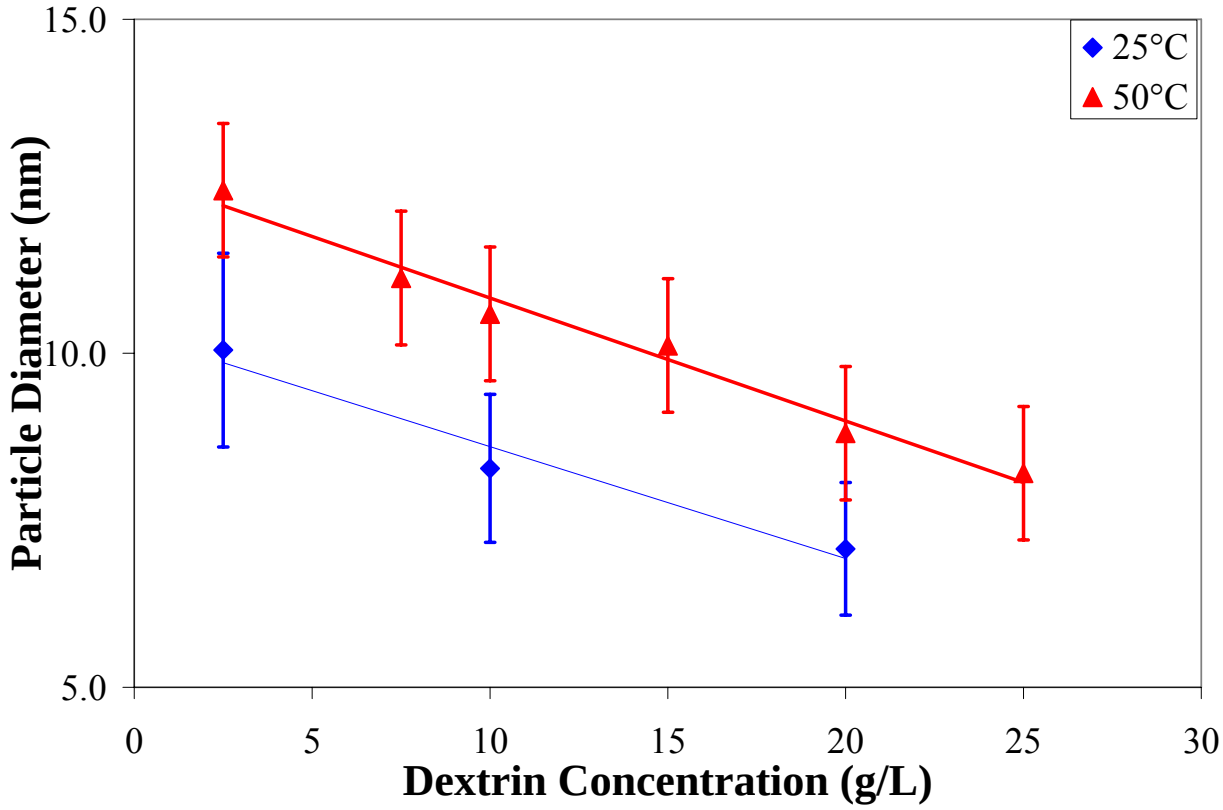

Figure 3-6: Average gold nanoparticles size as a product of generation temperature and dextrin concentration (adapted and modified from Anderson *et al.*, 2011).

3.3.3 Reaction mechanism

Gold particles were successfully generated over a large range of dextrin concentration, pH, and temperature. The effects of the various parameters on the generated particle size can be explained using the basic generation model. The paradigm is a four step generation modeled on

citrate particles and appears to be valid in the dextrin system [98]. The gold chloride is first reduced, then stabilized, a slow growth phase followed by a fast growth phase. The initial reduction is achieved upon the sodium carbonate pH adjustment. This is observed visually as the solution turns from yellow (Au(III)) to a dark tinted solution (smoke grey). This grey color persists and slowly turns darker with a purple tint, were ground state gold atoms are being stabilized into individual particles. The particles begin the slow growth and the solution beings turning a red tint. The fast growth phase usually last approximately 30 - 120 minutes (50°C) and the solution develops the characteristic deep red color of 5-50 nm gold nanoparticles. The UV-Vis absorbance of the reaction was monitored with time and the 520 nm absorbance peak was plotted in Figure 3-7.

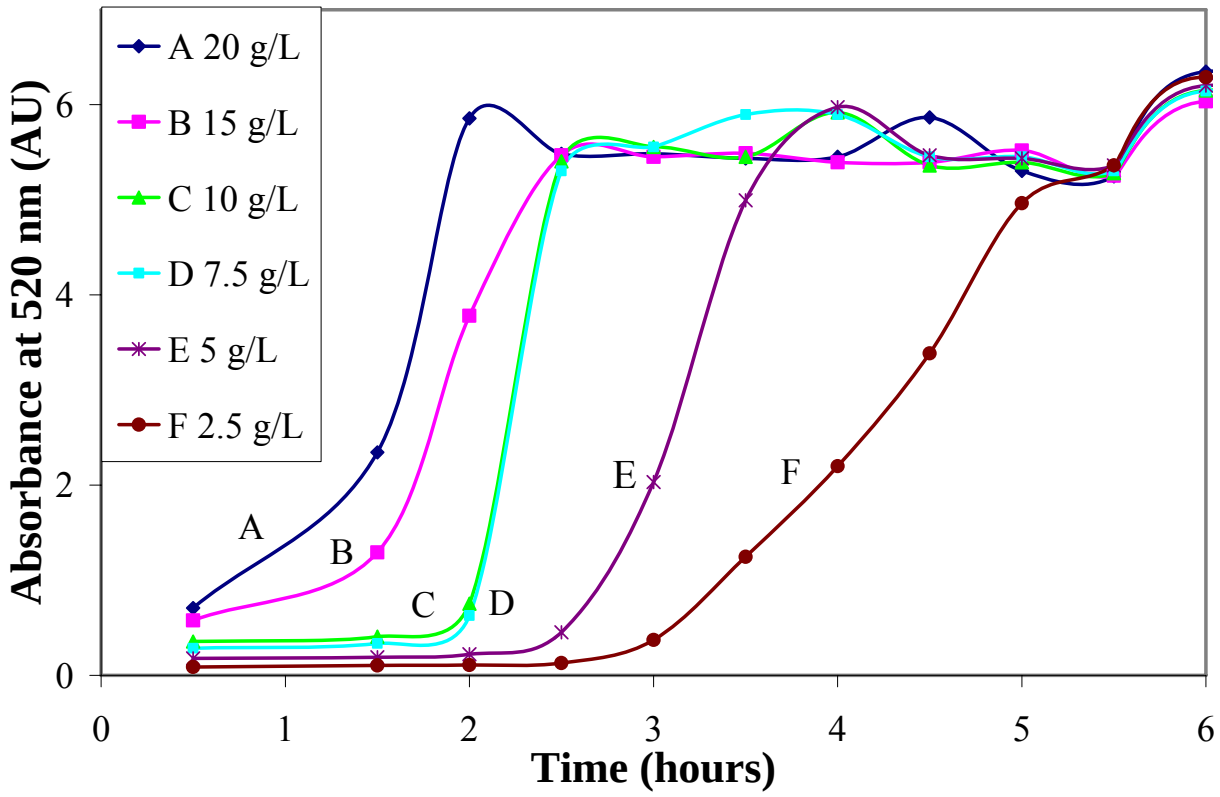

Figure 3-7: UV-Vis monitoring of reaction completion.

From Figure 3-7, a rapid increase in absorbance is seen after an initial lag phase. The absorbance at 520 nm is used to measure article concentration. From the absorbance data, an ideal curve is pictured in Figure 3-8 labeled with the proposed phases of growth. These conditions are the same as line C from Figure 3-7.

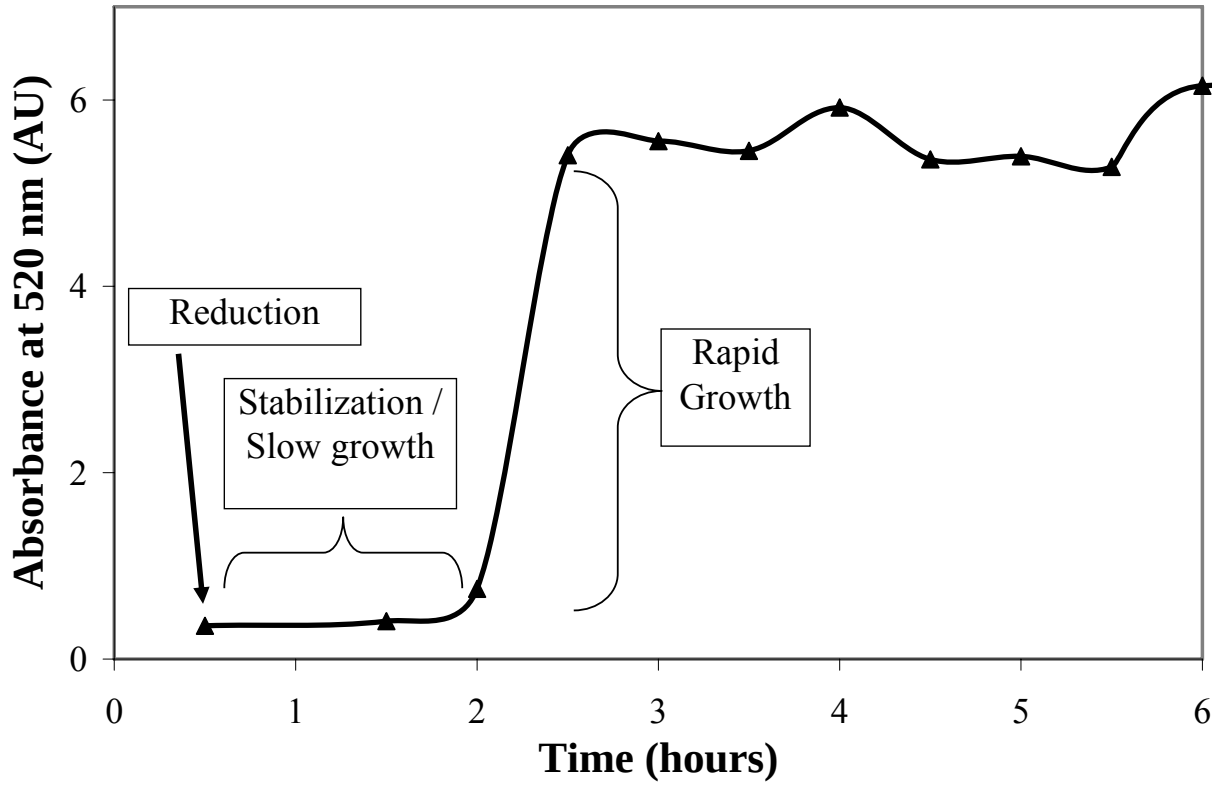

Figure 3-8: UV-Vis monitoring of proposed reaction mechanism.

The rapid growth phase shown is Figure 3-8 is the most apparent stage. During the stabilization and slow growth, a color change is observed visually (Figure 3-2, 1hr), but not seen in the UV-Vis data. The time at which rapid growth begins varies with temperature, pH, and dextrin concentration. It was observed that higher amount of dextrin, higher pH and higher temperatures shortened the time from the beginning of the reaction to when the rapid change in color occurred. These observations agree with conventional particle generation theory.

Particle size is a combination of available capping agent, or stabilization agent, and reaction rate. Using a higher ratio capping agent to gold concentration provides a greater surface area of gold

that can be stabilized, which allows generation of smaller particles. The higher capping agent concentration also helps maintain the stability of the particles, by providing free capping agent in solution to replace any molecules that disassociate from the particle surface. Faster reaction rates create smaller particles by promoting more nucleation points. As the reaction rapidly proceeds, all the available reactant, gold chloride, is consumed and a larger number of small particles are formed. Smaller particles are generated with increasing pH. It is thought the higher pH creates a more reactive dextrin molecule by promoting the opening of the terminal glucose molecule into an aldehyde in the presence of sodium carbonate. This aldehyde group is thought to be the reducing agent for the gold chloride. When the reaction temperature is increased, the rate of reaction increases, but the particle size increases. This is contrary to the rate of reaction theory proposed above. The increased temperature allows for the capping agent to disassociate/associate more rapidly on the forming particles. The rapid exchange of capping agent may occur rapidly enough to prevent the fusing of two free gold particle surfaces. This could explain why increasing temperature also increased particle diameter.

The system used for alkaline generation utilizes sodium carbonate, dextrin, and gold chloride. Determination by reactant substitution was conducted to help determine what components were participating in the reaction. When the pH was adjusted with either sodium carbonate or hydrochloric acid (HCl), the same grey tint formed in the gold chloride solution. Without dextrin, the sodium carbonate reaction maintained the tint for 24-48 hours upon metallic gold deposition on the gas/liquid interface. Without dextrin present, the HCl adjusted reaction proceeded to precipitate into purple aggregates visible with the human eye. Previous work suggests that standard citrate reactions reduce their reaction rates as pH increases by formation of

more stable and less reactive gold-hydroxyl species [98]. As the pH increases, the initial gold chloride ion exchanges chlorides ions for hydroxyl ions. As the pH increases the gold ion goes through the following species: $[AuCl_4]^-$, $[AuCl_3OH]^-$, $[AuCl_2OH_2]^-$, $[AuClOH_3]^-$, to $[AuOH_4]^-$. As the pH increases, equilibrium in the carbonate-bicarbonate-carbonic acid systems shifts to favor the carbonate species. Carbonate has pKa values of 6.33 and 10.35 for the range of pH being used. The balance of carbonate/bi-carbonate between pH 6.33 and 11 has similar trending in the same fashion as the reaction rate data show. The dextrin/carbonate system does not produce particles below pH 7.0 while producing AuNPs within minutes at pH 11.0. The combination of carbonate and alkaline pH are both required for synthesis. The presence of dextrin in the system is required for stable particle formation. When dextrin is removed from the system, a purple precipitate forms after 24-48 hours of synthesis time.

To determine the capping agent, FTIR readings were conducted on successfully generated particles at 10 g/L dextrin, pH 9.0, 50°C and 2mM gold chloride. A volume of 1 mL of generated particles was washed 3 times in water to remove excess reactants and pH adjusted with 50 µL of 0.1 M sodium hydroxide. The change in pH resulted in precipitate formation after 2 hours. Samples were centrifuged to remove the metallic AuNP cores. The supernatant was compared to stock dextrin and autoclaved dextrin samples. Figure 3-8 shows the FTIR data.

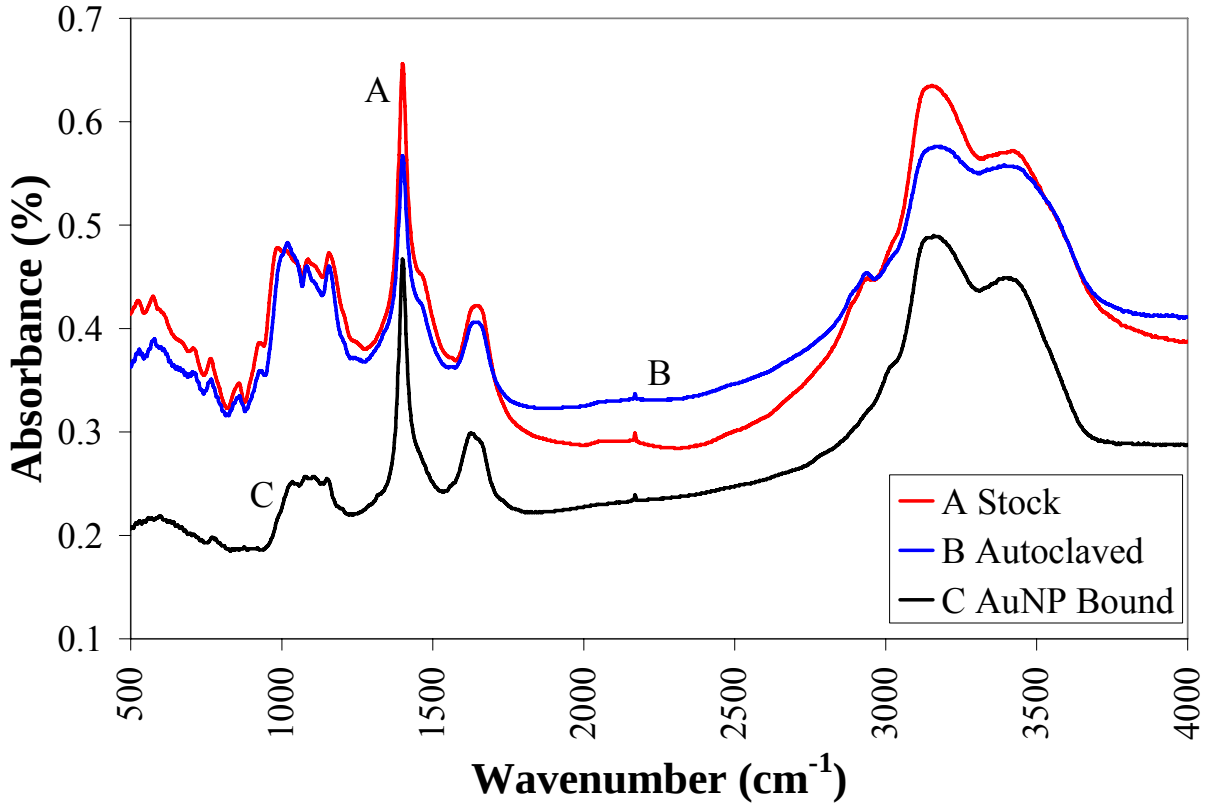

Figure 3-9: FTIR of capping agent. (a) Stock dextrin; (b) Pre-synthesis reactant; and (c) Freed capping dextrin (adapted and modified from Anderson *et al.*, 2011).

From Figure 3-9, the recovered dextrin from the generated particles had the same absorbance pattern as both the starting samples. Dextrin that has undergone a ring opening would be expected to have a carboxylic acid signature at 1714 cm^{-1}, 1414 cm^{-1}, or 1294 cm^{-1} wavenumber. The lack of the carboxylic group suggests the dextrin that is protecting the AuNP core is unreacted. A lack of reacted dextrin on the AuNP surface does not remove dextrin as a reduction agent for the gold chloride. Dextrin is a linear polysaccharide of glucose molecules connected via alpha(1-4) and alpha(1-6) bonding. The monosaccharide glucose, a reducing sugar, was used to generate AuNPs at 10 g/L. The synthesis was more rapid than the dextrin

reaction resulting in large purple precipitate. During the generation, the desired red color was seen briefly, but it was not possible to stabilize the reaction at that stage. When dextrin and glucose were mixed together (10 g/L dextrin, 5 g/L glucose) the reaction proceeded at a rate between pure dextrin and pure glucose. The resulting particles generated were stable for approximately 14 days, with significant precipitation beginning after 24 hours. The combination of the different sugars suggests that the dextrin is a reactive species in AuNP formation.

The exact mechanism of AuNP was not empirically determined. From the data, stable gold nanoparticle generation requires pH > 7.0, sodium carbonate, gold chloride and dextrin. Gold nanoparticles formation may be accomplished by aldose / ketose reduction of gold chloride. The degree of sugar ring opening may be increased by increased pH and carbonate concentration. The higher pH may also stabilize the gold chloride for a slow and even particle growth. This system of gold nanoparticles generation consistently produces uniform particles with controllable size based on the generation conditions.

3.3.4 Gold nanoparticle functionalization

Common methodologies for utilizing gold nanoparticles involve replacing the capping agent for a functional group or other recognition molecule. The process of ligand exchange involves disassociation of the capping agent, such as dextrin or citrate, and the more permanent attachment of the molecule of interest [11]. Thiols are most commonly used for attachment chemistry to gold surfaces. Gold nanoparticles generated at 2.5 g/L and 10.0 g/L (12.4 nm and 10.4 nm respectively) were functionalized with 6-FAM labeled, thiol linked DNA. Both sizes of

particles were successfully functionalized, Figure 3-9 shows exchange efficiency compared to citrate generated particles.

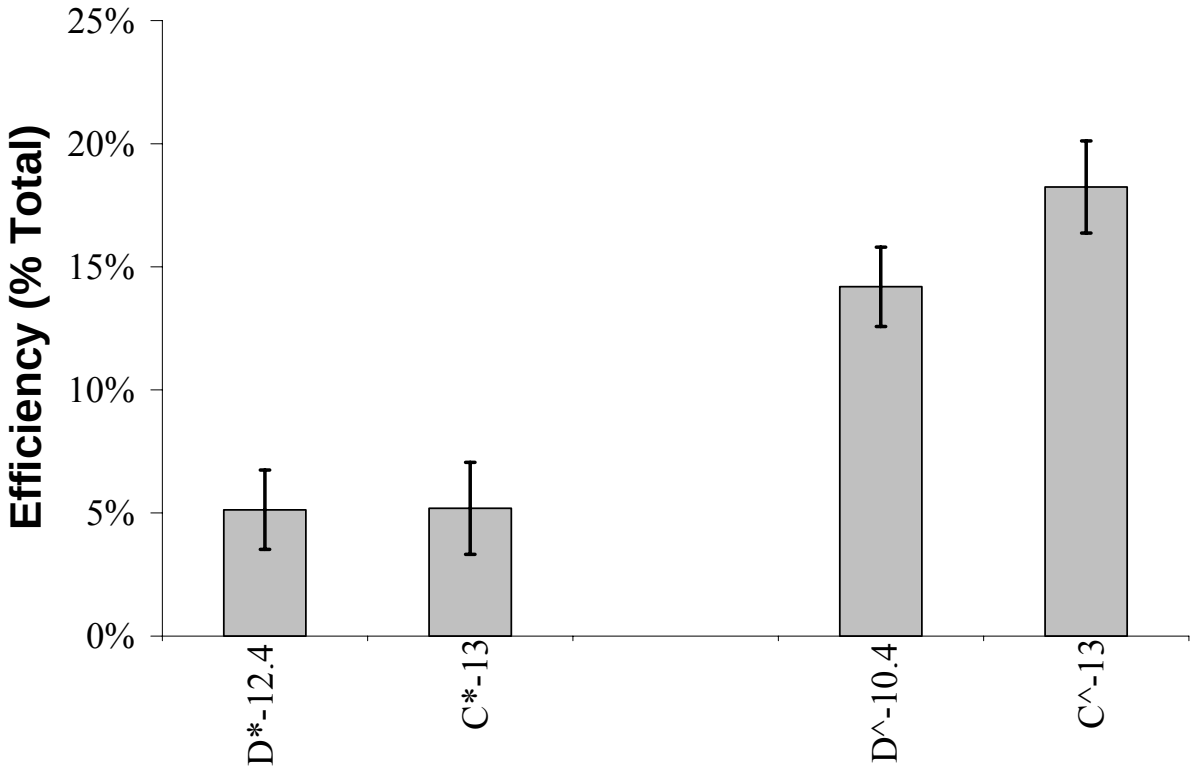

Figure 3-10: Comparison of dextrin and citrate generated gold nanoparticles for ligand exchange compatibility. D=dextrin generated; C=citrate generated; 12.4, 13, and 10.4 represent AuNP diameter used (adapted and modified from Anderson *et al.*, 2011).

Efficiency is reported in Figure 3-10 as the ratio of the amount of DTT liberated FAM-DNA verses the total DNA used in the functionalization reaction. From Figure 3-10, the left grouping of data, D*-12.4 nm and C*-13 nm, have the same efficiency. The right grouping, D^-10.4 and C^-13, show a lower efficiency for the dextrin particles. The smaller 10.4 nm diameter dextrin

AuNP have ~69% of the available surface area for DNA-capture compared to a 13 nm diameter particle. With surface area taken into account, the 77% signal seen from the smaller particles showed comparable DNA capture to the larger 13 nm diameter citrate particles. Dextrin generated gold nanoparticles were equivalent to citrate generated particles for use in assays after ligand exchange.

3.4 Conclusions

Dextrin coated gold nanoparticles were successfully generated with sizes ranging from 5.9 and 16.8 nm ± 1.6 nm. Particle size was controllable by varying generation pH, dextrin concentration, and reaction temperature. The produced AuNP were stable for 6 months when stored at room temperature in the generation media. The particles were successfully functionalized with DNA capping agents and used for the sandwich assay in Chapter 5.

This chapter is adapted from our recently published work in IEEE Transactions on Nanotechnology:

Anderson, J. Michael; Zhang, Deng; and Alocilja, C. Evangelyn. Spectral and Electrical Nanoparticle-Based Molecular Detection of *Bacillus Anthracis* Using Co-polymer Mass Amplification. Journal of Nanoparticle Research. 2011. 10(1):44-49.

DOI: 10.1109/TNANO.2010.2061235

Chapter 4: Spectral co-polymerization mass amplification detection of *Bacillus anthracis* Stern using sandwich assay identification

4.1 Introduction

Fluorescent methods of DNA reporting commonly rely on hybridization events with a separation step. Hybridization is not a rapid process as it is driven by the concentration of products and the DNA sequence being targeted [99]. The bio-barcode assay uses DNA specificity to achieve proper sequence recognition, and the use of magnetic particles provides a simple separation scheme [18]. The use of a second hybridization event and gold nanoparticles provides a vehicle for a 100 times amplification of target signal via small single-stranded DNA (ssDNA) reporter molecules (bio-barcodes) [100]. The signal from the bio-barcodes comes from a fluorescent label on the DNA strand, and for more sensitive detection two additional rounds of hybridization are required, with silver enhancement and laboratory specific detection hardware [101]. Simplification of the detection signal from the assay has been accomplished by electrochemical detection of the gold nanoparticles [102]. An alternative fluorescent method using self-assembling small ssDNA molecules has been developed [13]. The detection method utilizes a released co-polymerization partner from the gold nanoparticles and dye that have 1000 times increase in signal when bound to the double-strand DNA (dsDNA) formed from co-polymerization between the released gold nanoparticles DNA and a second probe DNA. Other enzyme free hybridization schemes have been explored, but amplification is limited, they possess high time requirements, or have long assay times [58, 60, 62, 63]. The method presented is enzyme free, provides amplification and detection requires under 25 minutes.

4.2 Materials and methods

The DNA dyes SYBR Gold (S11494), PicoGreen (P7581), and SYBR 101 (S21500) and a 100 bp DNA ladder (15628-019) were obtained and used without purification from Invitrogen Life Technologies. Single-stranded DNA sequences (oligonucleotides) and 6-carboxyflurescein (6-FAM or FAM) labeled ssDNA was purchased from Integrated DNA Technologies. Preparation and recovery of thiol-linked DNA was accomplished with 1,4-dithio-DL-threitol (DTT, D5545) obtained from Sigma-Aldrich. Attachment of amine labeled DNA to magnetic particles was conducted using sulfosuccinimidyl 4-N-maleimidomethyl cyclohexane-1-carboxylate (sulfo-SMCC, 22122) from Pierce-Thermo Scientific. Gold nanoparticles were synthesized using hydrogen tetrochloroaurate (III) trihydrate (203386) and sodium citrate dehydrate (W302600) from Sigma-Aldrich. Quantum dots (QDs, 7.2 nm evidot 490) suspended in toluene were obtained from Evident Technologies and functionalized with aminoethanethiol (AET, AC15377-0259) from Fisher Scientific.

4.2.1 DNA target generation

The *pagA* gene was the target of the sandwich assay. A culture of *Bacillus anthraci*s Sterne (*Bacillus*) was refreshed and cultured over night in trypticase soy broth. A volume of 1 mL of culture was digested with proteinase K for 75 minutes at 50°C. The resulting lysate was purified using ethanol precipitation. The samples were suspended to 75% isopropanol / 25% lysate and centrifuged for 30 minutes at 4°C, then decanted and the process repeated with 100% ethanol and then 70% ethanol. Final resuspension was in double distilled 18 MΩ water. The recovered genomic DNA was then amplified by polymerase chain reaction (PCR) to create 119 base pair (bp) sequence for use in the sandwich assay. Table 4-1 listed the reaction conditions.

Amplification reactions were purified using a DNA binding column (Qiagen MinElute PCR Purification Kit, 28004).

Table 4-1. Probe sequences generated for *pagA* gene in *Bacillus anthracis* Sterne.

Sequence Name	Sequence	Amplicon Size
Bac-FWD-Primer	5´ AAA ATG GAA GAG TGA GGG TG 3´	119 bp
Bac-REV-Primer	5´ CCG CCT TTC TAC CAG ATT TA 3'	

DNA concentration was determined using a UV absorbance spectrophotometer (SmartSpec 3000, BioRad Laboratories), and the length of the purified sample was confirmed in a 2% w/v agarose gel by electrophoresis in Figure 4-1.

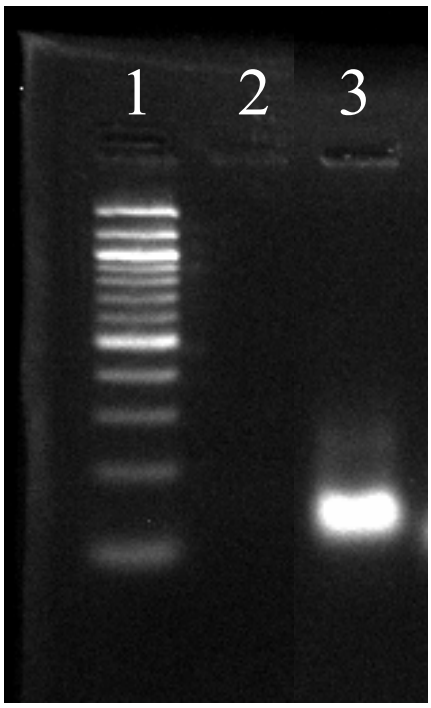

Figure 4-1: PCR of *Bacillus anthracis* DNA for the *pagA* gene. Lane 1: 500 µg of 100 bp ladder. Lane 2: blank. Lane 3: PCR product using primer in Table 4-1.

Upon size confirmation and purification from Figure 4-1, the PCR product was serially diluted and then heated to 95°C for 10 minutes to denature the amplified DNA to ssDNA. Next, the hot DNA was rapidly cooled in an isopropanol bath (-20°C) to create single-stranded product as input for the sandwich assay.

4.2.2 Sandwich assay

4.2.2.1 Magnetic microparticle functionalization

The amine functionalized magnetic microparticles (MMP) (BM546, Bangs Laboratories, Inc.) were conjugated to the 5' end of the MMP-Bac-Probe via sulfo-SMCC shown in Figure 4-2 and listed in Table 4-2. SMCC is a thiol to amine bifunctional cross-linking agent that introduces a 0.83 nm spacer arm. The MMPs were washed 3x times in buffer (0.1 M phosphate, 0.3 M sodium chloride, pH 7.2) and 1 mg of MMP were resuspended in 1 mL in the same buffer. Sulfo-SMCC (0.3 g) was added to the MMP and allowed to react for 2 hours. The MMP-SMCC particles were washed to remove excess sulfo-SMCC and released N-hydroxysulfosuccinimide (sulfo-NHS) and the MMP-Bac-Probe was added and allowed to react for 8 hours. The thiolated DNA probes were activated by reduction in 0.1 M DTT under constant agitation at room temperature for 2 hours. Excess and reacted DTT was removed from the DNA reduction reaction using a Sephadex filtration column (GE Healthcare #Nap-5) per manufacturer instructions. Upon reaction, the MMP-DNA solution was washed three times and resuspended in blocking buffer (0.2 M Tris, pH 8.5) for 1 hour. The MMP-DNA particles were washed again and stored in reduced strength buffer (0.01 M phosphate, 0.2 M sodium chloride, pH 7.4) prior to use.

Table 4-2. Thiol functionalized species of DNA for particle decoration.

Sequence Name	Sequence
MMP Probe	5´-SH-AAA AAA AAA AGGA AGA GTG AGG GTG GAT ACA GGC T-3´
AuNP Probe	5´ AGA TTT AAA TCT GGT AGA AAG GCG GAA AAA AAA AA - Thiol 3'
AuNP-6FAM	5' 6FAM - ATC AGT CAG TCA GTC AGT CA - Thiol 3'
AuNP-AB	5' Thiol - TTA TTC GTA GCG TGA TGC CAA G 3'

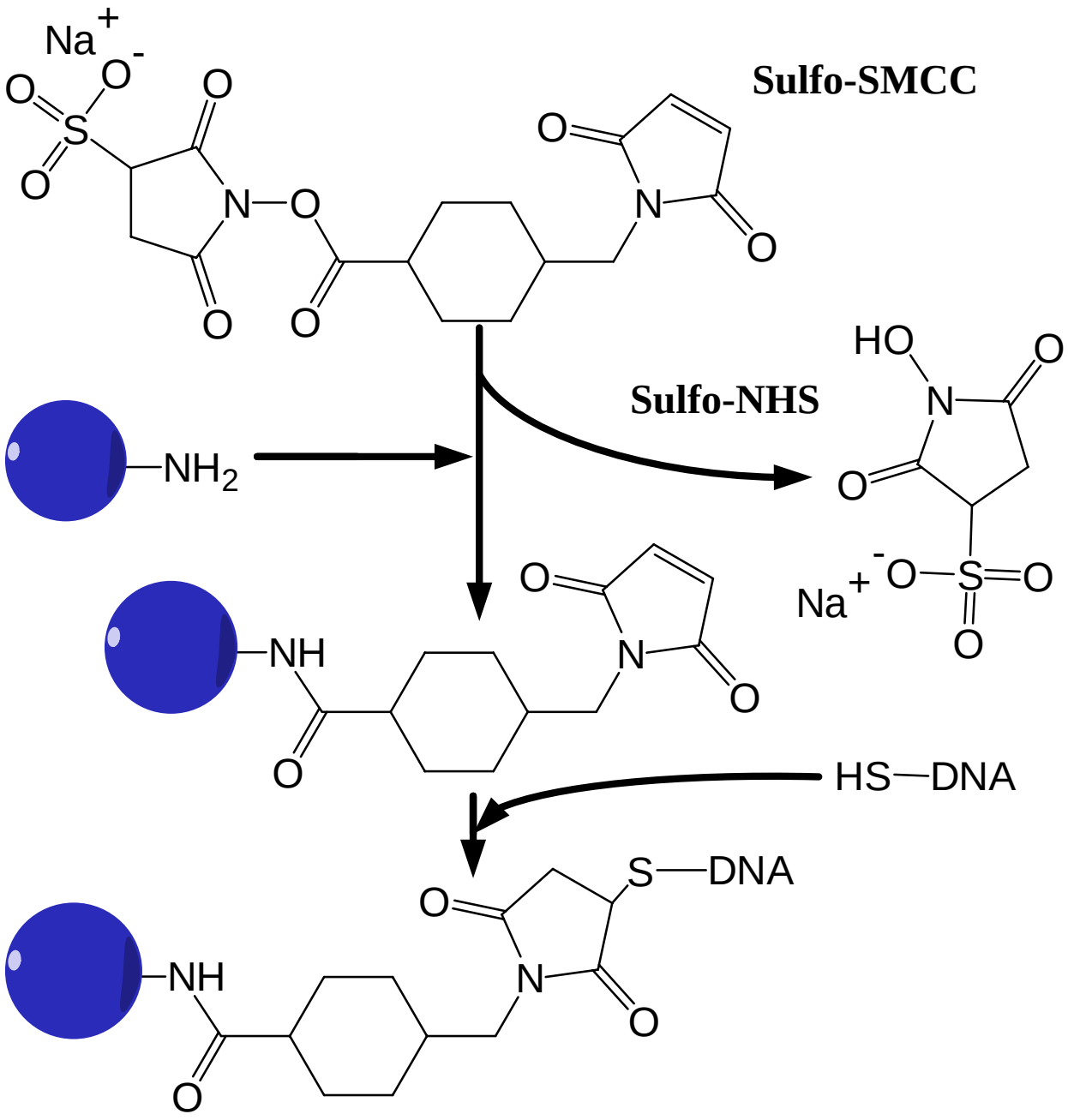

Figure 4-2: SMCC labeling of the MMP with DNA. The amine labeled microparticle attaches to the cross-linker sulfo-SMCC, releasing sulfo-NHS. The reactive microparticle then bonds to the sulfhydryl group on the DNA.

4.2.2.2 Gold nanoparticles generation and functionaliztion

Citrate generated gold nanoparticles were synthesized using a modified protocol from standard citrate generate AuNPs [11]. A 50 mL solution of hydrogen tetrochloroaurate (III) trihydrate (1 mM) was heated on a hotplate in a clean 125 mL Erlenmeyer flask until boiling. A volume of 5 mL of sodium citrate (38.8 mM) was added slowly in a dropwise fashion to the gold chloride stirring constantly. Upon development of the characteristic wine red color, the solution was taken off the hot plate and allowed to cool on the bench top. After cooling, the gold nanoparticles (AuNP) were stored in a 50 mL polypropylene centrifuge tube, protected from light at room temperature. Particles were previously characterized using this generation technique and successfully used in a biosensor [103].

The gold nanoparticles were functionalized with 0.05 nmol of AuNP-Bas-Probe and 5 nmol of co-polymerization probe (Table 4-2) via ligand exchange [11]. Briefly, a reactive thiol bonds to a free location on the gold surface after a weakly bound citrate molecule disassociates. The thiol bond is sufficiently stronger than the electrostatic bonding of the citrate molecule and forms a semi-permanent surface bond. Thiolated DNA was activated in the same manner as described in section 4.2.2.1. The reduced and reactive DNA was mixed with 1 mL of washed gold nanoparticles at 4 nM (1nM: 1 absorbance unit (AU) at 520 nm) in 18 MΩ water. Salt additions were added over a 48 hour period to facilitate close packing of the DNA oligonucleotides on the gold nanoparticles surface [15]. Particles were stored in the reaction solution for a maximum of 30 days on the bench top until use.

4.2.2.3 Target capture

The DNA input for the assay was prepared as described in section 4.2.1. The desired mass of DNA was volume adjusted to 40 µL and mixed with 0.08 mg of probe functionalized DNA microparticles and adjusted to a final volume of 200 µL using assay buffer (150 mM sodium chloride, 10 mM phosphate, 0.1% sodium dodecyl sulfate, and pH 7.4). The samples were inversion mixed at 45°C for 60 minutes. Upon hybridization, magnetic separation was used to wash the unbound DNA from the particles and resuspended to 200 µL of assay buffer containing 40 µL of the desired functionalized gold nanoparticles (1 nM). The MMPs-DNA and AuNPs were allowed to incubate and hybridize for 2 hours at 45°C under inversion mixing. The reactions were magnetically separated and washed twice to obtain the final MMP-target-AuNP sandwiches. The recovered sandwich structures were resuspended in 200 µL of 0.1 M DTT and heated to 95°C for 10 minutes, and centrifuged at 13,000 x g for 30 minutes to pellet the now free MMP and AuNPs. The supernatant containing the DNA was then used for detection.

4.2.3 Co-polymerization sequence design

Co-polymerization is defined as the process of having 2 or more ssDNA oligonucleotides partially hybridize with a second strand leaving a portion of sequence for additional hybridization events. By engineering overlapping sections that were complimentary to each other, two co-polymerization probes were generated that upon hybridization formed long dsDNA species with repeating subunits. The two probe system was designed as shown in Figure 4-3 [13].

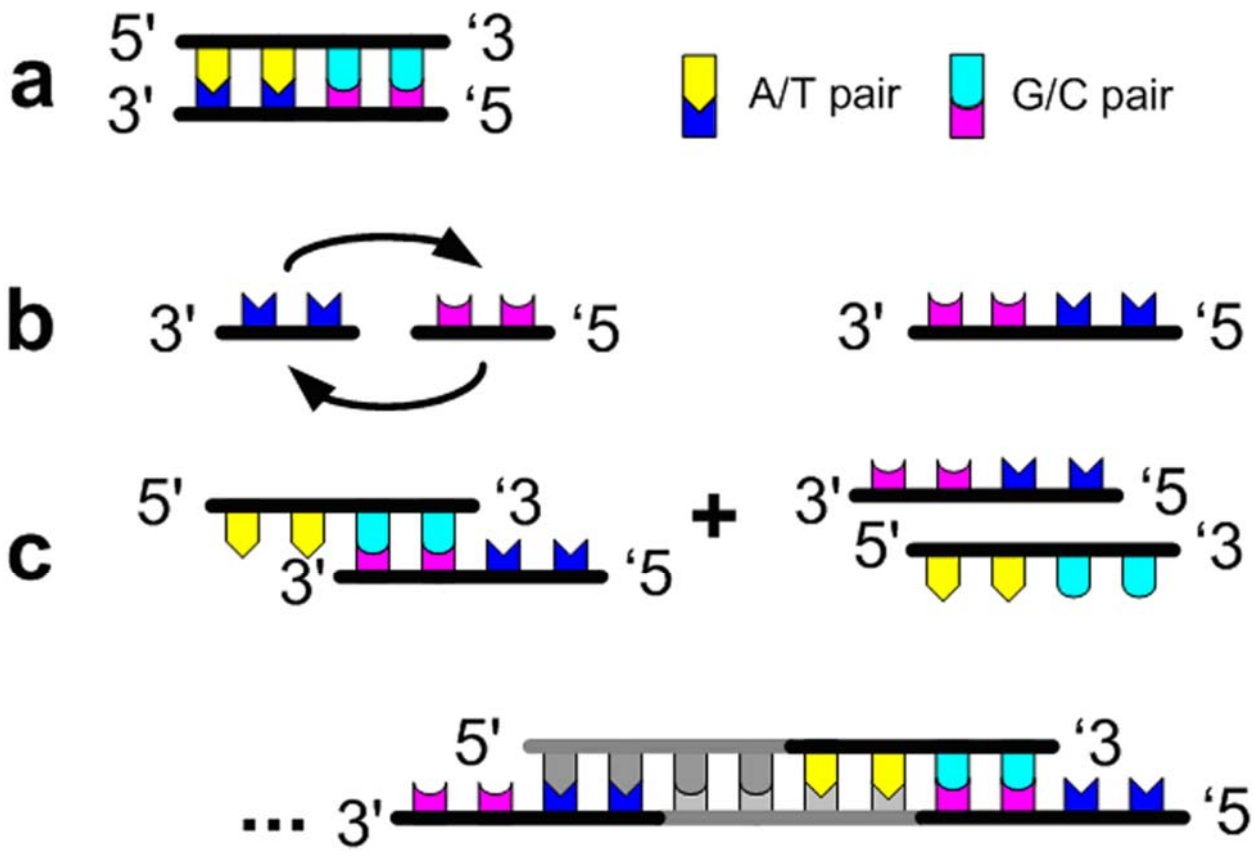

Figure 4-3: Cartoon representation of co-polymerization. (a) Initial dsDNA region; (b) Rearrangement of lower strand to created second co-polymerization partner; (c) possible initial hybridization and subsequent hybridization events (adapted and modified from Anderson, Zhang, and Alocilja, 2011).

A perfectly aligned 22 base pair (bp) DNA sequence was divided into two 11 base regions. One stand of the dsDNA molecule remained unchanged. The second strand has a translation of the bases. Bases 1-11 are moved into the 12-22 base position maintaining 5'-3' order. When one of each strand hybridizes, two different molecules can form. When sufficient quantity of both

strands is present a total of 4 different end groups can form as a result of the 5'-3' directionality of DNA, shown in Figure 4-4.

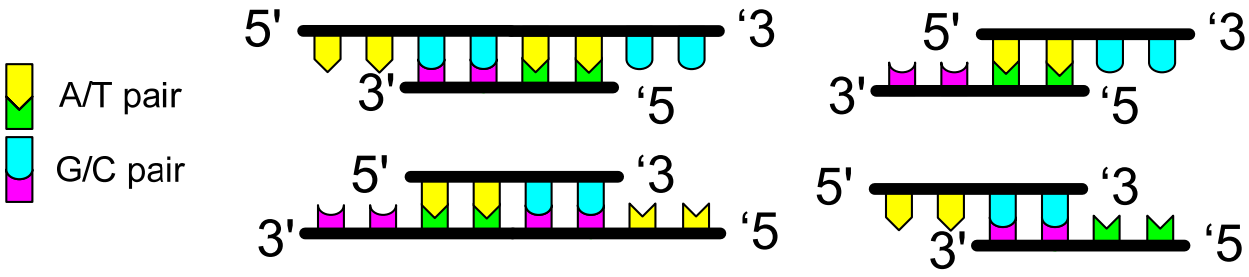

Figure 4-4: Possible terminal end configuration based on the two part co-polymerization (adapted and modified from Anderson, Zhang, and Alocilja, 2011).

The two strands of DNA generated were tested and designed to prevent self-hair pinning and improper self hybridization. Sequences were tested with the OligoAnalyzer (Integrated DNA Technologies, http://www.idtdna.com/analyzer/Applications/OligoAnalyzer/) and MFOLD (http://www.idtdna.com/analyzer/Applications/OligoAnalyzer/).

4.2.4 Co-polymerization detection

Sensitivity of the co-polymerization readout was accomplished using fluorescent detection with PicoGreen DNA dye. The gold nanoparticles linked with the DNA species AuNP-AB were tested from 0.1 ng to 100 ng against the hybridization probe (BA, Table 4-3) of 5 ng – 100 ng per 100 µL in hybridization buffer (10x PicoGreen, 10 mM Tris, 100 mM sodium chloride, 1 mM ethylenediaminetetraacetic acid, pH 8). Hybridization samples were mixes and heated to 95°C in a thermal cycler block for 3 minutes and allowed to cool to room temperature in the block. After cooling, the 100 µL volume was measured in a plate based spectrophotometer (Victor 1420,

Perkin Elmer) with an excitation filter of 492 nm ± 4 nm and emission filter of 535 nm ± 12.5 nm.

All samples that were visualized using electrophoretic separation for detection were run in 2% w/v agarose gels. Samples were separated using tric-boric-ethylenediaminetetraacetic acid (TBE) buffer at 1x and run at 30 V for 2 hours. Images were excited at 254 nm and emission was detected using a 540 nm long pass cut off ethidium bromide filter (Fotodyne 60-2030).

4.2.5 Quantum dot attachment

Cadmium/zinc core/shell quantum dots were purchased from Evident Technologies. The QDs were stabilized with trioctylphosphine oxide (TOPO) in toluene by the manufacturer. Before being conjugated to the SYBR101 dye, the QDs were functionalized with AET to provide a reactive amine group with water solubility. A quantity of 5 nanomoles of quantum dots was suspended in 5 mL of chloroform. Aminoethanethiol (0.5 M) in absolute ethanol was added to the QD/chloroform solution drop wise until flocculation began. The solution was flushed with nitrogen to purge oxygen and vortexed for 10 minutes. Then 0.5 mL of 18 MΩ water was added and the tube was reflushed with nitrogen. The sample was then vortexed again for 10 minutes to promote a phase change from the chloroform to water as the QDs were functionalized with AET. The solution was allowed to separate on the bench top for 30 minutes into an upper water layer containing AET-capped QDs and a lower chloroform phase. Capping was confirmed visually by observing yellow coloration of the water phase being that was confirmed by excitation with a 254 nm light source because under 254 nm excitation the QDs fluoresce. Before AET capping,

the chloroform phase fluoresces and post capping only the aqueous phase fluoresces thereby confirming AET functionalization.

Quantum dots were attached to the amine reactive dye SYBR 101. SYBR 101 is a double-strand intercalating dye with a succinimidyl ester group which reacts with primary amines. The SYBR 101 was resuspended in dimethyl sulfoxide (DMSO) to 10 mg/mL. A volume of 10 μL of the SYBR 101 dye was added to the 0.5 mL of AET water solubilized QDs and 0.5 mL reaction buffer (0.2 M phosphate, 0.3 M sodium chloride, pH 7.2) and mixed. After 2 hours of reaction, the SYBR 101 dye attached to the amine group on the QD's and was centrifuged to pellet the QD-SYBR particles. The pellet was resuspended in 500 μL of 0.1 M phosphate buffer. A volume of 10 μL of SYBR 101 (10 mg/mL, estimated molecular mass 550 g/mol, estimated 180 nmol / 10 μL) was reacted with 400 nmol of AET in a volume of 100 μL of the same buffer as the QD-SYBR reaction. This blocked the reactive ester of SYBR101 for use in DNA binding.

Electrochemical detection of the QDs was accomplished using a screen printed carbon electrode (SPCE). The SPCE was measured using a benchtop potentiostat (Princeton Applied Research, Potentiostat/galvanostat 263A). The fluorescence detection of the QD ions was accomplished using differential pulse voltammetry (DPV), with voltage sweeping from +1.5 to 0 V at 33.3 mV/s (step potential 10 mV and modulation amplitude of 50 mV). Samples were first dried onto the carbon electrode surface and then incubated for 5 minutes in 80 μL of 0.1 M hydrochloric acid. Within the SPCE/QD/hydrochloric acid electrochemical system, cadmium has a reduction/oxidation peak centered about -0.88 V.

4.3 Results and discussion

4.3.1 Co-polymerization sequences

The generated sequences are listed in Table 4-3. Results from MFOLD show an energy input is required for both sequences to form self base pairing structures. The sequence AB has a change in Gibbs free energy of +0.46 kcal/mol and BA has +1.07 kcal/mol as their most stable structures. This required input of free energy indicates an unstable or unfavorable confirmation. The sequences were then compared against each other using OligoAnalyzer for mispriming alone, and with the other strand present. Free energy was minimized for self priming of each sequence with AB and BA each having -3.61 kcal/mol. The most stable mis-priming between AB and BA has a free energy of -4.95 kcal/mol, where proper priming is approximately 5 times more stable with energies of -18.55 and -20.00 kcal/mol.

Table 4-3. Engineered co-polymerization ssDNA strands.

Sequence Name	Sequence
AB	5' TTA TTC GTA GCG TGA TGC CAA G 3'
BA	5’ GCT ACG AAT AAC TTG GCA TCA C 3’

4.3.2 Dye specificity

Determination of dye binding was accomplished by challenging each dye against ssDNA and dsDNA. Separation via electrophoresis removed excess or unbound dye leaving only the stained DNA to be visually imaged. Electrophoresis functions by applying a driving voltage to push

negatively charge materials though a polymer matrix. The ratio of charge to mass in a sample will determine how far it moves in a fixed amount of time at a fixed amount of driving voltage. DNA has a relatively constant charge per base value, giving the charge to mass ratio a constant value. This results in band movement in the agarose gel being a consistent measure of the size (length) for DNA.

The effects of three different DNA specific dyes were tested and the results are shown in Figure 4-5.

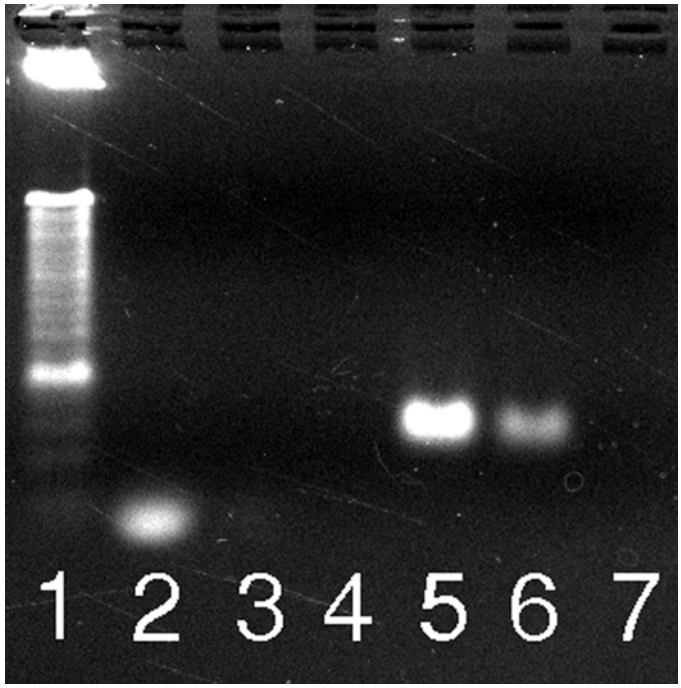

Figure 4-5: Agarose gel showing DNA dye testing. Lane 1: 1 μg of 100 bp ladder with SYBR Gold. Lanes 2-4 were run with 45 ng BA ssDNA. Lanes 5-7 were run with 15 ng of co-polymerized dsDNA. SYBR Gold, PicoGreen, and ethidium bromide were used to stain lanes 2 and 5, 3 and 6, and 4 and 7 respectfully per manufacture instructions (adapted and modified from Anderson, Zhang, and Alocilja, 2011).

All three dyes in Figure 4-5 [13] have excitation and emission spectra compatible with the UV excitation (SYBR Gold: 480 nm and UV-C excitation, 537 nm emission; SYBR 101 and PicoGreen: 480 nm and UV-C excitation, 520 nm emission; ethidium bromide: 302 nm excitation, 595 nm emission). PicoGreen dye binds to both ssDNA and dsDNA, but fluoresces much greater when bound to dsDNA. This makes PicoGreen a very good dsDNA dye reporter.

SYBR Gold also bonds to both ssDNA and dsDNA, but was designed to fluoresce strongly when bound to both. Lane 2 is stained with SYBR Gold and clearly showed the location of the ssDNA BA probe, lanes 3 and 4 do not show signal for the same DNA when using PicoGreen or ethidium bromide. Lanes 5-7 were run at a 2:1 ratio of BA:AB to ensure complete binding of the proposed AB reporter. SYBR Gold has the strongest signal in lane 5, as it will bind and cause fluorescence in both the dsDNA portion and the unhybridized ssDNA portion. Lane 6 showed a strong signal using PicoGreen and lane 7 showed no signal. The lack of signal in lane 7 resulted from being below the detection limit for ethidium bromide in the agarose gel.

When comparing lanes 2 and 3 to lane 5 and 6, it was seen that a third of the total DNA mass in lane 5 and 6 was significantly brighter than in lanes 2 and 3. The increased quantum yield (or efficiency) of SYBR Gold and PicoGreen upon binding to dsDNA was responsible. The lack of signal in lane 3, but strong signal in lane 6 confirmed that PicoGreen could be used as a dsDNA reporter for the co-polymerization detection.

Compatibility of the SYBR 101 dye system was tested with the co-polymerization product. The SYBR 101-QD and PicoGreen dyes were used to stain three AB:BA ratios, which are shown below in Figure 4-6.

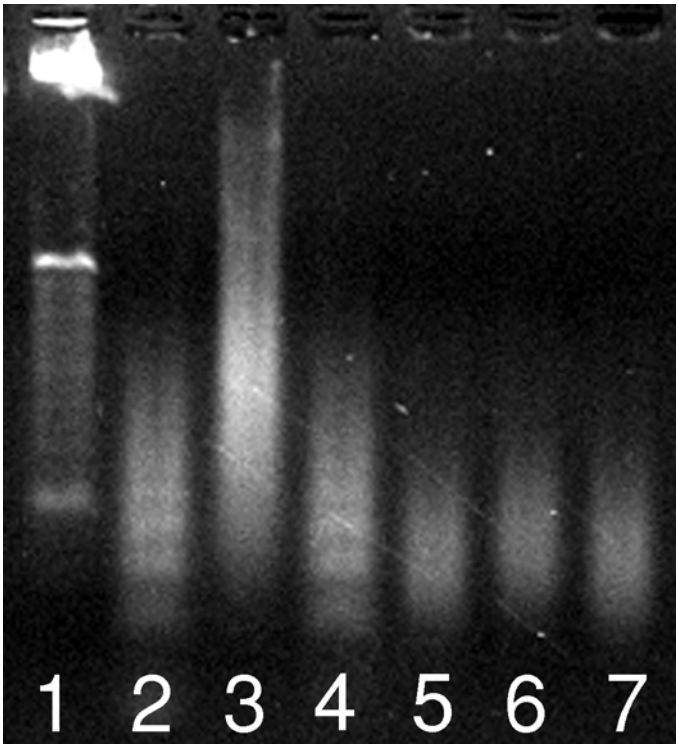

Figure 4-6: Gel electrophoresis of SYBR 101-QD dye specificity. Lane 1: 100 µg of 100 bp ladder. Lanes 2-4 and 5-6 are 450 ng of AB:BA at 10:1, 1:1, and 1:10 ratio respectively. Lane 1 stained with SYBR Gold, lanes 2-4 stained with PicoGreen and lanes 5-7 stained with SYBR101-QD (adapted and modified from Anderson, Zhang, and Alocilja, 2011).

In Figure 4-6 [13], lanes 2-4 show similar banding as in Figure 4-7 confirming successful hybridization co-polymerization. Lanes 5-7 show a less defined product in the same size region suggesting proper reaction and staining with SYBR 101-QD conjugated dye. The lack of signal higher up in the gel (larger fragments) may be the result of low sensitivity. As described in Figure 4-9 in section 4.3.5, the SYBR 101-QD particle has severely reduced fluorescence properties. The presence of banding in both dye types confirms compatibility of both dyes for dsDNA specific reactions and with the co-polymerization detection.

4.3.3 Hybridization banding

Characterization of the two part hybridization system was conducted by varying the ratio of AB to BA during hybridization. Each sample was run in an agarose gel and displayed in Figure 4-7 [13].

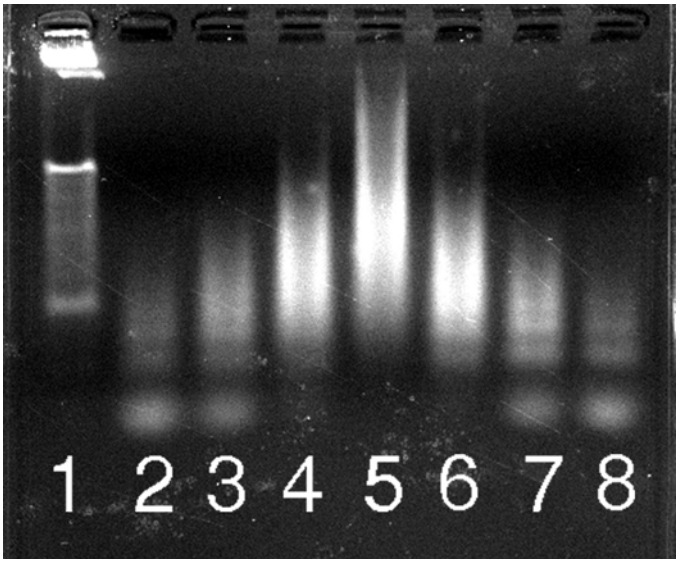

Figure 4-7: Optimization of co-polymer ratio. Lane 1: 1 μg of 100 bp ladder. Lanes 2-8 contain 150 ng of total DNA with 10:1, 5:1, 2:1, 1:1, 1:2, 1:5, and 1:10 ratio of AB:BA respectively stained with 1x of SYBR Gold (adapted and modified from Anderson, Zhang, and Alocilja, 2011).

SYBR Gold stain was used in order to determine where ssDNA and dsDNA were located. The lower bands in Figure 4-7, lanes 2, 3, 7 and 8 are the free, unhybridized ssDNA. When one DNA species is in excess, sufficient unbound DNA is seen as the lower band. As the ideal 1:1 ratio is

approached (lane 5) the amount of signal increases. SYBR Gold stains dsDNA more brightly than ssDNA, which is the cause of the darker bands in lanes 4-6. The formation of longer dsDNA fragments also were seen as a 1:1 ratio was approached. The longer fragments migrate slower in a gel and appear near the top of the gel. The dark band at approximately 25% down the gel is the 1500 bp indicator, which shows that at a 1:1 ratio and 75 ng of each ssDNA species the dsDNA fragments are close to 1500 base pairs in size. This longest size of generated dsDNA is approximately 70 units in series. The signal in lane 7 was stronger than in lane 3, which indicated that BA in excess creates more dsDNA than when AB is in excess. This follows primer guidelines, BA contains a G or C within the last two bases, and C and G are stronger binders with three hydrogen bonding partners each. The use of BA as the probe in excess was determined to be optimal for later sensitivity limit detection.

Comparison between lane 5 of Figure 4-7 and lane 3 of Figure 4-6 reveals a stronger signal with less dsDNA in Figure 4-7. The difference in hybridization is the method of staining. The stronger signal was the result of staining during the co-polymerization reaction, where in Figure 4-6 the staining was done post-hybridization. This may be explained in how PicoGreen binds to dsDNA. PicoGreen in an intercalating dye and requires approximately 4 bp per PicoGreen molecule [104]. A range of 3 to 5 PicoGreen dye molecules are able to bind each 22 bp region based on how closely the dye molecules are packed. Staining during hybridization may provide a more directed and efficient binding of PicoGreen to the developing dsDNA regions. When stained post-hybridization, the dye may bind less efficiently. Based on the data, PicoGreen was included during hybridization in the co-polymerization hybridization sensitivity trials.

4.3.4 Co-polymerization sensitivity

Co-polymerization probe sensitivity was determined by challenging a fixed amount of BA probe with a known amount of AB reporter. From the previous work, the BA species was in excess and PicoGreen dye was present during the co-polymerization hybridization. BA probe amounts between 5 – 100 ng and AB reporter amounts between 0.1 – 100 ng were tested and the detection values are shown in Figure 4-8 [13].

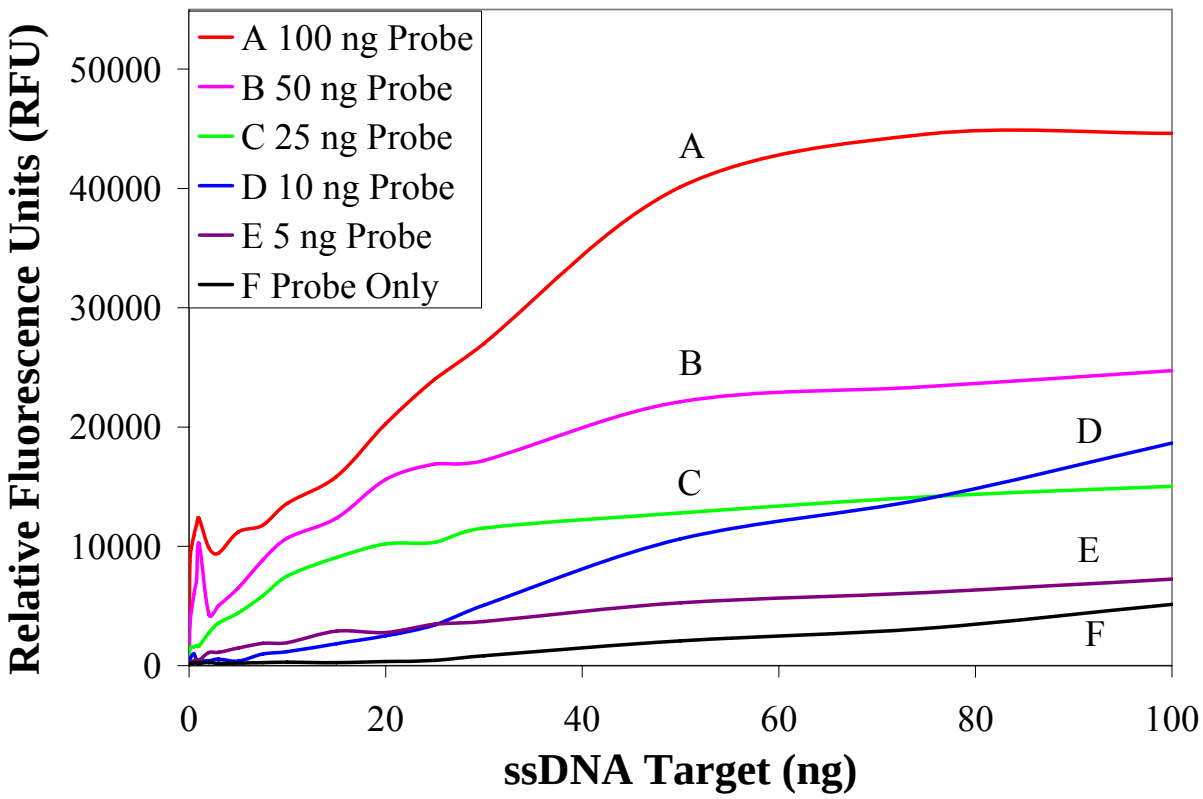

Figure 4-8: Probe sensitivity. Line A is the BA ssDNA probe only. Lines B-F are 5, 10, 25, 50 and 100 ng respectively of BA probe challenged against AB reporter (adapted and modified from Anderson, Zhang, and Alocilja, 2011).

From Figure 4-8 the line indicating probe only (A) has little to no signal. This was expected as PicoGreen does not have a strong fluorescent signal when only bound to ssDNA. The lines B-F represent an increasing amount of BA probe in the system. As each probe concentration was challenged with AB reporter, the signal increased in a linear fashion for 5-25 ng of probe.

Signals peaked and maintained strength beyond 30 ng of AB reporter for concentrations of BA probe 50 ng and less. Only when 100 ng of probe where used, did the signal continue to increase with reporter amount. The higher concentrations of probe, lines E and F, show irregularities when 0.1 ng to 2 ng of target AB reporter were used. For assay purposes, it was desired to have a constant signal increase and the probe amounts of 50 and 100 ng were removed from the analysis.

Optimal concentration of the co-polymerization probe were chosen to be 25 ng of BA reporter with 1x concentration of PicoGreen dye in 1x tris-borate-EDTA (TBE). At 25 ng of probe, the signal to noise ratio was 3:1 at 100 pg of AB reporter amount. This indicated that the co-polymerization had a detection sensitivity of 100 pg output from the sandwich assay.

To show improved fluorescent output, the co-polymerization method was compared to standard end-labeled DNA release. Co-testing was conducted with Dr. Zhang, using the lower limits of detection that he had achieved for co-polymerization detection [103]. Using 6-FAM liberated DNA as the final reporter, the limit of detection was found to be 1 ng at <1000 counts / 0.1 seconds. The lower limit for co-polymerization was found to be 100 pg of PCR DNA target yielding 1460 counts / 0.1 second. The copolymerization not only had a lower detection limit, but also a stronger signal. The added 20 minutes of assay time yield a more sensitive detection system by an order of magnitude with a stronger signal.

The local maxima in the 100 and 50 ng probe values from Figure 4-8 are thought to be a result of the binding modes of PicoGreen to the semi-dsDNA region. At high probe values the maximum

amount of ssDNA-dsDNA ratio is achieve. Essentially, every target AB molecule is bound to two BA probes. The PicoGreen binding near the ssDNA ends may be stabilized sufficiently to avoid reduced ssDNA efficiencies. Secondly, PicoGreen will also act as a minor groove binder at higher PicoGreen to DNA amounts. With an excess in BA probe, the ratio of PicoGreen to DNA is lower, forcing intercalation as the major binding mode. This binding mode is though to allow a greater number of dye molecules per dsDNA fragment. At higher PicoGreen to DNA ratios (lower total DNA), PicoGreen may be intercalating and also minor groove binding. With a stronger association from both binding modes, the number of dye molecules may be reduced per dsDNA segment. With sample target concentration being unknown, the higher BA probe concentrations were avoided to maintain a semi-dose response.

4.3.5 Quantum dot-dye attachment

Quantum dots were successful water solublized with AET. This was confirmed prior to SYBR 101 attachment. The quantum yield of the QDs was deceased after thiol surface functionalization. Previous work (Pong and Lee 2008) has reported up to a 50% decrease in signal after sulfur bonding. A quantity of 1 nmol of stock QD's were dissolved into a total volume of 100 μL in chloroform and compared against 1 nmol of AET capped QD's and measured in a fluorescent plate reader. The AET capped QDs showed a decrease in signal of 68.5% and were stable for 6 months at 4°C.

The fluorescent properties of the SYBR 101 dye were compared pre- and post-QD conjugation. A quantified mass of dsDNA was stained with both the SYBR 101 reacted with AET or with QDs and then separated with electrophoresis. The results are shown in Figure 4-9.

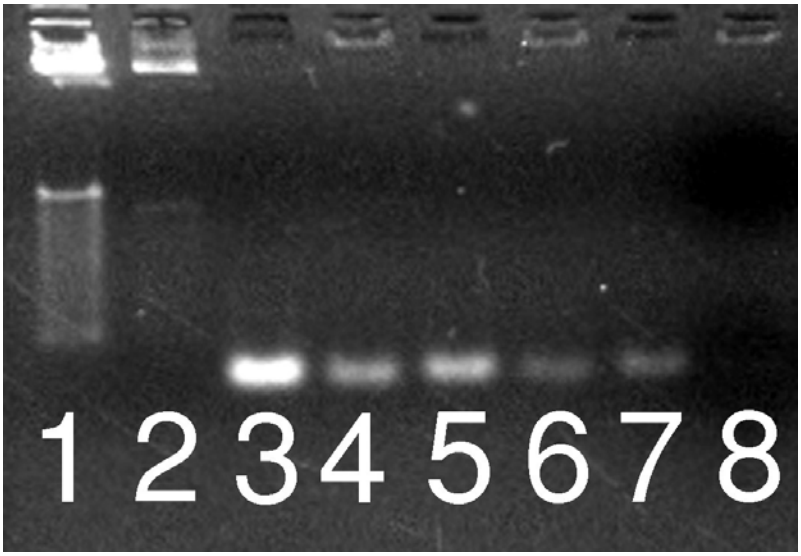

Figure 4-9: Fluorescence of QD conjugated SYBR 101 dye. Dilutions of 60 bp dsDNA stained with SYBR 101-AET or SYBR 101-QD. Lanes 1 and 2: 1 µg of 100 bp DNA ladder, lane 1 with SYBR 101-AET and lane 2 with SYBR 101-QD. Lanes 3, 5, and 7 were run with 75, 30 and 15 ng of SYBR 101-AET stained dsDNA. Lanes 4, 6, and 8 were run with 75, 30 and 15 ng of SYBR 101-QD stained dsDNA. Samples were run in a 2% w/v agarose gel at 30 V for 2 hours in 1x TBE (adapted and modified from Anderson, Zhang, and Alocilja, 2011).

Fluorescence was maintained after conjugation, but was reduced. Comparison of lanes 3 and 4, 5 and 6, and 7 and 8 show the QD conjugated dye has only 38% signal compared to SYBR 101-AET dye. This reduction in signal is a direct result of the QD conjugation. The QDs possess their own inherent fluorescence and it would be expected to have seen greater signal after QD conjugation, with a second fluorescent reporter. The severe reduction in signal is a result of quenching between SYBR 101 and the QD. The QD-SYBR conjugate had reduced signal while still binding DNA thus confirming successful conjugation of the dye and the quantum dot.

4.3.6 Electrochemical detection of quantum dot-dye

Proof of concept detection was accomplished with SYBR 101-QD dye in differential pulse voltametrtry (DVP). Samples of Zinc/cadmium, SYBR 101-QD and cadmium powder were tested as described in the methods section. Figure 4-10 [13] shows the plotted data from DPV.

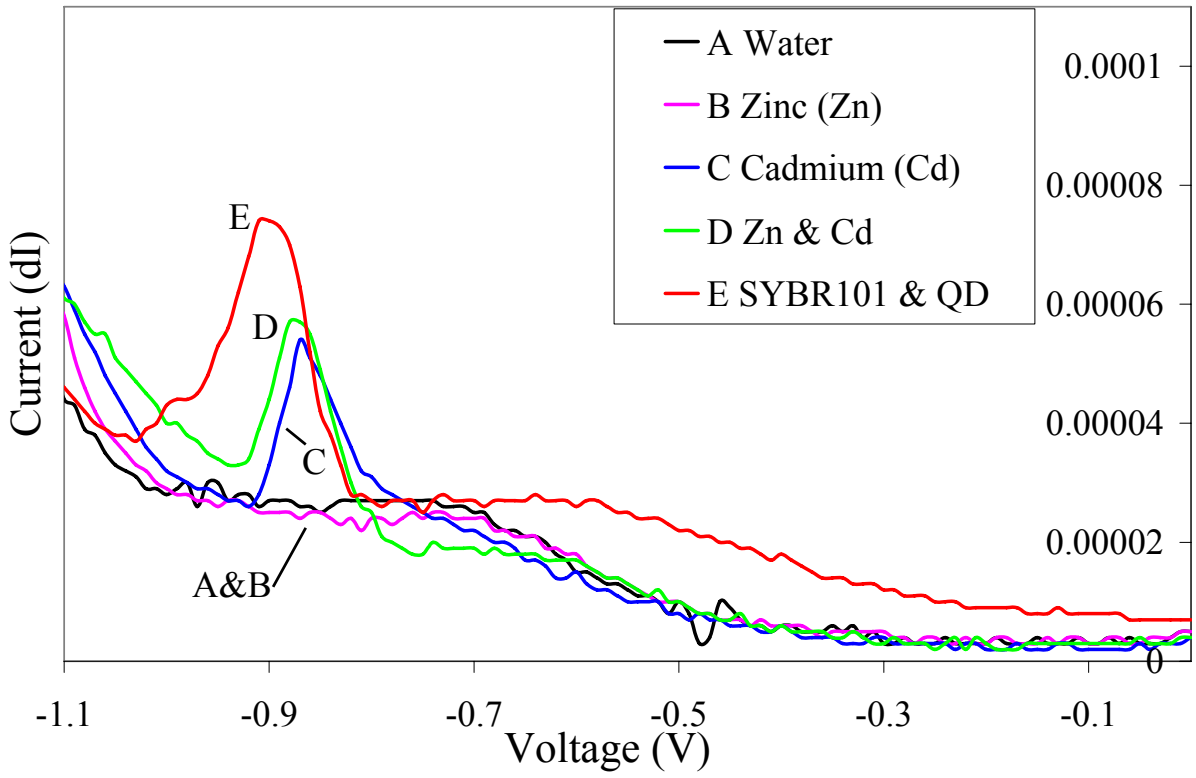

Figure 4-10: Differential pulse voltammetry of metallic particles. Peaks between -0.87 V and -0.90 V are seen indicating cadmium presence in all three metallic samples (adapted and modified from Anderson, Zhang, and Alocilja, 2011).

Sample Zn/Cad in Figure 4-10 DPV contained 20 µL of 1 mM cadmium chloride and 1 mM of zinc chloride, with a reduction peak of -0.87 V. When cadmium chloride alone was tested (1 mM), the same peak was seen indicating the -0.87 V peak was from cadmium alone. SYBR 101-QD samples (approximately 7.5 nmol) contained a similar strength signal with a -0.90 V reduction peak confirming the dye can be used in electrochemical detection. Electrochemical detection using QD-dye was not accomplished in the original paper as a method to separate the free dye from the bound dye was not available.

4.4 Conclusions

The successful generation of a co-polymerization hybridization system was accomplished. A system of two ssDNA species was generated and shown to partially hybridize in a continuous fashion generating longer dsDNA fragments. This system was incorporated into a sandwich assay for detection of *Bacillus anthracis* from cultured samples. Compared to standard end-labeled 6-FAM DNA systems, co-polymerization increased the detection sensitivity by 10 fold with a stronger signal and better signal to noise ratio than previous work. Optimal assay conditions were determined to be 25 ng of BA probe in a total volume of 100 µL (1x Picogreen, 1x tris-borate-EDTA buffer).

To fully investigate the unusual spike in the co-polymerization hybridization additional work will need to be conducted. The amount of dye used should be explored to try and force the increase in signal but at lower probe amounts. The co-polymerization system if forced into the conditions of appropriate dye to probe to target amount may provide a highly sensitive absence/presence test using fluorescent detection. A possible future set of experiments would

include varying the PicoGreen amounts from 1x through 0.01x with probe values from 10 ng through 1 pg. It would be expected to find a set of conditions at lower dye and probe levels that exhibit similar increase in fluorescent signal as was seen at the 50 ng and 100 ng probe amounts from Figure 4-8.

The successful attachment of quantum dots to a SYBR 101 dye molecule was accomplished and was shown to be compatible with the co-polymerization system. The SYBR 101-QD system was also shown to be detectable using electrical differential pulse voltammetry. The usage of the SYBR101-QD system for electrochemical detection was not realized in this work. Successful detection with the SYBR101-QD conjugate required a way to separate the bound dye from the unbound dye. The SYBR101-QD conjugate formed a colloidal suspension, preventing separation based on centrifugation. The size scale of the dye and DNA target remove the ability to filter the dye-target product from the free dye. Future work to include the SYBR101-QD into the detection system would require a plate based assay. An ssDNA strand tethered to a plate surface could act as a hybridization point for co-polymerization. The resulting immobilized dsDNA would retain bound SYBR101-QD when washed with buffer and separate the free SYBR101-QD dye from bound dye.

Chapter 5: Co-polymerization hybridization sandwich assay for detection of the Shiga-like toxin 1 in *Escherichia coli* O157:H7

5.1 Introduction

In the previous Chapters, 3 and 4, the generation of dextrin coated nanoparticles and self-assembling co-polymerization hybridization was presented. The dextrin coated gold nanoparticles (AuNPs) were successfully functionalized with DNA probes. These probes were then shown to be removable for basic fluorescent detection. The use of the designed co-polymerization DNA oligonucleotides was successful in detecting a target when allowed to hybridize, and fluoresced after dye intercalation binding. Chapter 5 describes the combination of these different technologies into a single biosensor system for detection of the Shiga-like toxin 1 (*stx1*) in *Escherichia coli* O157:H7 Sakai (*E. coli* O157:H7) strain. This biosensing system is comprised of two particles, gold nanoparticles and magnetic microparticles (MMP), both of which are labeled with DNA probes. These probes target the *stx1* gene, which is present in shiga toxigenic group of *Escherichia coli* (STEC) and enterohemorrhagic *E. coli* (EHEC). The Sakai strain of *E. coli* O157:H7 was used in this assay as it contains both of the Shiga-like toxin (*stx1* and *stx2)* genes common to the STEC and EHEC families of microorganisms. Shiga toxin and Shiga-like toxin are responsible for the illness associated with STEC and EHEC disease.

The two DNA coated particles were linked together when simultaneously hybridized to the *stx1* DNA target. The resulting sandwich structure of MMP-DNA-AuNP was magnetically separated and the desired form of detection was performed. The detection system was evaluated with electrical reduction-oxidation, standard end-label fluorescence, and co-polymerization detection

against genomic DNA extracted from *E. coli* O157:H7. While electrochemical detection has been miniaturized for possible field use, fluorescent detection has potential for field use with standard digital camera imaging and light emitting diode (LED) illumination.

5.2 Materials and methods

5.2.1 Primer and probe generation for Shiga-like toxin 1 (*stx1*) gene

The primer and probe sequences were designed to target the *stx1* gene sequence. A modified sequence was generated to target a 95 base pair (bp) region for hybridization assay detection [9]. The *stx1* gene is highly conserved in STEC and EHEC organisms and was chosen for the target sequence. Primers were designed with the properties listed in Table 5-1. Sequences are listed in Table 5-2.

Table 5-1. PCR primer properties and design optimization for the *stx1* gene.

	Generated	Optimal
Target Size	95 bp	90-110 bp
Target Tm	71.6 °C	65-75°C
Target GC%	47%	40-60%
FWD Primer Size	27	18-24 bp
REV Primer Size	27	18-24 bp
FWD Primer GC%	48%	40-60%
REV Primer GC%	44%	40-60%
FWD Primer Tm	60.2°C	45-55°C
REV Primer Tm	58.3°C	45-55°C

Table 5-2. *stx1* primers and amplified sequence (95 bp).

FWD Primer	5’ CAT CTG CCG GAC ACA TAG AAG GAA ACT 3’
REV Primer	5’ GGG AAG CGT GGC ATT AAT ACT GAA TTG 3’
Generated Target:	5'CATCTGCCGG ACACATAGAA GGAAACTCAT CAGATGCCAT TCTGGCAACT CGCGATGCAT GATGATGACA ATTCAGTATT AATGCCACGC TTCCC 3' Position 2,924,863 - 2,925,257 of gene sequence [105].

The chosen primer set was used for generation of probes for the hybridization assay. The primer sequences were incorporated into the probe set. Successful generation of the primers would also indicate the availability for probe binding. The probes generated are listed in Table 5-3.

Table 5-3. Sandwich assay particle probe sequences.

MMP Probe	5' Phosphate - AAA AAA AAA AAA CAT CTG CCG GAC ACA TAG AAG 3'
AuNP Probe	5' GTA TTA ATG CCA CGC TTC CCA AAA AAA AAA AA - Thiol 3'

The probes generated included a spacer arm of poly-adenosine to distance the binding sequence from the particle surface. The magnetic particle contained only a single species of DNA probe, where the gold nanoparticle was conjugated with two different DNA species. The probe attached

to the AuNP allowed for the sandwich assay to occur, where the second species of DNA was used for fluorescent reporting and detection. The second strand of DNA attached was determined by the method of fluorescent detection. The sequences that were generated and their uses are listed in Table 5-4 below.

Table 5-4. Co-polymerization sequences. Thiol sequences are for AuNP attachment. FAM was used for direct fluorescence testing, AB-Thiol and BA were used for standard co-polymerization detection and C-Linker, AB, and BA were used for tethered co-polymerization detection.

FAM	5' FAM - ATC AGT CAG TCA GTC AGT CA - Thiol 3'
C-Linker	5' GCT ACG AAT AAA TAG AAC AGT C - Thiol 3'
AB-Thiol	5' Thiol - TTA TTC GTA GCG TGA TGC CAA G 3'
AB	5' TTA TTC GTA GCG TGA TGC CAA G 3'
BA	5' GCT ACG AAT AAC TTG GCA TCA C 3'

5.2.2 Assay particle generation

The magnetic microparticles used were Fe3O4 particles of 1.5 μm diameter decorated with a primary amine on the surface (Bangs Labs #BM546). The gold nanoparticles used were generated as described in Chapter 3 (10 g/L dextrin, 50°C, pH 9.0 and 2 mM gold chloride).

5.2.2.1 Magnetic particle functionalization

The amine coated magnetic microparticles used in this assay were functionalized with the 5'-phosphoralated probe listed in Table 5-3 (MMP-Probe). The probe was attached using the zero length cross-linker 1-ethyl-3-(3-dimethylaminopropyl) carbodiimide) (EDC) and N-Hydroxysuccinimide (NHS) in 0.1 M 2-(N-morpholino)ethanesulfonic acid (MES) buffer at pH 6.0, Figure 5-1. The magnetic particles (5 mg) were added to EDC (5 mg), NHS (50 mg), and 10 nmol of phosphorylated DNA in a 15 mL polypropylene centrifuge tube. The 5' end phospohate of a DNA chain reacts with EDC in the same manner as a carboxyl and provided a means of covalent attachment. The reaction proceeded for 48 hours at 25°C under gentle agitation while protected from light. The particles were washed three time in the assay buffer (described in section 5.2.4 Sandwich assay) and resuspended to a final concentration of 0.8 mg/mL.

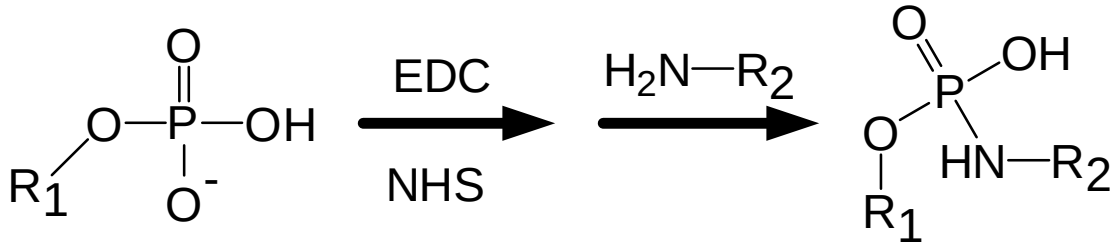

Figure 5-1: Probe attachment to magnetic particle via EDC/NHS cross-linker reaction. DNA probe (R1) with 5' end phosphate, Magnetic particle (R2) with surface primary amine.

5.2.2.2 Gold nanoparticles functionalization

The gold nanoparticles were functionalized with DNA through ligand exchange in the same fashion as citrate generated gold nanoparticles. Ligand exchange starts with a reactive thiol which bonds to a free gold surface after a dextrin molecule disassociates. The thiol bond is

sufficiently stronger than the electrostatic bonding of the dextrin, and forms a semi-permanent surface decoration. Three different species of gold nanoparticles were generated for each of the fluorescent readout methods. All gold nanoparticles were functionalized with 0.05 nmol of AuNP Probe (Table 5-3) and 5 nmol of a reporter (Table 5-4). The thiolated DNA probes were reduced in 0.1 M dithiothreitol (DTT) under constant agitation at room temperature. Excess and reacted DTT was removed from the DNA reduction reaction using a Sephadex filtration column (GE Healthcare #Nap-5) per manufacturer instructions. The reduced and reactive DNA was mixed with 1 mL of washed gold nanoparticles at 4 nM (1nM: 1 absorbance unit (AU) at 520 nm) in 18 megaohm (MΩ) water. Salt additions were added over a 48 hour period to facilitate close packing of the DNA oligonucleotides on the gold nanoparticles surface [11]. Particles were stored in the reaction solution for a maximum of 30 days on the bench top until use.

5.2.3 DNA target extraction

Bacterial cultures of *E. coli* O157:H7 Sakai were refreshed and allowed to grow for 4 hours resulting in a culture of live *E. coli* at concentration of about 10^8 colony forming units per milliliter (CFU/mL). The live culture was serially diluted eight times, each at 1:10, creating a dilution series. A volume of 1 mL of each of the dilutions was treated with the Trizol (Invitrogen #15596-026) reagent or proteinase K digestion followed by standard ethanol precipitation. Trizol extraction was also compared against phenol/chloroform extraction as the Trizol protocol also uses bi-phase extraction. Using Trizol, in brief, each culture sample was pelleted and resuspended in the Trizol reagent and vortexed. Chloroform was then added and vortexed again. The sample was allowed to separate in to a three phase system, with DNA in intraphase boundary and the lower phase. The upper phase is removed and then 100% ethanol was mixed

into the lower phase. The sample was centrifuged and washed two times with citrate buffer (10% ethanol, 0.1 M sodium citrate) following with a 70% ethanol precipitation. Following a final centrifugation, the DNA was resuspended in 300 µL of 8 mM sodium hydroxide. The total recovery time was 2 hours. Standard recovery starts by digestion with 100 µg of proteinase K added to the bacterial pellet that has been resuspended in lysis buffer (200 mM sodium chloride, 100 mM Tris, 5 mM ethylenediamminetetraacetate (EDTA), and 0.2% sodium dodecyl sulfate (SDS)). Digestion with proteinase K was accomplished at 65°C for 75 minutes. Samples were then ethanol precipitated using three rounds of centrifugation at 13,000 x g. The first centrifugation was carried out in 100% isopropanol, then 100% ethanol, and finally 70% ethanol, with the supernatant being removed each time. The final DNA sample was dried for 2 hours in a bio-safety cabinet and resuspended in the same fashion as the Trizol method. Total recovery time for ethanol precipitation was 4.75 hours. Phenol chloroform extraction samples were mixed in a phenol/chloroform solution (Invitrogen #15593-031), vortex for 3 minutes and then ethanol precipitated, with recovery requiring 3.5 hours. The recovered DNA was measured on a NanoDrop 1000 (Thermo Scientific) spectrophotometer.

5.2.4 Sandwich assay

The DNA input for the assay was prepared by heating the desired target (40 µL) in a thin walled 300 µL tube at 95°C for 5 minutes in a water bath to denature the DNA into single-stranded DNA. The tubes were then rapidly cooled in a -20°C isopropanol bath for 30 seconds to stabilize the denatured single-stranded DNA target. The 40 µL of DNA was mixed with 0.08 mg of probe functionalized DNA microparticles and adjusted to a final volume of 200 µL using assay buffer (150 mM sodium chloride, 10 mM phosphate, 0.1% SDS, and pH 7.4). The samples were

inversion mixed at 45°C for 60 minutes. Upon hybridization, magnetic separation was used to wash the unbound DNA from the particles and resuspended to 200 µL of assay buffer containing 40 µL of the desired functionalized gold nanoparticles (1 nM). The MMPs-DNA and AuNPs were allowed to incubate and hybridize for 2 hours at 45°C under inversion mixing. The reactions were magnetically separated and washed twice to obtain the final MMP-target-AuNP sandwiches. The choice of electrochemical detection or fluorescence amplification detection method determines the next steps in the process are described in section 5.2.5.

5.2.5 Detection

5.2.5.1 Reduction oxidation electrochemical detection

Electrochemical detection was accomplished by placing the magnetically separated sandwich structures from the previous section on to the carbon working electrode of a screen printed carbon electrode (SPCE) and allowed to dry for 1 hours in a biosafety cabinet (Figure 5-2) [32]. A volume of 50 µL of 0.1 M hydrochloric acid was placed on the SPCE as the electrolyte.

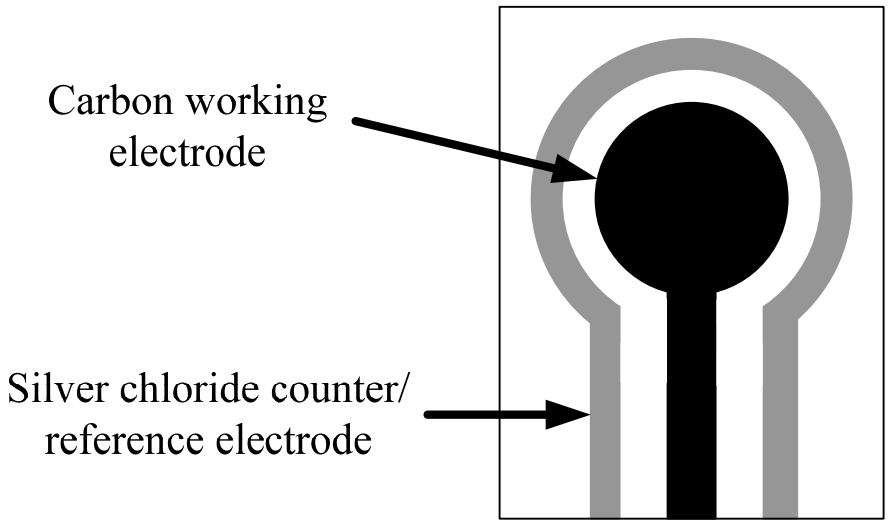

Figure 5-2: Schematic of the screen printed carbon electrode. Carbon working electrode with silver/silver chloride combination reference/counter electrode.

A voltage of +1.5 V was applied to the carbon electrode-sample for 120 seconds to condition the sample. The +1.5 V converted the ground state gold nanoparticles into gold(III). The SPCE was measured using a benchtop potentiostat (Princeton Applied Research, Potentiostat/galvanostat 263A). The readout of the gold ions was accomplished using differential pulse voltammetry (DPV), with voltage sweeping from +1.5 to 0 V at 33.3 mV/s (step potential 10 mV and modulation amplitude of 50 mV). Within the SPCE/gold/hydrochloric acid electrical system, gold reduction appears as a differential pulse voltammetry signal centered around +0.3 V.

5.2.5.2 Direct carboxyfluorescein (6-FAM) attachment

Detection of fluorescence was quenched in the presence of gold nanoparticles and detection requires liberation of the 6-FAM-DNA from the AuNP. The MMP-DNA-AuNP samples were resuspended in 5 M DTT and heated to 95°C for 15 minutes and then agitated for 45 minutes at 21°C. The samples were then centrifuged at 13,000 x g for 30 minutes and the supernatant was transferred into a 96 well plate. Detection was accomplished by excitation at 492 nm ± 4 nm and with an emission filter at 535 nm ± 12.5 nm.

5.2.5.3 Co-polymerization growth

The sandwiched MMP-DNA-AuNP from the sandwich assay was resuspended in 5 M DTT and the DNA was recovered in the supernatant the same way as in section 5.2.5.2. The recovered DNA (AuNP-Probe, Target, and AB-Thiol) sequences were added to 50 ng of BA probe, and

heated again to 95°C for 5 minutes and allowed to air cool to room temperature over a 10 minute period. The samples were then mixed with PicoGreen (Invitrogen #P7581) at 1x concentration and allowed to stain for 5 minutes. The stained DNA was then plated and fluorescence detection was conducted the same way as in section 5.2.5.2.

5.2.5.4 Co-polymerization tethering

The concentrated MMP-DNA-AuNP used with the "C-Linker" labeled AuNP was resuspended in a solution of assay buffer with 20 nM AB and 20 nM BA. The AB/BA co-polymerization solution was mixed to a concentration of 1 μM of each species in assay buffer and heated to 95°C for 15 minutes prior to the end of the sandwich assay. The AB/BA solution was allowed to air cool slowly to room temperature before addition to the sandwich structures. A volume of 25 μL of the AB/BA solution was resuspended with the MMP-DNA-AuNP sandwiched to 200 μL in assay buffer. The AB/BA sequences were allowed to hybridize to the C-Linker for 15 minutes at room temperature under constant inversion. The samples were magnetically separated, washed, and the DNA was liberated with DTT as described previously. The resulting supernatant contained the AuNP-Probe, target DNA, C-Linker, and AB/BA complexes. This was heated to 95°C for 5 minutes and later air cooled to promote hybridization. Finally, PicoGreen was added to a final concentration of 1x and the samples were read in a plate reader in the same fashion as described in 5.2.5.2.

5.3 Results and discussion

5.3.1 Primer and probe generation evaluation for Shiga-like toxin 1 (*stx1*) gene

Primer sequences were generated from the gene sequence reported in Fode-Vaughan (2003) to produce a 95 bp target. Primer compatibility was tested by polymerase chain reaction (PCR) of genomic DNA extract using the Trizol extraction method. A mass of 50 ng of extracted *E. coli* O157:H7 DNA was loaded into a PCR master mix (Invitrogen Fast SYBR® Green Master Mix #4385610) with 300 nM of primer in a 50 µL reaction volume. Genomic *E. coli* O157:H7 DNA was also amplified with a primer set reported in Sharma (2003) in combination for both the *stx1* and *stx2* genes. Table 5-5 listed the primers used to test the *stx1* gene presence and potential binding.

Table 5-5. Primer sequences for *stx1* and *stx2* used to test primers generated for sandwich assay.

Sequence Name	Sequence	Source	Amplicon Size
stx1-Forward-Anderson (FWD)	5’ CAT CTG CCG GAC ACA TAG AAG GAA ACT 3’		95 bp
stx1-Reverse-Anderson (REV)	5’ GGG AAG CGT GGC ATT AAT ACT GAA TTG 3’		
stx1-Forward-Sharma (S1F)	5' GAC TGC AAA GAC GTA TGT AGA TTC G 3'	Sharma 2003	150 bp
stx1-Reverse-Sharma (S1R)	5' ATC TAT CCC TCT GAC ATC AAC TGC 3'		
stx2-Forward-Sharma (S2F)	5' ATT AAC CAC ACC CCA CCG 3'	Sharma 2003	206 bp
stx2-Reverse-Sharma (S2R)	5' GTC ATG GAA ACC GTT GTC AC 3'		

The end product of PCR amplification reactions (10 µL) were loaded into a 2% w/v agarose gel and run at 30 V for 120 minutes in buffer (40 mM Tris, 20 mM acetic acid, and 1 mM EDTA).

The samples were prestained with a fluorescent dye, SYBR Green, from the master mix PCR kit. The results are show in Figure 5-3, with lane contents listed in Table 5-6.

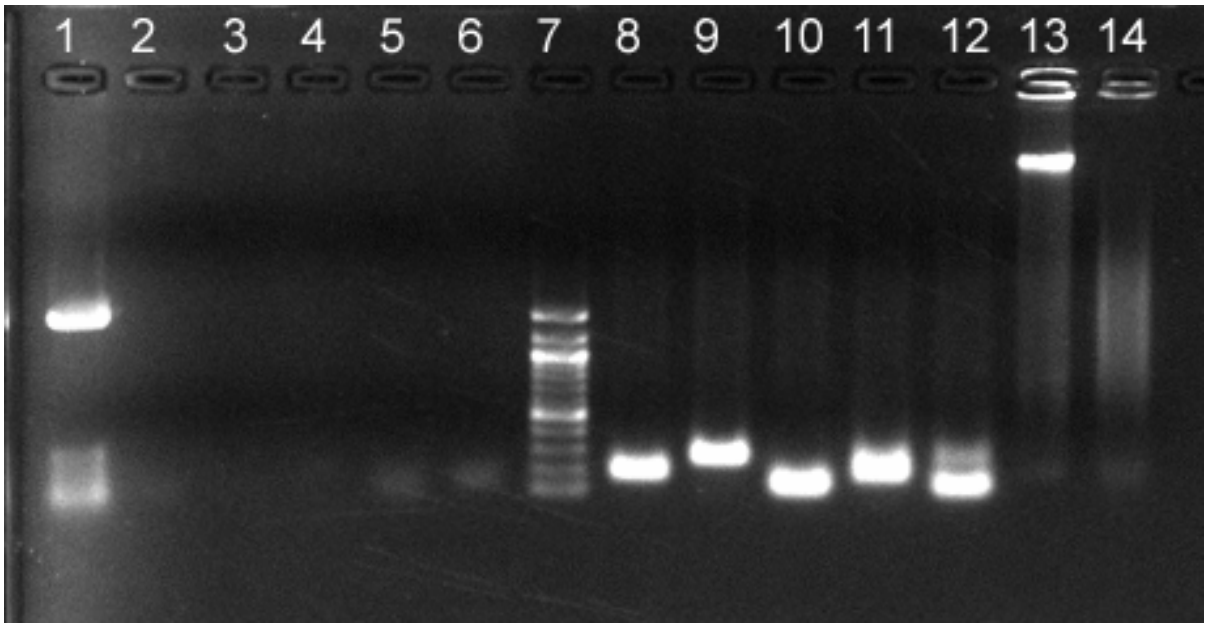

Figure 5-3: Agarose gel electrophoresis with PCR product. Combinations of *stx* primer sets shown. Lane contents are listed in Table 5-6.

Table 5-6. Lane description for Figure 5-3. Lanes 1,7 and 13 do not contain PCR reactants, lanes 2-6, 8-12, and 14 underwent PCR reaction.

Lane	Description	Contents
1	Ladder	10 bp per band
2	Primer Only	S1R / S1F
3	Primer Only	S2R / S2F
4	Primer Only	REV / FWD
5	Primer Only	S1R / S1F / S2R / S3F
6	Primer Only	REV / FWD / S2R / S3F
7	Ladder	100 bp per band
8	Template	S1R / S1F
9	Template	S2R / S2F
10	Template	REV / FWD
11	Template	S1R / S1F / S2R / S3F
12	Template	REV / FWD / S2R / S3F
13	Template	Extracted Genomic DNA
14	Template	PCR with No Primers

No significant product is seen in lanes 2-6 when the primers are run alone in the PCR reaction. This establishes that no self-priming (binding) is occurring and creating off-target amplicons. When the Sharma primers are run individually, as seen in lanes 8 and 9, only a single amplicon is seen with the expected product size of about 150 and 200 bps. The developed primer, lane 10, also creates the correct size amplicon of about 100 bp. When both the *stx1* and *stx2* primers from Sharma are mixed together, lanes 11 and 12, two products are observed. In lane 11, a larger band is generated that extends from the 150-200 bp size range. Lane 12 shows two distinct bands, both 100 and 200 bp in size, *stx2* from Sharma and the *stx1* primer generated. That two products are formed indicates that both genes are present in the target *E. coli* genome. Both *stx1* primer sets function as expected. The generated FWD and REV primer set created for the sandwich assay correctly bind the *stx1* gene and were used to generate probes for the magnetic microparticles and gold nanoparticles.

Probes were generated using the primer sequences with an appropriate poly-adenosine sequence added to create a stand off distance from the particle. This stand-off distance allowed for hybridization of the target DNA from *E. coli* while also having the attached fluorescent reporter on the gold nanoparticles.

5.3.2 Gold nanoparticles functionalization and detection mechanism

The gold nanoparticles were functionalized as previously described in the methods section. Three types of gold nanoparticles were generated based on the DNA species attached. Figure 5-4 shows the detection principle for 6-FAM labeled gold nanoparticles.

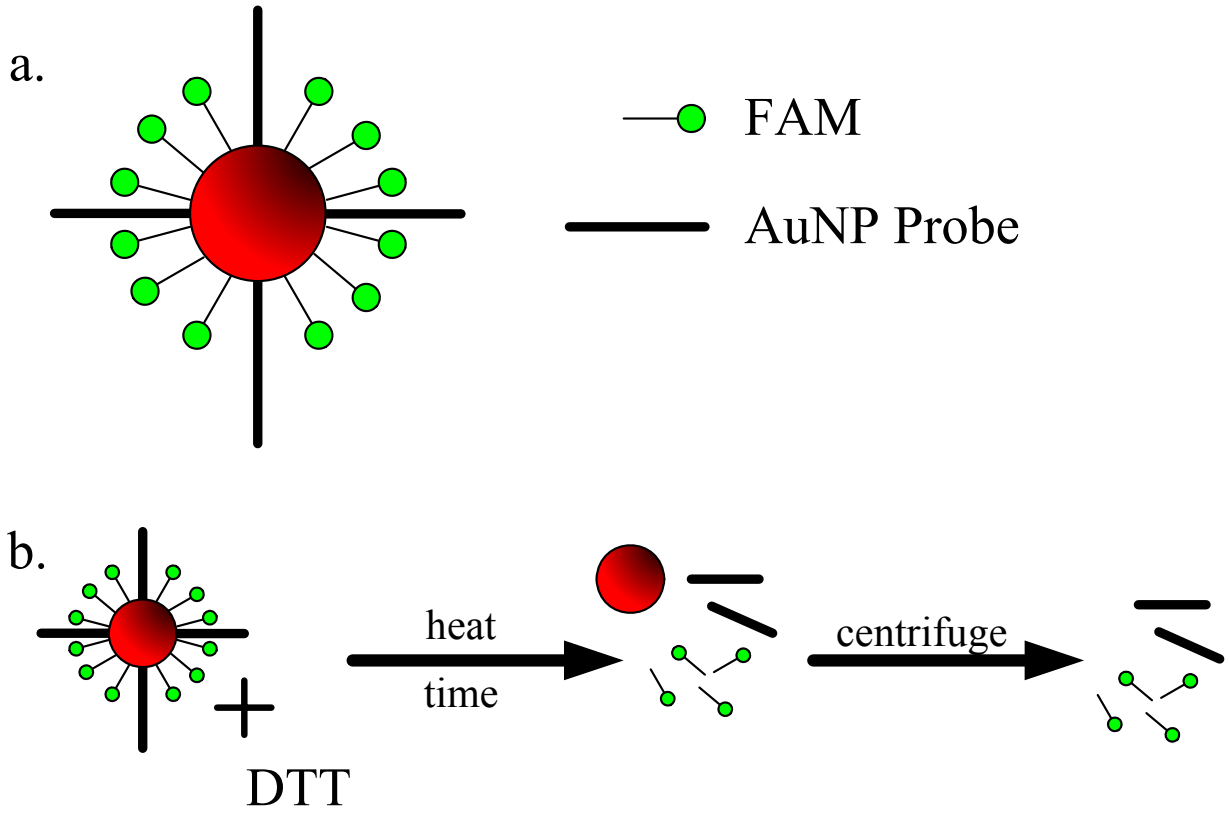

Figure 5-4: Direct fluorescence AuNP construction. (a) AuNP after generation; (b) Schematic of gold nanoparticle detection of end-labeled DNA after sandwich assay. DNA is liberated from the AuNP via DTT exchange.

The 6-FAM labeled DNA wad recovered from the gold nanoparticles after treatment with DTT as in Figure 5-4b and fluorescently detected as described in the methods section. Detection with co-polymerization hybridization as described in Chapter 3 is shown in Figure 5-5.

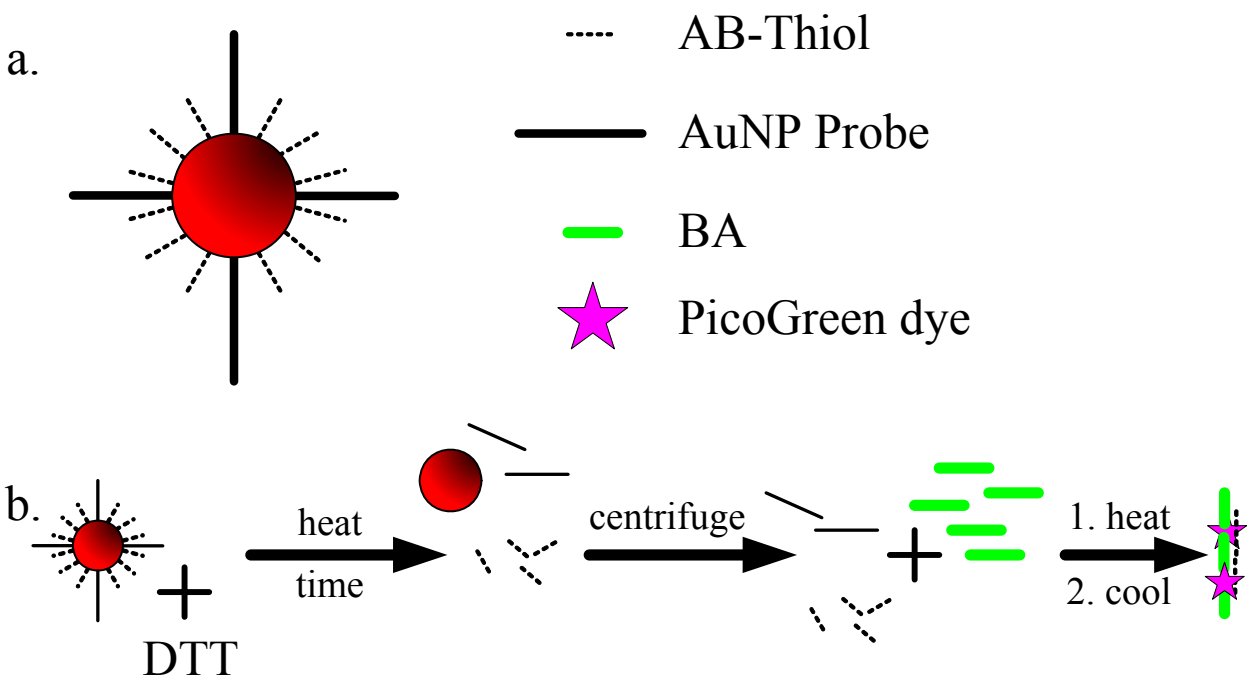

Figure 5-5: Standard co-polymerization AuNP construction. (a) AuNP after generation; (b) Schematic of co-polymerization detection after sandwich assay. The co-polymerization DNA reporter was liberated and then reacted.

Upon liberation of the attached DNA from the gold nanoparticles, the DNA was mixed with the co-polymerization hybridization partner and PicoGreen dye and heated. The DNA was then slowly cooled, forming double-stranded DNA sequences that fluoresce when bound to the dye. Detection was accomplished in the same manner as with the 6-FAM samples. The third fluorescent detection method was accomplished in the manner shown in Figure 5-6.

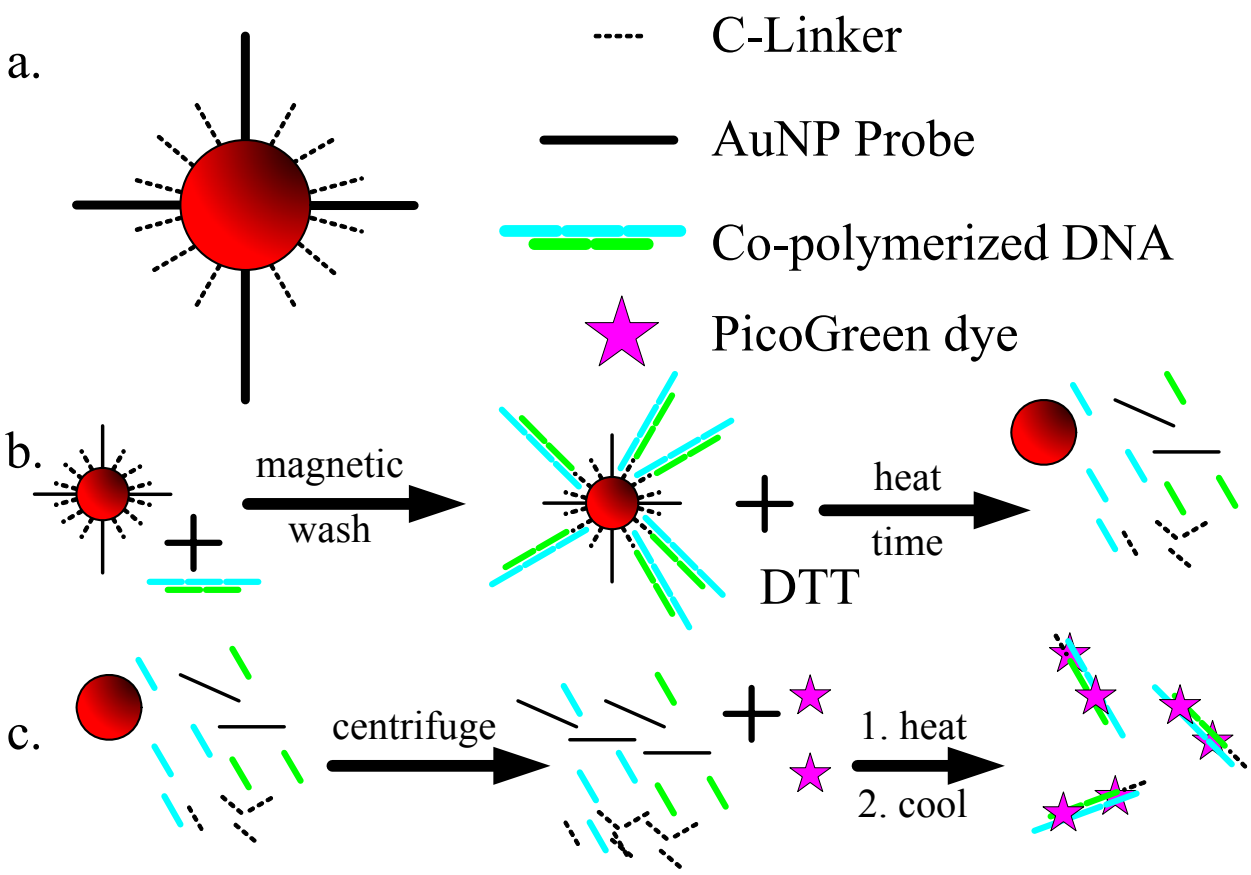

Figure 5-6: Tethered co-polymerization AuNP construction. (a) AuNP after generation; (b) Schematic of co-polymerization tethering detection. Co-polymerized DNA hybridizes to the AuNP before DTT liberation and detection.

The attachment of the C-Linker DNA species to the gold nanoparticles provided a hybridization attachment point for pre-co-polymerized DNA to attach. The co-polymerized DNA hybridized to the gold nanoparticles and separated while still part of the magnetic microparticle sandwich. After the second magnetic separation, the system was treated in the same fashion as the AB-Thiol system.

Successful generation of each of the three gold nanoparticles species was confirmed by a stable solution after ligand exchange, indicated by maintaining the original color. Control reactions without stabilizing DNA molecules turn purple and precipitate out of solution after the salting steps described in the methods of Chapter 5.

5.3.3 DNA extraction optimization

Optimization of a DNA extraction method was explored using Trizol, proteinase K digestion with ethanol precipitation, and phenol/chloroform extraction. The previous method used was enzyme digestion of the cellular material with ethanol purification. This method has a high recovery of DNA, but requires a large amount of equipment and 4 hours to complete. The Trizol kit uses a proprietary solvent system based on chloroform/phenol extraction. The Trizol kit is a two hour procedure requiring low equipment demands. Phenol/chloroform was explored as a control to the Trizol method. Table 5-7 lists the results of DNA recovery from 1 mL of 4 hour culture (~$1x10^8$ CFU).

Table 5-7. Comparison of DNA extraction methods.

Method	DNA Recovery (ng)	Standard Deviation (ng)
Ethanol	19408	3982
Trizol	29980	6060
Phenol	600	420

From the data, the Trizol method performs reasonably well compared to the ethanol precipitation in half the time. Trizol extraction also has the advantage of no perishable enzymes, no heating steps, and only requires a low speed centrifuge, leading to possible field based extraction. The standard phenol/chloroform extraction does not perform well compared to either of the other methods. It is believed that additional lysis agents are present in the Trizol reagent that increases DNA recovery. Trizol was used to obtain the target DNA input from the dilution series in the sandwich assay.

5.3.4 Detection

Detection was accomplished by either of two methods, electrochemical or fluorescence. Electrochemical detection uses the entire MMP-DNA-AuNP sandwich for detection, where fluorescence uses the DNA removed by DTT from the metallic particles in the assay.

5.3.4.1 Reduction oxidation detection optimization

Electrochemical detection was performed as described in the methods section of Chapter 5. The gold nanoparticle species used for electrochemical detection was the AB-Thiol particles. The final product from the assay was dried on the SPCE and then conditioned with 0.1 M hydrochloric acid for 120 seconds at +1.5 V. Dilutions were spilt between samples for the assay and bacterial culture plating for actual determination of cell count. A volume of 1 mL from each dilution was used for DNA extraction, assay hybridization, and gold reduction/oxidation measurement. The detection is displayed in Figure 5-7 below.

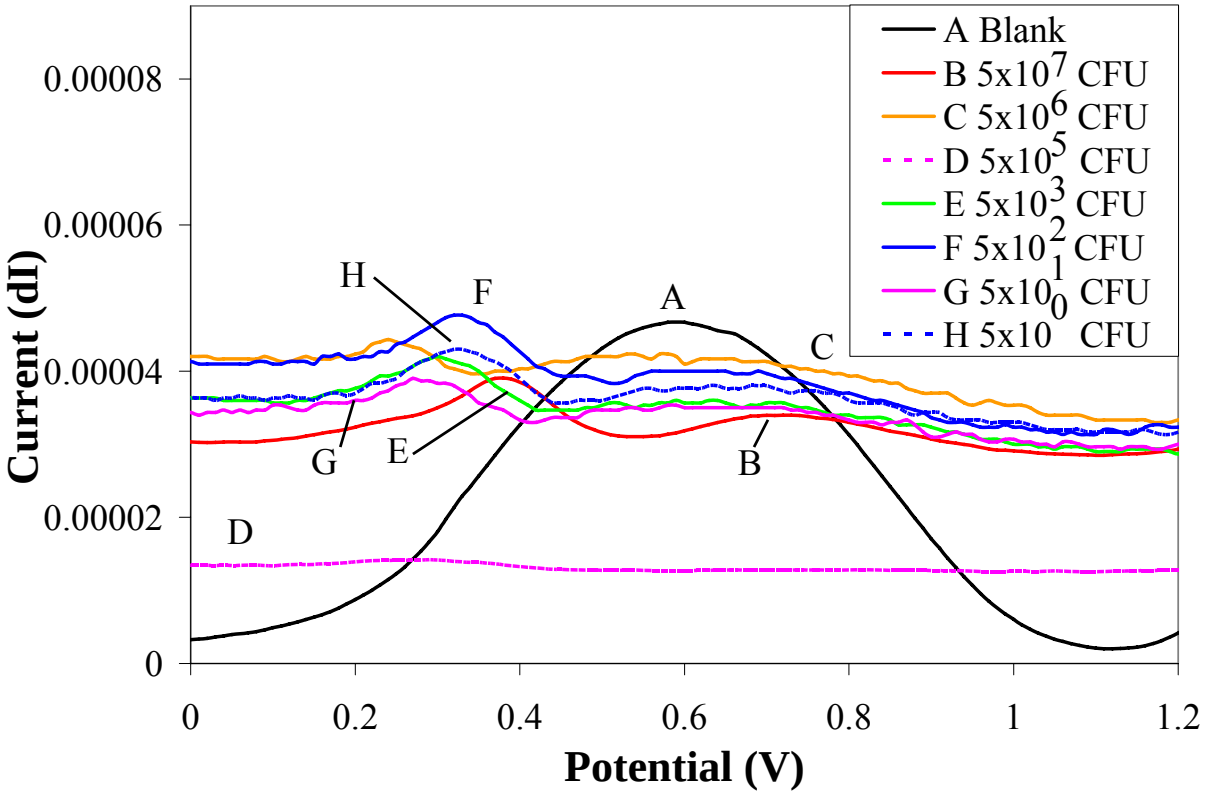

Figure 5-7: DPV response of gold nanoparticles after sandwich assay. Gold response is seen as a peak between +0.2 and +0.4 V. The peak in curve A is a result of the hydrochloric acid and MMP interaction with the system with AuNPs.

In Figure 5-7 most concentrations of target showed a positive capture. The low signal of sample $5x10^5$ CFU/mL still had the reduction peak at 0.3-0.4 V characteristic of the SPCE system. This set of data was from centrifuge tubes that leaked during hybridization, losing sample. Previous use of the sandwich assay with PCR generated targets showed a linear response with target

concentration [32]. The DNA recovery and assay procedure above did not show the same linear response.

The non-dose response of the reduction/oxidation plot may be the result of DNA extraction inefficiency, sandwich assay losses, magnetic separation loss, and SPCE detection sensitivity. The reduction/oxidation measurement was used to confirm proper functioning of the assay system as a whole, including the new probes, target extraction, and nanoparticles recovery. Detection of the thiol treated gold nanoparticles was attempted to verify the fluorescence in tandem and compare the sensitivities on the same samples. Figure 5-8 shows the electrical response from that system.

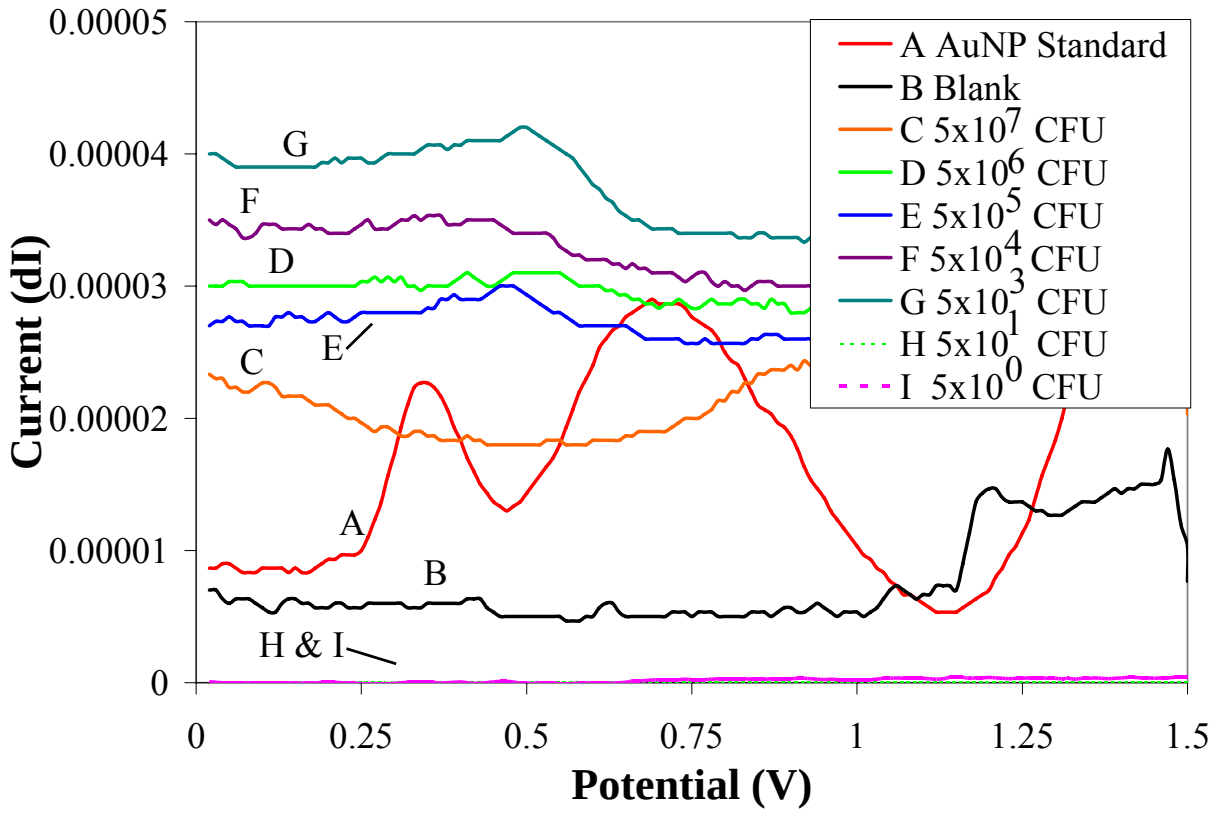

Figure 5-8: DPV response of thiol liberated AuNPs after sandwich assay.

From Figure 5-8 no gold reduction peak was seen in the 0.3 – 0.4 V range for the samples. The full amount of gold into the system showed the gold peak at +0.35 V confirming that the electrical system was functioning. The thiol addition and gold particle recovery were incompatible with the reduction of this system. The 5 M DTT in the system prevented the measurement either through gold surface stabilization or masking of the electrochemical signal. This result eliminated the ability to use both electrochemical and fluorescent detection of the sandwich structure because of the thiol. A third method was explored to recover the gold nanoparticles from the sandwich structure using high temperature (95°C) to break the hybridized DNA, Figure 5-9. This method of gold recovery would only be compatible with the C-Linker co-polymerization method, as the attached co-polymerized DNA would be freed and thus recoverable. Without the addition of DTT into the sandwich structure system, little or none of the thiol linked DNA would be free. The lack of DNA disassociation removed the direct FAM attachment and AB-thiol recovery and subsequent fluorescent detection.

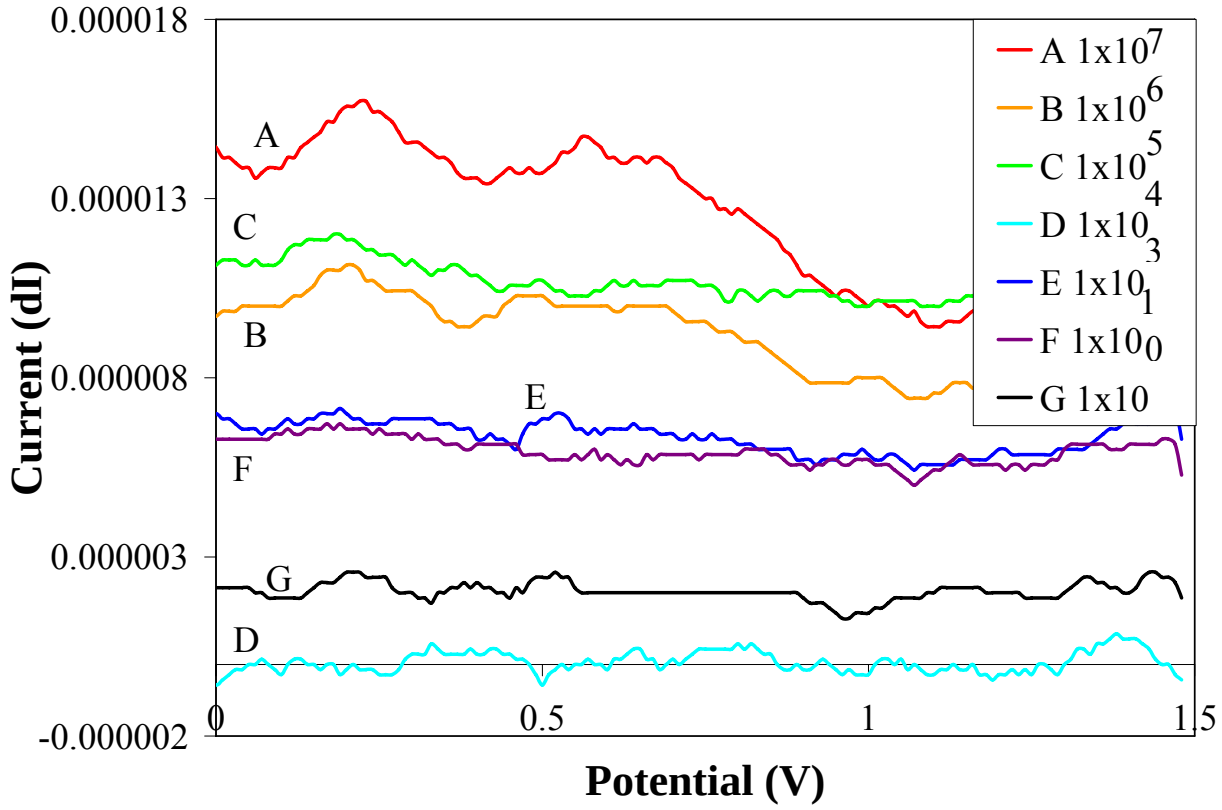

Figure 5-9: DVP response from sandwich assay. AuNPs were separated using 95°C without DTT to break sandwich structure.

The gold containing fraction after 15 minutes of incubation at 95°C did not exhibit any reduction/oxidation peaks or show appreciable signal. The corresponding MMP pellet was tested under the same gold detection method. The Figure 5-9 shows the presences of gold in five of the seven samples (lines A-C, E and F). The gold remaining after magnetic separation of the iron fraction indicated that the hybridized gold nanoparticles were not successfully freed by boiling alone. Based on the previous trials it was determined that electrochemical reduction/oxidation measurement can be performed on the whole sandwich structure alone, and a sample cannot be both electrochemically detected and fluorescently detected using this system.

5.3.4.2 Fluorescent readout

Fluorescent detection comparison was accomplished by splitting a serial dilution series of *E. coli* O157:H7 between each of the three fluorescence methods. DNA was extracted as before and the sandwich assay was performed using the appropriately generated gold nanoparticles. Detection of the labeled DNA was accomplished after a thiol liberation step. The gold and magnetic particles were pelleted at 13,000 x g for 25 minutes and the supernatant was readout. Figure 5-10 shows the signal from the dilution series for 6-FAM labeled gold nanoparticles.

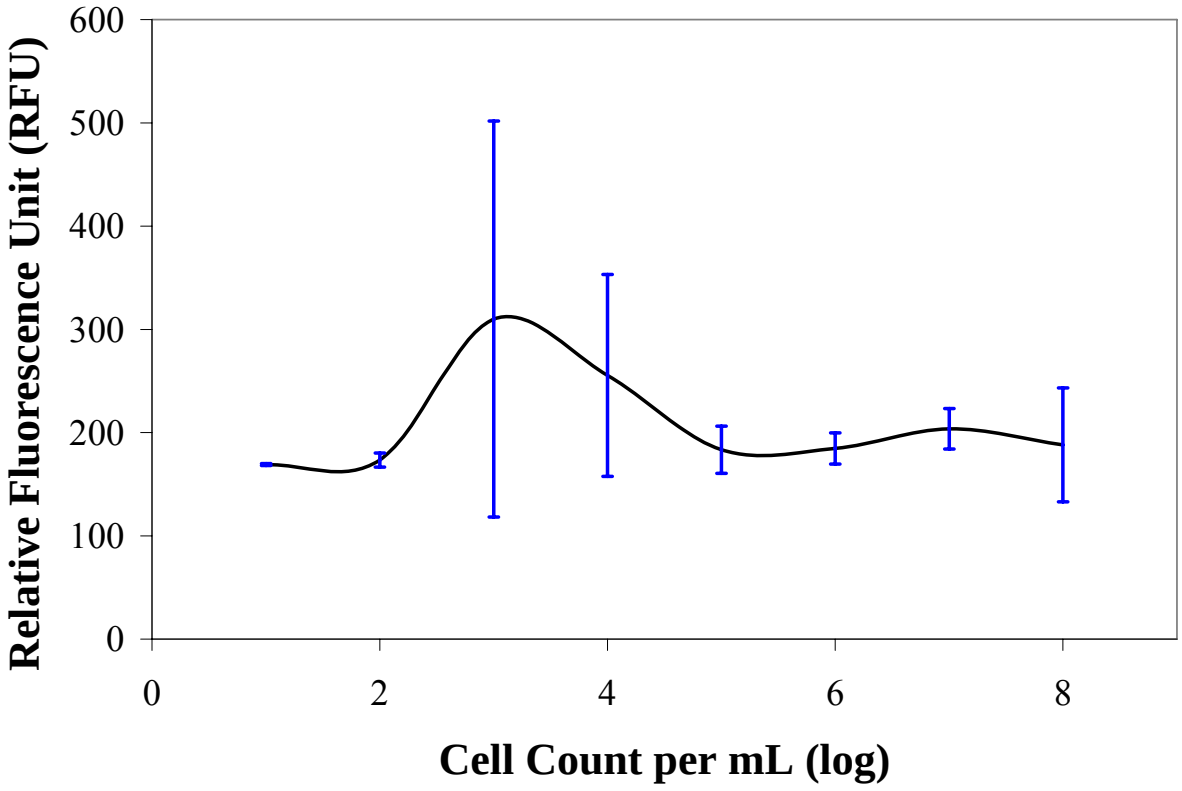

Figure 5-10: Fluorescence detection of 6-FAM end labeled DNA AuNPs. DNA was liberated using DTT exchange. Samples measured using fluorescein filters set.

The directly labeled DNA did not show a strong response to the amount of target after the sandwich assay. The result seen above in Figure 5-10 is a combination of multiple factors. The high amount of thiol used for liberating the DNA has the potential to attack the FAM reducing the signal. The low amount of reporter on the gold nanoparticles in addition to photo-bleaching during the assay and during gold-nanoparticle conjugation may also lead to the lower than expected signal. Previous efforts showing effective conjugation of 6-FAM-DNA to both citrate and dextrin generated gold nanoparticles utilized approximately 100 times the gold particles [12]. This work used lower DTT concentrations and the detection was in a smaller volume.

The AB-Thiol and C-Linker gold nanoparticles were tested per the methods section previous described and are shows in Figure 5-11.

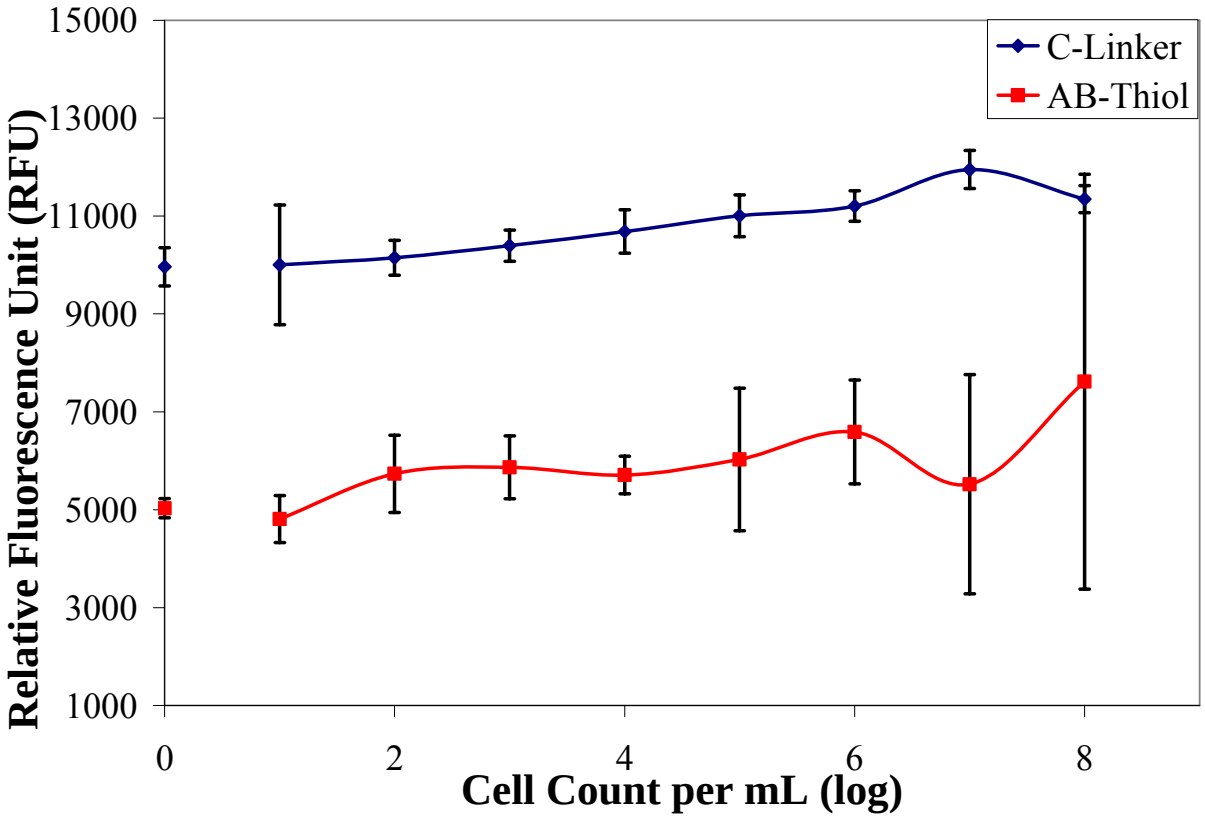

Figure 5-11: Fluorescence detection of co-polymerization amplification of sandwich assay. Blank samples are reported at the 0 cell count log value. Samples measured using fluorescein filters set.

Both of the co-polymerization methods showed a dose response. The AB-Thiol and C-Linker methods had detection in the 10^2 CFU/mL range. The difference between the two methods was seen in the signal strength and the higher range values. The AB-Thiol method has a weaker signal but was a simpler and faster method compared to the C-Linker amplification. The C-linker had a more consistent signal and larger signal, but required more time for detection. Both methods showed successful detection of the *stx1* target in *E. coli* O157:H7.

5.4 Conclusions

The described nanoparticle based biosensor in this chapter was successfully used to detect the *stx1* gene in *Escherichia coli* O157:H7 Sakai culture samples. To accomplish detection, a rapid and efficient DNA extraction method was determined and used to obtain PCR quality DNA target. The extraction method finalized was using the Trizol reagent, which only requires room temperature reactants and a low speed centrifuge. The nanoparticle sandwich assay was tested against serially diluted *E. coli* culture. Detection methods compared were reduction/oxidation and fluorescent co-polymerization hybridization. Both methods were capable of detecting target DNA from a 10^2 CFU/mL sample. Total assay time from sample to electrochemical detection or sample to fluorescence detection requires 7 hours.

The system developed and optimized in this study has comparable detection sensitivity and time requirements to other systems previously developed. The main strengths of the described system are the DNA extraction, low equipment needs, low cost, multiple detection formats, and an additional amplification step with co-polymerization hybridization.

Chapter 6: Conclusion and future work

The combined research presented in Chapters 3-5 described the engineering and development of a DNA based biosensor utilizing self assembling DNA sequences and carbohydrate coated gold nanoparticles to target the *stx1* gene in *Escherichia coli* O157:H7 Sakai. Current US government standards for water testing require 12-24 hours before detection. This detection is not specific to the pathogenic targets, but only identifies the presence of an indicator species commonly found along side pathogenic species of bacteria. The research in this dissertation presents a complete assay technique for DNA based identification in 7 hours, making it more specific and faster than currently approved methods.

Traditional DNA based biosensors require lengthy and involved DNA extraction processes to produce a pure input material for enzymatic amplification. In the presented system the extraction is accomplished with a commercial kit. The kit produces a DNA output compatible with the engineered assay system and requires less than 2 hours from sample to testing. The assay system uses a novel carbohydrate coated nanoparticle for amplification of the input signal. Carbohydrate generated gold nanoparticles were successfully generated under mild alkaline conditions and used in the sandwich assay for detection of the *stx1* gene in *Escherichia coli* O157:H7. The synthesis procedure was accomplished using dextrin, a carbohydrate, and sodium carbonate to initiate and form gold nanoparticles that were successfully decorated with DNA probes. Gold nanoparticle size was controllable based on generation conditions. The resulting particles were stable for over 6 months when left in the reaction solution and completely compatible for replacement of citrate generated particles for the uses in this dissertation.

A novel reporter system of self-assembling DNA molecules was designed for co-polymerization detection. Co-polymerization detection is currently capable of fluorescence measurement through the use of a dye with high quantum efficiency when bound to double-stranded DNA target. Co-polymerization is compatible with reduction / oxidation measurement through use of metallic tracers linked DNA intercalation dyes. To fully utilize electrochemical detection with co-polymerization, a means of separating free co-polymerization probe and excess dye needs to be developed. Normally the fluorescent dye will bind to the DNA probes on both particles, but does not contribute a fluorescent signal since the probes are single-stranded. The nanoparticle linked dye would bind the same single-strand probes, and would contribute a metallic reduction signal even in the absence of a target.

Successful detection using co-polymerization was accomplished when combined with a nano / microparticle sandwich assay and proper DNA extraction. DNA was successfully and rapidly extracted from live *Escherichia coli* O157:H7 Sakai and used directly as target in the sandwich assay. A DNA probe set was created and used to recognize the *stx1* gene from *E. coli* O157:H7 by the magnetic microparticle and gold nanoparticle. Both electrochemical detection of the gold nanoparticles and fluorescence detection with co-polymerization were successfully demonstrated. The hybridization based reporter system was shown to be capable of detecting as little as 10^5 colony forming units per milliliter. Electrochemical detection was capable of a presence / absence detection at 10^1 colony forming units per milliliter. The co-polymerization

method provided a rapid and sensitive fluorescent based detection method with increased sensitivity over end labeled reporter systems.

Future work is required to optimize both the electrochemical and fluorescent detection methods of co-polymerization hybridization. Further reduction in the DNA extraction and recovery time may be possible. Possible reduction in times could include reduced centrifuge times at higher speeds, additional wash steps with shorter washing times, reduction of the desalting step times, or simple removal of desalting steps. The removal of salt may not be necessary with the high salt hybridization buffer used during the sandwich assay. The dextrin gold nanoparticle generation method has potential for functionalizing the nanoparticles with biomaterials during the generation process. The conjugation of thiolated DNA and other functional groups during generation should be explored. Addition of the thiol group at different reaction times, thiol concentrations, reaction pH, or reaction temperatures may provide a one pot synthesis technique that produces functionalized gold nanoparticles. A primary amine functional group would be an ideal attachedment chemistry as it would allow for conjugation to carboxyl, hydroxyl, and thiol groups.

Exploration into exploiting the large signal increase at low dye to probe ratio in co-polymerization hybridization has potential for increased detection sensitivity. Optimization of PicoGreen and co-polymerization probe amounts may lead to a better signal to noise ratio. Reduction of background noise would also lead to higher sensitivities. The described assay system utilizes a polystyrene 96-well plate for readout. The aromatic nature of polystyrene binds free ssDNA probe and stabilizes the PicoGreen interaction with non-specifically bound ssDNA.

The stabilized dye fluorescence created higher background signal than polypropylene microcentrifuge tubes. Future use of polypropylene 96-well plates would help reduce background noise. The combination of optimized dye and probe concentration in polypropylene plate would help achieve maximum sensitivity for the fluorescent detection readout of the co-polymerization assay.

The sandwich assay was the longest step of the entire detection process. Reduction in time during hybridization would have the greatest impact on improving the assay speed. Optimization of hybridization time and temperature conditions may lead to a reduction of the assay time. Currently, the assay is performed at a single temperature, which is 10°C less than the melting temperature of the probes. Heating the initial binding step to a temperature twenty of more degrees higher than the melting temperature and allowing for a slower rate of cooling may promote faster hybridization of the magnetic microparticles in the same fashion as the co-polymerization hybridization self-assembly. The same optimization would then be possible with the gold nanoparticle hybridization step, providing further reduction in assay time.

The addition of electrochemical readout to the co-polymerization hybridization method would further add additional sensitivity to the assay. The addition of a metallic nanoparticle to the co-polymerization probe would be one way to introduce electrochemistry. Attachment of a QD could be accomplished through a modification to the probe's phosphate backbone. An internal thiol or phosphorothioate would provide a reactive sulfur atom for QD attachment. By introducing a QD-DNA structure to the tethered co-polymerization method in Chapter 5, a method of free QD-DNA removal would be possible. The QD attachment would also present the

opportunity for multiplexed detection through different metallic compositions, allowing for detection of multiple metals with differential pulse voltammetry.

In summary, this research demonstrates the successful integration of rapid DNA extraction, specific target detection with a sandwich assay, and both electrochemical and fluorescent detection capabilities. The use of electrochemical detection provides a rapid and sensitivity absence/presence test, and the fluorescence detection provides a promising tool for sample quantification.

APPENDICES

APPENDIX A: DATA

A.1 CHAPTER 3 DATA

Table A-1. Absorbance data of gold nanoparticles for Figure 3-1.

Time:	0 hr	1 hr	1.5 hr	2 hr	3 hr	4 hr	5 hr
Wavelength (nm)	Absorbance (AU)						
400	0.395	0.393	0.438	0.740	2.063	2.088	2.029
401	0.393	0.392	0.436	0.738	2.059	2.080	2.026
402	0.391	0.390	0.435	0.735	2.057	2.077	2.023
403	0.389	0.389	0.433	0.733	2.054	2.075	2.020
404	0.388	0.387	0.432	0.731	2.051	2.071	2.017
405	0.387	0.386	0.430	0.730	2.047	2.068	2.014
406	0.385	0.385	0.429	0.728	2.044	2.065	2.009
407	0.383	0.383	0.427	0.726	2.043	2.064	2.007
408	0.382	0.382	0.426	0.724	2.041	2.064	2.006
409	0.381	0.381	0.425	0.722	2.038	2.060	2.002
410	0.379	0.379	0.423	0.720	2.035	2.057	1.999
411	0.378	0.378	0.422	0.719	2.032	2.055	1.997
412	0.377	0.377	0.421	0.717	2.030	2.052	1.995
413	0.376	0.376	0.420	0.716	2.029	2.049	1.994
414	0.374	0.374	0.419	0.714	2.024	2.047	1.991
415	0.373	0.373	0.417	0.713	2.022	2.045	1.990
416	0.372	0.373	0.417	0.712	2.022	2.043	1.987
417	0.371	0.372	0.416	0.710	2.021	2.041	1.984
418	0.369	0.370	0.415	0.708	2.020	2.040	1.982
419	0.368	0.369	0.413	0.707	2.018	2.036	1.981
420	0.367	0.368	0.412	0.705	2.017	2.035	1.980
421	0.367	0.368	0.412	0.705	2.015	2.033	1.979
422	0.366	0.367	0.411	0.704	2.015	2.031	1.977
423	0.364	0.366	0.410	0.702	2.014	2.031	1.976
424	0.363	0.365	0.409	0.701	2.011	2.030	1.974
425	0.363	0.365	0.409	0.700	2.011	2.029	1.973
426	0.362	0.364	0.408	0.699	2.011	2.028	1.972
427	0.361	0.363	0.406	0.698	2.008	2.026	1.972
428	0.360	0.362	0.406	0.697	2.009	2.026	1.974
429	0.359	0.361	0.405	0.696	2.009	2.026	1.973
430	0.359	0.361	0.405	0.695	2.007	2.026	1.971

Table A-1. Continued

431	0.358	0.360	0.404	0.694	2.007	2.024	1.969
432	0.356	0.359	0.402	0.692	2.009	2.023	1.968
433	0.356	0.358	0.402	0.692	2.008	2.024	1.969
434	0.355	0.358	0.402	0.691	2.006	2.025	1.970
435	0.354	0.357	0.401	0.690	2.006	2.025	1.970
436	0.353	0.356	0.399	0.689	2.005	2.024	1.969
437	0.352	0.355	0.399	0.688	2.006	2.024	1.970
438	0.351	0.354	0.398	0.687	2.008	2.024	1.972
439	0.351	0.354	0.398	0.687	2.008	2.025	1.972
440	0.350	0.353	0.397	0.686	2.010	2.027	1.974
441	0.349	0.352	0.396	0.685	2.012	2.030	1.976
442	0.348	0.351	0.395	0.684	2.012	2.033	1.976
443	0.348	0.351	0.395	0.684	2.012	2.034	1.977
444	0.347	0.350	0.394	0.683	2.015	2.035	1.979
445	0.345	0.349	0.393	0.682	2.018	2.038	1.980
446	0.344	0.348	0.392	0.681	2.020	2.040	1.983
447	0.344	0.348	0.392	0.681	2.022	2.040	1.985
448	0.344	0.348	0.392	0.681	2.024	2.044	1.987
449	0.343	0.346	0.391	0.680	2.027	2.047	1.990
450	0.342	0.345	0.390	0.679	2.029	2.051	1.993
451	0.340	0.344	0.388	0.678	2.032	2.054	1.996
452	0.340	0.344	0.388	0.678	2.036	2.057	1.999
453	0.340	0.344	0.388	0.678	2.037	2.061	2.002
454	0.339	0.343	0.388	0.678	2.040	2.064	2.006
455	0.338	0.342	0.387	0.677	2.044	2.068	2.009
456	0.337	0.342	0.386	0.677	2.045	2.073	2.011
457	0.337	0.341	0.385	0.676	2.050	2.078	2.016
458	0.337	0.341	0.385	0.677	2.057	2.082	2.021
459	0.337	0.341	0.385	0.677	2.063	2.089	2.026
460	0.336	0.340	0.384	0.677	2.072	2.096	2.033
461	0.335	0.339	0.384	0.676	2.079	2.103	2.040
462	0.335	0.339	0.384	0.676	2.084	2.108	2.046
463	0.335	0.340	0.384	0.678	2.090	2.116	2.054
464	0.335	0.340	0.384	0.678	2.096	2.126	2.063
465	0.334	0.339	0.384	0.678	2.106	2.134	2.070
466	0.333	0.338	0.383	0.677	2.115	2.141	2.076
467	0.333	0.338	0.383	0.678	2.121	2.150	2.083
468	0.333	0.338	0.383	0.679	2.129	2.161	2.094
469	0.334	0.338	0.384	0.680	2.139	2.172	2.103
470	0.333	0.338	0.383	0.680	2.148	2.181	2.111
471	0.332	0.337	0.382	0.680	2.158	2.190	2.121

Table A-1. Continued

472	0.332	0.337	0.382	0.681	2.171	2.204	2.133
473	0.332	0.337	0.383	0.682	2.183	2.217	2.145
474	0.333	0.338	0.384	0.684	2.195	2.230	2.156
475	0.333	0.338	0.384	0.685	2.206	2.245	2.167
476	0.332	0.338	0.383	0.686	2.216	2.259	2.180
477	0.332	0.337	0.383	0.686	2.232	2.273	2.192
478	0.332	0.337	0.384	0.687	2.248	2.290	2.204
479	0.333	0.338	0.384	0.690	2.261	2.303	2.221
480	0.333	0.339	0.385	0.692	2.276	2.323	2.237
481	0.333	0.339	0.385	0.693	2.290	2.343	2.250
482	0.332	0.338	0.385	0.694	2.308	2.356	2.267
483	0.332	0.338	0.385	0.695	2.323	2.373	2.284
484	0.332	0.339	0.385	0.696	2.339	2.394	2.299
485	0.334	0.340	0.387	0.699	2.356	2.413	2.314
486	0.334	0.340	0.387	0.701	2.373	2.428	2.329
487	0.333	0.340	0.387	0.702	2.390	2.449	2.341
488	0.333	0.339	0.387	0.703	2.409	2.471	2.358
489	0.333	0.340	0.387	0.705	2.428	2.489	2.380
490	0.334	0.340	0.388	0.708	2.445	2.511	2.398
491	0.335	0.341	0.389	0.710	2.461	2.536	2.416
492	0.335	0.341	0.390	0.711	2.479	2.558	2.436
493	0.335	0.341	0.390	0.713	2.496	2.581	2.449
494	0.334	0.341	0.390	0.714	2.515	2.604	2.466
495	0.334	0.342	0.390	0.716	2.536	2.629	2.484
496	0.335	0.343	0.391	0.719	2.552	2.655	2.496
497	0.336	0.343	0.392	0.722	2.568	2.682	2.511
498	0.336	0.344	0.393	0.723	2.586	2.702	2.531
499	0.336	0.344	0.393	0.725	2.597	2.717	2.551
500	0.336	0.343	0.393	0.726	2.615	2.741	2.563
501	0.336	0.343	0.393	0.727	2.634	2.756	2.581
502	0.337	0.344	0.394	0.730	2.647	2.773	2.592
503	0.337	0.345	0.395	0.732	2.661	2.802	2.597
504	0.338	0.345	0.395	0.734	2.674	2.821	2.609
505	0.338	0.345	0.396	0.736	2.689	2.842	2.622
506	0.337	0.345	0.395	0.737	2.703	2.853	2.627
507	0.337	0.345	0.395	0.738	2.710	2.863	2.640
508	0.338	0.345	0.396	0.740	2.718	2.885	2.653
509	0.338	0.346	0.397	0.742	2.727	2.898	2.653
510	0.339	0.347	0.398	0.744	2.732	2.898	2.667
511	0.339	0.347	0.398	0.745	2.748	2.909	2.681
512	0.339	0.347	0.398	0.745	2.760	2.920	2.681

Table A-1. Continued

513	0.338	0.346	0.398	0.746	2.760	2.920	2.681
514	0.339	0.347	0.398	0.747	2.760	2.920	2.681
515	0.339	0.348	0.400	0.749	2.769	2.934	2.689
516	0.340	0.349	0.400	0.751	2.779	2.960	2.697
517	0.340	0.349	0.401	0.752	2.769	2.960	2.697
518	0.340	0.349	0.400	0.753	2.769	2.948	2.689
519	0.340	0.348	0.400	0.753	2.779	2.960	2.689
520	0.340	0.348	0.400	0.753	2.779	2.960	2.697
521	0.340	0.349	0.401	0.754	2.779	2.948	2.697
522	0.341	0.349	0.402	0.755	2.779	2.960	2.697
523	0.342	0.350	0.403	0.756	2.779	2.960	2.697
524	0.342	0.350	0.403	0.757	2.762	2.948	2.697
525	0.341	0.350	0.402	0.756	2.743	2.948	2.689
526	0.341	0.350	0.402	0.756	2.750	2.934	2.681
527	0.341	0.350	0.402	0.756	2.750	2.920	2.674
528	0.342	0.351	0.403	0.756	2.734	2.920	2.661
529	0.343	0.351	0.404	0.757	2.727	2.909	2.653
530	0.343	0.352	0.405	0.757	2.717	2.883	2.646
531	0.343	0.352	0.404	0.757	2.700	2.858	2.631
532	0.342	0.351	0.404	0.756	2.687	2.839	2.619
533	0.342	0.351	0.404	0.755	2.673	2.819	2.607
534	0.343	0.351	0.404	0.755	2.659	2.802	2.589
535	0.343	0.352	0.405	0.755	2.646	2.777	2.574
536	0.344	0.353	0.406	0.756	2.626	2.750	2.558
537	0.345	0.353	0.406	0.755	2.597	2.725	2.537
538	0.344	0.353	0.406	0.754	2.582	2.695	2.517
539	0.344	0.353	0.406	0.753	2.570	2.667	2.498
540	0.344	0.353	0.405	0.751	2.543	2.636	2.476
541	0.344	0.353	0.406	0.751	2.514	2.600	2.446
542	0.345	0.354	0.406	0.750	2.486	2.560	2.419
543	0.345	0.355	0.407	0.750	2.455	2.525	2.397
544	0.346	0.355	0.407	0.749	2.423	2.487	2.365
545	0.346	0.355	0.407	0.748	2.389	2.441	2.327
546	0.346	0.355	0.407	0.746	2.357	2.402	2.293
547	0.345	0.354	0.406	0.744	2.322	2.364	2.260
548	0.345	0.354	0.406	0.743	2.283	2.322	2.226
549	0.346	0.355	0.407	0.741	2.248	2.277	2.190
550	0.346	0.356	0.407	0.741	2.209	2.232	2.153
551	0.347	0.357	0.408	0.740	2.170	2.189	2.113
552	0.348	0.357	0.408	0.739	2.129	2.148	2.075
553	0.348	0.356	0.407	0.737	2.088	2.105	2.037

Table A-1. Continued

554	0.347	0.356	0.407	0.734	2.051	2.063	1.996
555	0.347	0.356	0.407	0.732	2.012	2.020	1.955
556	0.347	0.356	0.407	0.731	1.970	1.975	1.915
557	0.348	0.357	0.407	0.730	1.931	1.932	1.875
558	0.349	0.357	0.407	0.729	1.891	1.891	1.836
559	0.349	0.358	0.408	0.727	1.850	1.849	1.796
560	0.349	0.358	0.407	0.725	1.811	1.808	1.757
561	0.348	0.357	0.407	0.723	1.773	1.768	1.718
562	0.348	0.357	0.406	0.720	1.734	1.728	1.678
563	0.348	0.356	0.406	0.718	1.696	1.688	1.640
564	0.348	0.357	0.406	0.717	1.656	1.647	1.601
565	0.349	0.357	0.406	0.715	1.618	1.609	1.563
566	0.349	0.358	0.407	0.713	1.581	1.572	1.527
567	0.350	0.358	0.406	0.712	1.545	1.534	1.491
568	0.349	0.358	0.406	0.709	1.509	1.498	1.456
569	0.349	0.357	0.405	0.706	1.474	1.463	1.422
570	0.348	0.357	0.405	0.704	1.439	1.428	1.387
571	0.348	0.356	0.404	0.701	1.406	1.394	1.352
572	0.349	0.356	0.404	0.700	1.373	1.360	1.318
573	0.349	0.357	0.404	0.698	1.339	1.327	1.286
574	0.349	0.357	0.404	0.696	1.307	1.295	1.254
575	0.350	0.358	0.404	0.694	1.277	1.264	1.223
576	0.349	0.357	0.403	0.692	1.247	1.234	1.193
577	0.348	0.356	0.402	0.689	1.219	1.204	1.164
578	0.348	0.355	0.401	0.686	1.190	1.176	1.136
579	0.347	0.355	0.401	0.683	1.161	1.148	1.107
580	0.348	0.355	0.401	0.682	1.134	1.121	1.079
581	0.348	0.355	0.401	0.680	1.108	1.094	1.051
582	0.348	0.356	0.400	0.678	1.081	1.067	1.024
583	0.349	0.356	0.400	0.675	1.055	1.041	0.998
584	0.348	0.355	0.400	0.673	1.029	1.015	0.972
585	0.347	0.354	0.398	0.670	1.005	0.991	0.947
586	0.346	0.353	0.397	0.668	0.981	0.967	0.923
587	0.346	0.353	0.396	0.665	0.958	0.944	0.899
588	0.345	0.352	0.396	0.662	0.935	0.922	0.877
589	0.346	0.352	0.396	0.660	0.913	0.900	0.855
590	0.346	0.353	0.396	0.659	0.892	0.879	0.833
591	0.346	0.353	0.395	0.657	0.871	0.858	0.811
592	0.346	0.352	0.395	0.654	0.851	0.838	0.791
593	0.345	0.351	0.393	0.652	0.831	0.817	0.770
594	0.344	0.351	0.392	0.648	0.811	0.798	0.750

Table A-1. Continued

595	0.343	0.350	0.391	0.645	0.792	0.779	0.731
596	0.343	0.349	0.390	0.643	0.773	0.760	0.712
597	0.343	0.348	0.389	0.641	0.755	0.742	0.693
598	0.343	0.349	0.389	0.638	0.737	0.725	0.676
599	0.343	0.349	0.389	0.636	0.720	0.708	0.659
600	0.343	0.349	0.389	0.635	0.703	0.691	0.642
601	0.343	0.348	0.388	0.633	0.687	0.674	0.626
602	0.342	0.347	0.386	0.630	0.670	0.658	0.610
603	0.340	0.346	0.385	0.627	0.654	0.642	0.594
604	0.339	0.345	0.383	0.624	0.639	0.627	0.579
605	0.339	0.344	0.382	0.621	0.624	0.612	0.563
606	0.339	0.344	0.382	0.619	0.610	0.598	0.549
607	0.339	0.344	0.381	0.617	0.596	0.584	0.535
608	0.339	0.344	0.381	0.615	0.582	0.571	0.521
609	0.339	0.344	0.381	0.613	0.569	0.557	0.507
610	0.338	0.343	0.380	0.611	0.555	0.544	0.493
611	0.337	0.342	0.378	0.608	0.543	0.531	0.480
612	0.336	0.341	0.377	0.605	0.530	0.519	0.467
613	0.335	0.339	0.375	0.602	0.517	0.506	0.455
614	0.334	0.339	0.374	0.600	0.505	0.494	0.443
615	0.333	0.338	0.373	0.598	0.493	0.482	0.431
616	0.333	0.338	0.373	0.596	0.482	0.471	0.419
617	0.334	0.337	0.372	0.594	0.470	0.459	0.408
618	0.334	0.337	0.372	0.592	0.459	0.448	0.396
619	0.333	0.337	0.371	0.591	0.448	0.437	0.385
620	0.332	0.336	0.370	0.588	0.437	0.427	0.373
621	0.331	0.335	0.368	0.585	0.427	0.416	0.363
622	0.330	0.334	0.367	0.582	0.416	0.405	0.352
623	0.329	0.333	0.365	0.580	0.406	0.395	0.342
624	0.329	0.332	0.365	0.578	0.396	0.385	0.332
625	0.329	0.331	0.364	0.576	0.386	0.375	0.322
626	0.328	0.331	0.364	0.575	0.377	0.366	0.313
627	0.328	0.331	0.363	0.573	0.368	0.358	0.305
628	0.328	0.331	0.363	0.571	0.360	0.349	0.297
629	0.327	0.330	0.362	0.569	0.352	0.341	0.289
630	0.326	0.329	0.360	0.566	0.344	0.333	0.281
631	0.325	0.327	0.358	0.563	0.336	0.325	0.274
632	0.323	0.326	0.357	0.560	0.328	0.318	0.266
633	0.322	0.325	0.355	0.558	0.321	0.310	0.259
634	0.322	0.324	0.354	0.556	0.313	0.303	0.251

Table A-1. Continued

635	0.322	0.324	0.354	0.554	0.306	0.296	0.244
636	0.322	0.324	0.353	0.553	0.299	0.289	0.237
637	0.321	0.323	0.353	0.551	0.292	0.282	0.230
638	0.321	0.323	0.352	0.550	0.285	0.275	0.223
639	0.321	0.322	0.351	0.547	0.278	0.268	0.216
640	0.320	0.321	0.350	0.545	0.272	0.262	0.209
641	0.318	0.320	0.348	0.542	0.265	0.255	0.202
642	0.317	0.318	0.346	0.540	0.258	0.249	0.196
643	0.316	0.318	0.345	0.538	0.252	0.242	0.189
644	0.316	0.317	0.345	0.536	0.246	0.236	0.183
645	0.315	0.316	0.344	0.535	0.240	0.230	0.177
646	0.315	0.317	0.343	0.533	0.234	0.224	0.170
647	0.315	0.316	0.343	0.531	0.228	0.218	0.164
648	0.315	0.316	0.342	0.530	0.222	0.212	0.159
649	0.314	0.315	0.341	0.528	0.216	0.207	0.153
650	0.313	0.314	0.340	0.526	0.211	0.201	0.147
651	0.312	0.312	0.338	0.523	0.205	0.196	0.142
652	0.311	0.311	0.336	0.521	0.200	0.191	0.136
653	0.310	0.310	0.335	0.519	0.195	0.185	0.131
654	0.309	0.309	0.334	0.516	0.189	0.180	0.125
655	0.309	0.308	0.334	0.515	0.184	0.175	0.120
656	0.308	0.309	0.333	0.514	0.180	0.170	0.116
657	0.308	0.309	0.333	0.512	0.175	0.166	0.111
658	0.308	0.308	0.332	0.511	0.170	0.161	0.106
659	0.308	0.307	0.331	0.509	0.166	0.156	0.101
660	0.307	0.306	0.330	0.507	0.161	0.152	0.097
661	0.305	0.305	0.329	0.505	0.157	0.147	0.092
662	0.304	0.304	0.327	0.502	0.152	0.143	0.088
663	0.303	0.302	0.326	0.500	0.148	0.139	0.083
664	0.302	0.301	0.324	0.498	0.144	0.134	0.079
665	0.301	0.300	0.323	0.496	0.140	0.130	0.075
666	0.301	0.300	0.322	0.495	0.135	0.126	0.071
667	0.301	0.300	0.322	0.493	0.132	0.122	0.067
668	0.300	0.299	0.322	0.492	0.128	0.118	0.063
669	0.300	0.299	0.321	0.491	0.124	0.115	0.059
670	0.300	0.298	0.320	0.489	0.120	0.111	0.056
671	0.299	0.297	0.318	0.487	0.116	0.107	0.052
672	0.297	0.296	0.317	0.485	0.113	0.103	0.048
673	0.296	0.294	0.316	0.482	0.109	0.100	0.044
674	0.295	0.293	0.314	0.480	0.106	0.096	0.041
675	0.294	0.292	0.313	0.478	0.102	0.093	0.038

Table A-1. Continued

676	0.293	0.291	0.312	0.476	0.099	0.090	0.034
677	0.292	0.290	0.311	0.475	0.096	0.086	0.031
678	0.292	0.290	0.310	0.473	0.092	0.083	0.028
679	0.292	0.290	0.310	0.472	0.089	0.080	0.025
680	0.291	0.289	0.309	0.471	0.086	0.077	0.022
681	0.291	0.288	0.308	0.469	0.083	0.074	0.019
682	0.290	0.288	0.307	0.467	0.080	0.071	0.016
683	0.289	0.286	0.306	0.465	0.077	0.068	0.013
684	0.287	0.285	0.304	0.463	0.074	0.065	0.010
685	0.286	0.283	0.302	0.461	0.071	0.062	0.007
686	0.284	0.282	0.301	0.458	0.068	0.059	0.004
687	0.283	0.281	0.299	0.457	0.066	0.057	0.001
688	0.283	0.280	0.298	0.455	0.063	0.054	-0.001
689	0.282	0.279	0.298	0.454	0.060	0.052	-0.004
690	0.282	0.279	0.297	0.453	0.058	0.049	-0.007
691	0.282	0.278	0.297	0.451	0.055	0.046	-0.009
692	0.281	0.278	0.296	0.449	0.053	0.044	-0.011
693	0.280	0.277	0.295	0.448	0.050	0.042	-0.014
694	0.279	0.275	0.293	0.446	0.048	0.039	-0.016
695	0.278	0.274	0.292	0.444	0.046	0.037	-0.019
696	0.277	0.273	0.291	0.442	0.043	0.034	-0.021
697	0.275	0.272	0.289	0.440	0.041	0.032	-0.023
698	0.274	0.270	0.287	0.438	0.039	0.030	-0.025
699	0.273	0.269	0.286	0.436	0.037	0.028	-0.028
700	0.272	0.268	0.285	0.434	0.035	0.026	-0.030

Table A-2. Additional absorbance data of gold nanoparticles for Figure 3-1.

Time:	**6 hr**	**12 hr**	**24 hr**
Wavelength (nm)	Absorbance (AU)		
400	2.282	2.301	2.373
401	2.279	2.297	2.369
402	2.276	2.293	2.364
403	2.272	2.288	2.360
404	2.271	2.284	2.358
405	2.267	2.286	2.355
406	2.264	2.282	2.351
407	2.258	2.275	2.347
408	2.254	2.274	2.340
409	2.253	2.269	2.336
410	2.248	2.266	2.335
411	2.244	2.265	2.333
412	2.240	2.261	2.329
413	2.236	2.259	2.322
414	2.235	2.255	2.322
415	2.233	2.250	2.322
416	2.229	2.248	2.315
417	2.226	2.247	2.311
418	2.223	2.244	2.309
419	2.222	2.243	2.307
420	2.221	2.243	2.308
421	2.219	2.237	2.306
422	2.214	2.235	2.304
423	2.211	2.236	2.300
424	2.212	2.235	2.298
425	2.212	2.232	2.299
426	2.211	2.228	2.297
427	2.207	2.227	2.295
428	2.204	2.226	2.296
429	2.204	2.223	2.293
430	2.203	2.221	2.290
431	2.200	2.219	2.290
432	2.200	2.219	2.289
433	2.199	2.221	2.288
434	2.197	2.219	2.287
435	2.196	2.218	2.287
436	2.197	2.220	2.287

Table A-2. Continued

437	2.198	2.222	2.288
438	2.199	2.223	2.288
439	2.199	2.223	2.287
440	2.199	2.221	2.288
441	2.200	2.222	2.291
442	2.201	2.226	2.294
443	2.203	2.227	2.294
444	2.204	2.227	2.295
445	2.204	2.229	2.299
446	2.207	2.231	2.303
447	2.211	2.233	2.305
448	2.210	2.235	2.307
449	2.211	2.236	2.308
450	2.215	2.240	2.310
451	2.218	2.244	2.315
452	2.220	2.248	2.318
453	2.223	2.251	2.321
454	2.227	2.252	2.327
455	2.232	2.256	2.331
456	2.236	2.263	2.337
457	2.240	2.267	2.344
458	2.246	2.273	2.351
459	2.249	2.278	2.355
460	2.255	2.285	2.359
461	2.261	2.292	2.366
462	2.269	2.299	2.375
463	2.274	2.308	2.382
464	2.279	2.314	2.388
465	2.288	2.321	2.397
466	2.296	2.332	2.410
467	2.304	2.340	2.421
468	2.312	2.348	2.428
469	2.318	2.354	2.435
470	2.328	2.361	2.443
471	2.342	2.373	2.457
472	2.354	2.385	2.471
473	2.362	2.397	2.483
474	2.373	2.410	2.497
475	2.386	2.422	2.512
476	2.398	2.436	2.529
477	2.409	2.449	2.543

Table A-2. Continued

478	2.421	2.463	2.556
479	2.436	2.480	2.574
480	2.448	2.493	2.588
481	2.464	2.506	2.607
482	2.480	2.522	2.627
483	2.492	2.543	2.644
484	2.510	2.564	2.665
485	2.526	2.582	2.687
486	2.542	2.593	2.707
487	2.563	2.612	2.727
488	2.582	2.636	2.748
489	2.601	2.658	2.771
490	2.617	2.676	2.795
491	2.633	2.689	2.819
492	2.653	2.708	2.844
493	2.676	2.734	2.865
494	2.695	2.756	2.888
495	2.715	2.773	2.912
496	2.736	2.795	2.937
497	2.752	2.812	2.963
498	2.773	2.826	2.979
499	2.789	2.846	2.995
500	2.802	2.865	3.014
501	2.821	2.883	3.046
502	2.841	2.906	3.068
503	2.856	2.920	3.080
504	2.868	2.928	3.101
505	2.883	2.946	3.127
506	2.898	2.963	3.154
507	2.915	2.972	3.154
508	2.934	2.982	3.154
509	2.948	2.991	3.184
510	2.954	3.001	3.205
511	2.954	3.011	3.205
512	2.966	3.011	3.216
513	2.979	3.021	3.227
514	2.979	3.031	3.227
515	2.985	3.031	3.227
516	2.991	3.031	3.244
517	3.004	3.031	3.244
518	3.018	3.031	3.227

Table A-2. Continued

519	3.018	3.031	3.227
520	3.018	3.031	3.232
521	3.008	3.031	3.238
522	3.008	3.031	3.238
523	3.008	3.031	3.238
524	3.008	3.031	3.238
525	3.008	3.031	3.221
526	2.998	3.024	3.205
527	2.998	3.018	3.205
528	2.991	3.008	3.179
529	2.982	2.988	3.154
530	2.969	2.969	3.150
531	2.951	2.960	3.136
532	2.945	2.954	3.101
533	2.940	2.931	3.065
534	2.923	2.906	3.046
535	2.901	2.893	3.028
536	2.878	2.873	2.998
537	2.863	2.844	2.964
538	2.846	2.819	2.931
539	2.821	2.791	2.894
540	2.802	2.764	2.854
541	2.781	2.739	2.817
542	2.756	2.712	2.778
543	2.731	2.679	2.736
544	2.702	2.640	2.697
545	2.669	2.600	2.652
546	2.635	2.561	2.604
547	2.604	2.523	2.559
548	2.572	2.488	2.515
549	2.536	2.451	2.472
550	2.503	2.408	2.426
551	2.469	2.368	2.379
552	2.431	2.325	2.334
553	2.391	2.282	2.289
554	2.355	2.243	2.244
555	2.322	2.202	2.200
556	2.286	2.161	2.156
557	2.247	2.120	2.112
558	2.207	2.079	2.068
559	2.169	2.036	2.024

Table A-2. Continued

560	2.131	1.995	1.980
561	2.093	1.956	1.939
562	2.055	1.916	1.898
563	2.019	1.876	1.858
564	1.982	1.838	1.817
565	1.945	1.800	1.777
566	1.907	1.762	1.738
567	1.871	1.725	1.700
568	1.836	1.689	1.663
569	1.801	1.653	1.626
570	1.768	1.618	1.590
571	1.733	1.584	1.556
572	1.700	1.551	1.522
573	1.667	1.518	1.488
574	1.633	1.486	1.455
575	1.601	1.454	1.423
576	1.569	1.424	1.392
577	1.538	1.394	1.362
578	1.510	1.366	1.332
579	1.482	1.338	1.303
580	1.454	1.310	1.275
581	1.425	1.282	1.247
582	1.396	1.255	1.220
583	1.369	1.228	1.192
584	1.341	1.203	1.166
585	1.315	1.178	1.142
586	1.290	1.155	1.117
587	1.265	1.132	1.093
588	1.241	1.109	1.070
589	1.218	1.086	1.047
590	1.194	1.064	1.025
591	1.170	1.042	1.002
592	1.148	1.020	0.980
593	1.126	0.999	0.959
594	1.105	0.979	0.940
595	1.085	0.960	0.921
596	1.064	0.942	0.903
597	1.045	0.924	0.884
598	1.025	0.907	0.866
599	1.005	0.889	0.848
600	0.986	0.871	0.830

Table A-2. Continued

601	0.967	0.854	0.813
602	0.949	0.838	0.796
603	0.932	0.822	0.780
604	0.916	0.807	0.765
605	0.899	0.792	0.750
606	0.883	0.777	0.735
607	0.867	0.761	0.720
608	0.851	0.747	0.705
609	0.835	0.732	0.690
610	0.820	0.718	0.676
611	0.805	0.705	0.663
612	0.791	0.692	0.651
613	0.778	0.680	0.638
614	0.764	0.668	0.627
615	0.751	0.656	0.615
616	0.738	0.644	0.604
617	0.724	0.632	0.592
618	0.711	0.621	0.581
619	0.699	0.610	0.570
620	0.686	0.599	0.559
621	0.675	0.589	0.549
622	0.664	0.580	0.540
623	0.654	0.570	0.530
624	0.643	0.561	0.521
625	0.632	0.551	0.512
626	0.622	0.542	0.502
627	0.611	0.532	0.492
628	0.600	0.522	0.483
629	0.590	0.513	0.473
630	0.580	0.504	0.465
631	0.571	0.496	0.457
632	0.562	0.488	0.449
633	0.553	0.480	0.441
634	0.545	0.472	0.434
635	0.536	0.464	0.426
636	0.527	0.456	0.418
637	0.519	0.448	0.411
638	0.510	0.441	0.403
639	0.502	0.433	0.396
640	0.493	0.426	0.389
641	0.486	0.419	0.383

Table A-2. Continued

642	0.479	0.413	0.377
643	0.472	0.407	0.371
644	0.465	0.401	0.366
645	0.457	0.394	0.359
646	0.450	0.388	0.353
647	0.443	0.381	0.347
648	0.436	0.375	0.341
649	0.429	0.369	0.335
650	0.422	0.363	0.330
651	0.416	0.358	0.325
652	0.410	0.353	0.320
653	0.405	0.348	0.316
654	0.399	0.344	0.311
655	0.394	0.338	0.307
656	0.388	0.333	0.302
657	0.382	0.328	0.297
658	0.376	0.323	0.293
659	0.370	0.318	0.288
660	0.365	0.313	0.283
661	0.360	0.309	0.279
662	0.355	0.305	0.275
663	0.350	0.301	0.272
664	0.346	0.297	0.268
665	0.342	0.293	0.265
666	0.337	0.289	0.261
667	0.332	0.285	0.257
668	0.328	0.281	0.253
669	0.323	0.277	0.249
670	0.318	0.273	0.245
671	0.313	0.269	0.241
672	0.310	0.265	0.238
673	0.306	0.262	0.235
674	0.303	0.259	0.233
675	0.300	0.256	0.230
676	0.296	0.253	0.227
677	0.292	0.250	0.224
678	0.288	0.247	0.221
679	0.284	0.243	0.218
680	0.281	0.239	0.214
681	0.277	0.236	0.211
682	0.273	0.233	0.208

Table A-2. Continued

683	0.270	0.230	0.205
684	0.267	0.227	0.203
685	0.264	0.225	0.201
686	0.261	0.223	0.199
687	0.258	0.220	0.197
688	0.256	0.218	0.194
689	0.253	0.215	0.192
690	0.250	0.212	0.189
691	0.246	0.209	0.186
692	0.243	0.206	0.184
693	0.240	0.204	0.181
694	0.237	0.201	0.179
695	0.234	0.199	0.177
696	0.232	0.197	0.175
697	0.230	0.195	0.174
698	0.228	0.193	0.172
699	0.226	0.192	0.170
700	0.224	0.190	0.169

Table A-3. Particle diameter data for Table 3-3.

	Figure 3-3b		Figure 3-3d		Figure 3-3f	
Size (nm)	Count (n)	Fraction (%)	Count (n)	Fraction (%)	Count (n)	Fraction (%)
0-1	0	0.0%	0	0.0%	0	0.0%
1-2	0	0.0%	0	0.0%	0	0.0%
2-3	0	0.0%	0	0.0%	0	0.0%
3-4	1	0.2%	0	0.0%	0	0.0%
4-5	9	1.4%	0	0.0%	0	0.0%
5-6	45	7.1%	3	0.5%	1	0.2%
6-7	134	21.1%	6	0.9%	0	0.0%
7-8	206	32.4%	21	3.3%	0	0.0%
8-9	154	24.3%	44	6.9%	7	1.1%
9-10	70	11.0%	62	9.8%	27	4.3%
10-11	14	2.2%	75	11.8%	63	9.9%
11-12	2	0.3%	66	10.4%	55	8.7%
12-13	0	0.0%	32	5.0%	45	7.1%
13-14	0	0.0%	6	0.9%	34	5.4%
14-15	0	0.0%	0	0.0%	15	2.4%
15-16	0	0.0%	1	0.2%	0	0.0%
16-17	0	0.0%	0	0.0%	1	0.2%
17-18	0	0.0%	0	0.0%	0	0.0%
18-19	0	0.0%	0	0.0%	0	0.0%
19-20	0	0.0%	0	0.0%	0	0.0%
	8.64	Average Diameter (nm)	11.19	Average Diameter (nm)	12.56	Average Diameter (nm)
	1.21	Standard Deviation (nm)	1.58	Standard Deviation (nm)	1.53	Standard Deviation (nm)
	635	Total Count (n)	316	Total Count (n)	248	Total Count (n)

Table A-4. Dextrin generation conditions for gold nanoparticle size data for Figure 3-4.

Dextrin Concentration (g/L)	Diameter (nm)	Standard Deviation (nm)
25	8.20	1.07
20	8.80	1.26
15	10.12	1.48
10	10.59	1.79
7.5	11.13	2.65
2.5	12.44	1.49

Table A-5. Data for pH generation conditions for gold nanoparticle size data Figure 3-5.

Generation pH	Dextrin Concentration (g/L)	Diameter (nm)	Standard Deviation (nm)
7	20	13.70	2.44
8	20	10.15	1.24
9	20	9.17	1.45
10	20	6.99	1.25
11	20	5.89	0.94
7	10	14.58	2.55
8	10	13.33	4.22
9	10	10.58	1.82
10	10	9.47	1.63
11	10	9.23	1.36
9	2.5	16.83	2.26
10	2.5	13.62	1.23
11	2.5	12.22	1.02

Table A-6. Data for temperature generation of gold nanoparticle size data for Figure 3-6.

Generation Temp (°C)	Dextrin Concentration (g/L)	Diameter (nm)	Standard Deviation (nm)
25	20	7.07	0.99
25	10	8.28	1.11
25	2.5	10.05	1.45
50	25	8.20	1.07
50	20	8.80	1.26
50	15	10.12	1.48
50	10	10.59	1.79
50	7.5	11.13	2.65
50	2.5	12.44	1.49

Table A-7. Data for UV absorbance vs. time for Figure 3-7.

Time (hrs)	Dextrin generation condition					
	20g/L	15g/L	10g/L	7.5g/L	5g/L	2.5g/L
0.5	0.708	0.578	0.357	0.284	0.178	0.087
1.5	2.345	1.293	0.407	0.336	0.189	0.104
2	5.858	3.780	0.753	0.628	0.221	0.108
2.5	5.482	5.468	5.406	5.306	0.453	0.129
3	5.486	5.454	5.558	5.558	2.033	0.372
3.5	5.436	5.490	5.454	5.896	4.996	1.247
4	5.454	5.394	5.920	5.896	5.976	2.199
4.5	5.868	5.394	5.362	5.454	5.468	3.385
5	5.306	5.520	5.394	5.454	5.436	4.964
5.5	5.246	5.254	5.282	5.306	5.362	5.362
6	6.348	6.036	6.152	6.144	6.202	6.290
12	6.410	6.036	6.062	6.106	6.152	5.090
24	6.300	5.862	6.488	6.656	6.548	6.348

Table A-8. Data for UV-Vis absorbance of dextrin species for Figure 3-9.

Wave Number (cm^{-1})	Absorbance (%)		
	Stock	Auto-claved	AuNP Bound
501	41.5%	36.3%	20.8%
507	41.9%	36.9%	20.7%
513	42.1%	36.9%	21.0%
519	42.5%	37.6%	21.1%
525	42.7%	37.7%	21.2%
530	42.5%	37.8%	21.4%
536	42.0%	37.6%	21.1%
542	41.5%	37.1%	21.4%
548	41.6%	37.4%	21.3%
553	41.8%	37.3%	21.5%
559	42.2%	38.0%	21.7%
565	42.6%	38.1%	21.6%
571	43.0%	38.8%	21.6%
577	43.0%	38.9%	21.5%
582	42.5%	38.6%	21.6%
588	41.9%	38.3%	21.7%
594	41.9%	38.1%	21.8%
600	41.7%	38.2%	21.8%
606	41.5%	37.9%	21.6%
611	41.3%	38.0%	21.5%
617	41.0%	37.5%	21.5%
623	40.4%	37.3%	21.3%
629	40.0%	36.9%	21.4%
634	39.6%	36.6%	21.2%
640	39.4%	36.5%	21.3%
646	39.1%	36.2%	21.0%
652	39.0%	36.3%	20.9%
658	38.9%	36.0%	20.9%
663	38.8%	36.2%	20.7%
669	38.7%	35.9%	20.8%
675	38.5%	35.9%	20.5%
681	38.2%	35.6%	20.5%
687	37.9%	35.4%	20.2%
692	37.8%	35.5%	20.2%
698	37.9%	35.4%	20.2%
704	38.0%	35.8%	20.0%

Wave Number (cm^{-1})	Absorbance (%)		
	Stock	Auto-claved	AuNP Bound
2225	28.7%	33.1%	23.5%
2231	28.6%	33.1%	23.5%
2237	28.6%	33.1%	23.5%
2243	28.6%	33.1%	23.5%
2249	28.6%	33.1%	23.5%
2254	28.5%	33.1%	23.5%
2260	28.5%	33.1%	23.5%
2266	28.5%	33.1%	23.6%
2272	28.5%	33.1%	23.6%
2278	28.5%	33.1%	23.6%
2283	28.5%	33.1%	23.6%
2289	28.5%	33.1%	23.6%
2295	28.5%	33.2%	23.7%
2301	28.4%	33.2%	23.7%
2306	28.4%	33.2%	23.7%
2312	28.4%	33.2%	23.7%
2318	28.4%	33.2%	23.7%
2324	28.5%	33.2%	23.8%
2330	28.5%	33.2%	23.8%
2335	28.5%	33.3%	23.8%
2341	28.5%	33.3%	23.8%
2347	28.5%	33.4%	23.8%
2353	28.6%	33.4%	23.9%
2359	28.6%	33.4%	23.9%
2364	28.6%	33.5%	23.9%
2370	28.7%	33.5%	23.9%
2376	28.7%	33.5%	24.0%
2382	28.7%	33.5%	24.0%
2387	28.8%	33.6%	24.0%
2393	28.8%	33.6%	24.1%
2399	28.8%	33.7%	24.1%
2405	28.9%	33.7%	24.1%
2411	28.9%	33.8%	24.2%
2416	29.0%	33.8%	24.2%
2422	29.0%	33.9%	24.3%
2428	29.2%	34.0%	24.3%

Table A-8. Continued

710	38.0%	35.6%	20.1%	2434	29.2%	34.0%	24.3%
715	37.8%	35.6%	19.9%	2440	29.3%	34.1%	24.4%
721	37.0%	34.9%	19.8%	2445	29.4%	34.1%	24.4%
727	36.4%	34.5%	19.6%	2451	29.5%	34.2%	24.5%
733	35.9%	34.1%	19.5%	2457	29.5%	34.3%	24.5%
739	35.6%	33.8%	19.5%	2463	29.6%	34.3%	24.5%
744	35.5%	33.9%	19.3%	2468	29.7%	34.4%	24.6%
750	35.8%	34.0%	19.3%	2474	29.8%	34.5%	24.6%
756	36.4%	34.7%	19.3%	2480	29.9%	34.5%	24.6%
762	37.0%	34.9%	19.5%	2486	29.9%	34.5%	24.7%
768	37.0%	35.1%	19.8%	2492	30.0%	34.6%	24.7%
773	36.3%	34.4%	19.7%	2497	30.1%	34.6%	24.7%
779	35.6%	34.0%	19.7%	2503	30.1%	34.7%	24.8%
785	35.0%	33.4%	19.5%	2509	30.2%	34.7%	24.8%
791	34.5%	33.0%	19.3%	2515	30.2%	34.8%	24.8%
796	33.9%	32.7%	19.2%	2521	30.3%	34.8%	24.9%
802	33.3%	32.1%	19.0%	2526	30.4%	34.9%	24.9%
808	32.8%	32.0%	19.0%	2532	30.4%	34.9%	24.9%
814	32.5%	31.6%	18.8%	2538	30.5%	35.0%	25.0%
820	32.3%	31.7%	18.7%	2544	30.6%	35.1%	25.0%
825	32.4%	31.6%	18.6%	2549	30.7%	35.1%	25.0%
831	32.9%	32.1%	18.5%	2555	30.8%	35.2%	25.1%
837	33.5%	32.4%	18.7%	2561	30.9%	35.2%	25.1%
843	34.0%	32.8%	18.6%	2567	30.9%	35.3%	25.1%
849	34.3%	33.1%	18.7%	2573	31.0%	35.4%	25.2%
854	34.6%	33.3%	18.7%	2578	31.1%	35.4%	25.2%
860	34.7%	33.5%	18.6%	2584	31.2%	35.5%	25.3%
866	34.0%	32.9%	18.7%	2590	31.3%	35.6%	25.3%
872	33.2%	32.6%	18.7%	2596	31.4%	35.6%	25.4%
877	32.9%	32.0%	18.8%	2602	31.4%	35.7%	25.4%
883	33.2%	32.2%	18.6%	2607	31.5%	35.8%	25.5%
889	34.0%	32.5%	18.6%	2613	31.6%	35.8%	25.5%
895	34.8%	33.0%	18.7%	2619	31.7%	35.9%	25.6%
901	35.5%	33.4%	18.7%	2625	31.9%	36.0%	25.7%
906	36.2%	33.9%	18.7%	2630	32.1%	36.1%	25.7%
912	37.2%	34.6%	18.7%	2636	32.2%	36.2%	25.8%
918	38.1%	35.2%	18.8%	2642	32.3%	36.3%	25.8%
924	38.6%	35.8%	18.7%	2648	32.5%	36.4%	25.9%
930	38.6%	35.8%	18.6%	2654	32.7%	36.6%	25.9%
935	38.5%	35.9%	18.6%	2659	32.8%	36.7%	26.0%

Table A-8. Continued

941	38.3%	35.5%	18.7%	2665	33.0%	36.7%	26.0%
947	38.9%	35.5%	18.8%	2671	33.1%	36.8%	26.1%
953	40.6%	36.3%	19.0%	2677	33.3%	36.9%	26.1%
958	42.5%	37.6%	19.2%	2683	33.4%	37.0%	26.2%
964	44.3%	39.0%	19.6%	2688	33.5%	37.1%	26.2%
970	45.8%	40.6%	19.9%	2694	33.7%	37.2%	26.3%
976	47.0%	42.4%	20.5%	2700	33.8%	37.3%	26.3%
982	47.7%	44.1%	21.2%	2706	34.0%	37.4%	26.4%
987	47.8%	45.6%	21.7%	2711	34.1%	37.5%	26.4%
993	47.7%	46.5%	22.1%	2717	34.3%	37.6%	26.5%
999	47.5%	47.0%	22.5%	2723	34.4%	37.7%	26.6%
1005	47.4%	47.2%	23.1%	2729	34.6%	37.9%	26.7%
1011	47.5%	47.8%	23.7%	2735	34.8%	37.9%	26.7%
1016	47.5%	48.2%	24.2%	2740	35.0%	38.0%	26.8%
1022	47.3%	48.2%	24.7%	2746	35.2%	38.2%	26.9%
1028	47.1%	47.8%	25.0%	2752	35.4%	38.3%	27.0%
1034	46.8%	47.3%	25.1%	2758	35.5%	38.4%	27.1%
1039	46.6%	47.1%	25.1%	2764	35.8%	38.6%	27.3%
1045	46.5%	46.7%	25.0%	2769	36.0%	38.7%	27.4%
1051	46.3%	46.5%	25.0%	2775	36.2%	38.9%	27.6%
1057	46.0%	45.7%	24.8%	2781	36.3%	39.0%	27.7%
1063	45.4%	44.8%	24.9%	2787	36.6%	39.1%	27.8%
1068	44.9%	44.1%	25.2%	2792	36.7%	39.3%	27.9%
1074	45.5%	45.0%	25.6%	2798	37.0%	39.4%	28.0%
1080	46.3%	45.9%	25.7%	2804	37.2%	39.6%	28.0%
1086	46.6%	45.9%	25.5%	2810	37.4%	39.7%	28.1%
1092	46.5%	45.4%	25.5%	2816	37.7%	39.9%	28.3%
1097	46.3%	44.8%	25.5%	2821	37.9%	40.1%	28.3%
1103	46.2%	44.6%	25.7%	2827	38.2%	40.3%	28.4%
1109	46.1%	44.4%	25.7%	2833	38.5%	40.5%	28.6%
1115	45.9%	44.2%	25.5%	2839	38.9%	40.7%	28.7%
1120	45.6%	43.8%	25.3%	2845	39.2%	40.9%	28.8%
1126	45.3%	43.6%	25.0%	2850	39.6%	41.2%	29.0%
1132	45.0%	43.2%	25.1%	2856	40.0%	41.5%	29.1%
1138	45.0%	43.3%	25.0%	2862	40.4%	41.8%	29.3%
1144	45.6%	44.1%	25.2%	2868	40.9%	42.1%	29.4%
1149	46.6%	45.3%	25.5%	2873	41.4%	42.5%	29.6%
1155	47.3%	46.0%	25.3%	2879	41.8%	42.9%	29.8%
1161	47.1%	45.7%	24.8%	2885	42.2%	43.3%	30.0%
1167	46.7%	44.8%	23.9%	2891	42.5%	43.5%	30.2%
1173	46.0%	43.5%	23.5%	2897	42.7%	43.7%	30.4%

Table A-8. Continued

1178	45.2%	42.2%	23.0%	2902	43.0%	43.9%	30.5%
1184	44.2%	40.9%	22.8%	2908	43.3%	44.1%	30.7%
1190	43.1%	39.9%	22.7%	2914	43.7%	44.4%	31.0%
1196	42.3%	39.3%	22.6%	2920	44.2%	44.7%	31.3%
1201	41.7%	39.0%	22.6%	2926	44.6%	45.1%	31.5%
1207	41.2%	38.6%	22.3%	2931	44.7%	45.3%	31.7%
1213	40.5%	38.0%	22.1%	2937	44.8%	45.4%	31.9%
1219	39.7%	37.5%	22.1%	2943	44.9%	45.3%	32.1%
1225	39.2%	37.2%	22.0%	2949	44.7%	45.1%	32.3%
1230	38.9%	37.2%	22.1%	2954	44.7%	44.9%	32.5%
1236	38.8%	37.1%	22.0%	2960	44.7%	44.8%	32.7%
1242	38.8%	37.2%	22.1%	2966	44.8%	44.8%	33.0%
1248	38.7%	37.1%	22.1%	2972	44.9%	45.0%	33.3%
1254	38.5%	37.0%	22.2%	2978	45.2%	45.0%	33.7%
1259	38.4%	36.9%	22.2%	2983	45.4%	45.2%	34.1%
1265	38.2%	36.9%	22.3%	2989	45.8%	45.5%	34.5%
1271	38.0%	36.8%	22.4%	2995	46.3%	45.7%	34.9%
1277	38.0%	36.8%	22.5%	3001	46.7%	46.1%	35.5%
1282	38.1%	37.0%	22.7%	3006	47.2%	46.3%	35.8%
1288	38.2%	37.1%	22.9%	3012	47.6%	46.6%	36.2%
1294	38.3%	37.3%	23.0%	3018	48.0%	46.8%	36.4%
1300	38.5%	37.5%	23.1%	3024	48.4%	47.0%	36.5%
1306	38.7%	37.8%	23.3%	3030	48.7%	47.3%	36.7%
1311	38.9%	38.0%	23.5%	3035	49.0%	47.4%	36.8%
1317	39.3%	38.3%	23.9%	3041	49.4%	47.7%	37.1%
1323	39.6%	38.5%	24.0%	3047	50.0%	48.1%	37.4%
1329	40.0%	38.9%	24.0%	3053	50.7%	48.6%	37.9%
1335	40.5%	39.4%	24.2%	3059	51.4%	49.1%	38.5%
1340	40.9%	39.7%	24.4%	3064	52.4%	49.7%	39.3%
1346	41.4%	40.0%	24.8%	3070	53.5%	50.5%	40.1%
1352	42.0%	40.4%	25.2%	3076	54.6%	51.2%	41.0%
1358	42.8%	41.0%	25.9%	3082	55.9%	52.0%	42.0%
1363	43.9%	41.8%	26.7%	3087	57.1%	52.9%	43.1%
1369	45.4%	42.8%	27.9%	3093	58.5%	53.7%	44.2%
1375	47.6%	44.3%	29.7%	3099	59.7%	54.6%	45.3%
1381	51.1%	46.8%	32.7%	3105	60.8%	55.3%	46.3%
1387	55.6%	49.9%	36.8%	3111	61.7%	55.9%	47.2%
1392	60.3%	52.9%	41.3%	3116	62.4%	56.4%	47.8%
1398	65.0%	56.3%	46.1%	3122	62.9%	56.8%	48.3%
1404	64.6%	56.0%	45.8%	3128	63.1%	57.1%	48.5%

Table A-8. Continued

1410	59.7%	52.8%	41.2%	3134	63.3%	57.2%	48.7%
1416	54.9%	49.5%	36.7%	3140	63.4%	57.3%	48.8%
1421	51.6%	47.2%	33.7%	3145	63.4%	57.4%	48.8%
1427	49.3%	45.5%	31.6%	3151	63.5%	57.4%	48.8%
1433	47.8%	44.4%	30.3%	3157	63.4%	57.5%	48.9%
1439	46.8%	43.7%	29.4%	3163	63.4%	57.6%	48.9%
1444	46.0%	43.2%	28.8%	3168	63.3%	57.6%	48.9%
1450	45.6%	42.8%	28.4%	3174	63.2%	57.6%	48.9%
1456	45.4%	42.6%	28.0%	3180	63.1%	57.5%	48.8%
1462	45.3%	42.4%	27.6%	3186	62.9%	57.5%	48.7%
1468	45.0%	42.0%	27.1%	3192	62.6%	57.5%	48.4%
1473	44.5%	41.4%	26.8%	3197	62.5%	57.4%	48.4%
1479	43.7%	40.7%	26.3%	3203	62.2%	57.3%	48.1%
1485	42.9%	40.0%	26.0%	3209	62.0%	57.3%	48.0%
1491	42.1%	39.4%	25.6%	3215	61.7%	57.2%	47.7%
1496	41.3%	38.8%	25.2%	3221	61.4%	57.1%	47.4%
1502	40.7%	38.3%	25.0%	3226	61.0%	56.9%	47.2%
1508	40.0%	37.9%	24.7%	3232	60.7%	56.6%	46.8%
1514	39.4%	37.5%	24.6%	3238	60.2%	56.6%	46.5%
1520	38.9%	37.2%	24.4%	3244	59.8%	56.4%	46.2%
1525	38.4%	36.9%	24.3%	3249	59.4%	56.1%	45.9%
1531	38.0%	36.6%	24.2%	3255	59.0%	56.0%	45.6%
1537	37.7%	36.5%	24.2%	3261	58.7%	55.8%	45.3%
1543	37.5%	36.3%	24.3%	3267	58.2%	55.7%	45.0%
1549	37.3%	36.3%	24.3%	3273	57.8%	55.5%	44.6%
1554	37.2%	36.3%	24.6%	3278	57.5%	55.4%	44.4%
1560	37.2%	36.3%	24.8%	3284	57.2%	55.3%	44.1%
1566	37.1%	36.3%	25.0%	3290	57.0%	55.2%	44.0%
1572	37.0%	36.2%	25.1%	3296	56.8%	55.1%	43.8%
1577	36.9%	36.3%	25.4%	3302	56.6%	55.1%	43.7%
1583	37.1%	36.5%	25.8%	3307	56.5%	55.0%	43.7%
1589	37.4%	36.8%	26.3%	3313	56.4%	55.0%	43.7%
1595	37.9%	37.2%	27.0%	3319	56.4%	55.1%	43.8%
1601	38.6%	37.8%	27.7%	3325	56.4%	55.2%	43.9%
1606	39.4%	38.4%	28.4%	3330	56.6%	55.2%	43.9%
1612	40.1%	39.0%	29.0%	3336	56.6%	55.4%	44.0%
1618	40.9%	39.7%	29.5%	3342	56.7%	55.3%	44.1%
1624	41.6%	40.2%	29.8%	3348	56.7%	55.4%	44.2%
1630	42.0%	40.5%	29.8%	3354	56.7%	55.5%	44.3%
1635	42.1%	40.6%	29.8%	3359	56.8%	55.5%	44.4%

Table A-8. Continued

1641	42.2%	40.6%	29.5%	3365	56.8%	55.5%	44.4%
1647	42.2%	40.6%	29.4%	3371	56.8%	55.6%	44.7%
1653	42.2%	40.6%	29.3%	3377	57.0%	55.7%	44.8%
1658	42.0%	40.4%	29.0%	3383	57.0%	55.7%	44.8%
1664	41.7%	40.1%	28.8%	3388	57.0%	55.7%	44.8%
1670	41.0%	39.5%	28.2%	3394	57.0%	55.8%	44.9%
1676	40.0%	38.7%	27.3%	3400	57.0%	55.7%	44.9%
1682	38.9%	37.9%	26.5%	3406	57.1%	55.7%	44.9%
1687	37.9%	37.1%	25.8%	3411	57.1%	55.7%	44.9%
1693	36.9%	36.4%	25.1%	3417	57.2%	55.7%	44.8%
1699	36.0%	35.8%	24.7%	3423	57.2%	55.7%	44.7%
1705	35.1%	35.3%	24.2%	3429	57.1%	55.6%	44.7%
1711	34.5%	34.8%	23.9%	3435	57.0%	55.6%	44.6%
1716	34.0%	34.5%	23.7%	3440	56.9%	55.5%	44.4%
1722	33.5%	34.2%	23.5%	3446	56.7%	55.4%	44.2%
1728	33.0%	33.9%	23.4%	3452	56.6%	55.3%	44.0%
1734	32.7%	33.7%	23.4%	3458	56.3%	55.2%	43.7%
1739	32.3%	33.5%	23.2%	3464	56.0%	54.9%	43.3%
1745	31.9%	33.3%	23.0%	3469	55.8%	54.7%	43.0%
1751	31.6%	33.2%	22.8%	3475	55.5%	54.6%	42.7%
1757	31.3%	33.0%	22.7%	3481	55.1%	54.4%	42.2%
1763	31.1%	32.9%	22.6%	3487	54.9%	54.2%	41.8%
1768	31.0%	32.9%	22.6%	3492	54.6%	54.1%	41.4%
1774	30.8%	32.8%	22.5%	3498	54.2%	53.7%	41.0%
1780	30.6%	32.7%	22.5%	3504	53.9%	53.5%	40.6%
1786	30.5%	32.7%	22.4%	3510	53.7%	53.3%	40.1%
1792	30.4%	32.6%	22.4%	3516	53.2%	53.1%	39.7%
1797	30.2%	32.6%	22.3%	3521	52.9%	52.8%	39.2%
1803	30.1%	32.5%	22.3%	3527	52.6%	52.6%	38.8%
1809	30.0%	32.5%	22.2%	3533	52.2%	52.3%	38.4%
1815	29.9%	32.4%	22.2%	3539	52.0%	52.2%	38.1%
1820	29.8%	32.4%	22.2%	3545	51.7%	51.9%	37.7%
1826	29.7%	32.4%	22.3%	3550	51.5%	51.6%	37.3%
1832	29.6%	32.4%	22.2%	3556	51.3%	51.3%	36.8%
1838	29.6%	32.3%	22.2%	3562	50.9%	51.0%	36.5%
1844	29.5%	32.3%	22.2%	3568	50.5%	50.7%	36.0%
1849	29.5%	32.3%	22.2%	3573	50.3%	50.3%	35.6%
1855	29.4%	32.3%	22.3%	3579	49.8%	50.0%	35.2%
1861	29.4%	32.3%	22.2%	3585	49.5%	49.6%	34.7%
1867	29.3%	32.3%	22.3%	3591	49.0%	49.1%	34.2%
1873	29.3%	32.3%	22.3%	3597	48.7%	48.7%	33.9%

Table A-8. Continued

1878	29.2%	32.3%	22.3%	3602	48.4%	48.4%	33.4%
1884	29.2%	32.3%	22.3%	3608	48.0%	48.0%	33.0%
1890	29.2%	32.3%	22.3%	3614	47.5%	47.5%	32.5%
1896	29.1%	32.3%	22.3%	3620	47.1%	47.1%	32.1%
1901	29.1%	32.3%	22.3%	3626	46.7%	46.7%	31.8%
1907	29.0%	32.3%	22.4%	3631	46.2%	46.3%	31.4%
1913	29.0%	32.3%	22.4%	3637	45.8%	45.9%	31.0%
1919	29.0%	32.3%	22.4%	3643	45.4%	45.5%	30.7%
1925	29.0%	32.3%	22.4%	3649	45.0%	45.2%	30.5%
1930	29.0%	32.4%	22.4%	3654	44.5%	44.9%	30.2%
1936	28.9%	32.4%	22.5%	3660	44.3%	44.5%	30.0%
1942	28.9%	32.4%	22.5%	3666	43.8%	44.3%	29.9%
1948	28.9%	32.4%	22.5%	3672	43.5%	44.0%	29.7%
1954	28.9%	32.4%	22.5%	3678	43.3%	43.8%	29.6%
1959	28.8%	32.4%	22.6%	3683	43.0%	43.5%	29.4%
1965	28.8%	32.4%	22.6%	3689	42.8%	43.4%	29.4%
1971	28.8%	32.4%	22.6%	3695	42.5%	43.2%	29.3%
1977	28.8%	32.4%	22.6%	3701	42.3%	43.0%	29.2%
1982	28.8%	32.4%	22.7%	3707	42.1%	42.9%	29.1%
1988	28.7%	32.5%	22.7%	3712	41.9%	42.7%	29.2%
1990	28.7%	32.5%	22.7%	3714	41.8%	42.7%	29.1%
1992	28.7%	32.5%	22.7%	3716	41.7%	42.7%	29.1%
1994	28.7%	32.5%	22.7%	3718	41.7%	42.6%	29.1%
1996	28.7%	32.5%	22.7%	3720	41.6%	42.6%	29.1%
1998	28.7%	32.5%	22.7%	3722	41.6%	42.6%	29.1%
2004	28.7%	32.5%	22.8%	3728	41.5%	42.5%	29.0%
2009	28.7%	32.6%	22.8%	3734	41.4%	42.4%	29.1%
2015	28.8%	32.6%	22.8%	3739	41.2%	42.3%	29.0%
2021	28.8%	32.6%	22.8%	3745	41.2%	42.3%	29.0%
2027	28.9%	32.7%	22.9%	3751	41.0%	42.2%	29.0%
2033	28.9%	32.7%	22.9%	3757	40.9%	42.1%	28.9%
2038	29.0%	32.8%	22.9%	3762	40.8%	42.0%	28.8%
2044	29.0%	32.8%	23.0%	3768	40.7%	42.0%	28.8%
2050	29.1%	32.9%	23.0%	3774	40.6%	41.9%	28.8%
2056	29.1%	32.9%	23.0%	3780	40.3%	41.8%	28.9%
2062	29.1%	32.9%	23.0%	3786	40.3%	41.7%	28.9%
2067	29.1%	32.9%	23.0%	3791	40.3%	41.7%	28.9%
2073	29.1%	32.9%	23.0%	3797	40.1%	41.7%	28.9%
2079	29.1%	33.0%	23.0%	3803	40.1%	41.7%	28.9%
2085	29.1%	33.0%	23.1%	3809	40.1%	41.6%	28.9%

Table A-8. Continued

2090	29.1%	33.0%	23.1%	3815	40.0%	41.5%	28.9%
2096	29.1%	33.0%	23.1%	3820	39.9%	41.4%	28.8%
2102	29.1%	33.0%	23.1%	3826	39.8%	41.5%	28.8%
2108	29.1%	33.0%	23.2%	3832	39.8%	41.4%	28.8%
2114	29.1%	33.0%	23.2%	3838	39.7%	41.4%	28.9%
2119	29.1%	33.0%	23.2%	3843	39.7%	41.4%	28.8%
2125	29.1%	33.1%	23.2%	3849	39.6%	41.3%	28.8%
2131	29.1%	33.1%	23.2%	3855	39.6%	41.4%	28.9%
2137	29.1%	33.1%	23.2%	3861	39.5%	41.2%	28.8%
2143	29.1%	33.1%	23.2%	3867	39.4%	41.3%	28.8%
2148	29.1%	33.1%	23.3%	3872	39.4%	41.3%	28.8%
2154	29.2%	33.2%	23.3%	3878	39.3%	41.2%	28.8%
2160	29.2%	33.2%	23.4%	3884	39.2%	41.2%	28.8%
2166	29.3%	33.3%	23.5%	3890	39.2%	41.3%	28.7%
2171	29.7%	33.6%	23.8%	3896	39.2%	41.3%	28.8%
2177	29.1%	33.2%	23.4%	3901	39.1%	41.3%	28.8%
2183	29.0%	33.2%	23.4%	3907	39.1%	41.2%	28.8%
2189	28.9%	33.1%	23.4%	3913	39.1%	41.2%	28.7%
2195	28.9%	33.2%	23.4%	3919	39.1%	41.2%	28.8%
2200	28.8%	33.1%	23.4%	3950	38.9%	41.3%	28.8%
2206	28.8%	33.1%	23.4%	3967	38.8%	41.1%	28.8%
2212	28.8%	33.1%	23.4%	3982	38.7%	41.1%	28.8%
2218	28.7%	33.1%	23.5%	3994	38.7%	41.1%	28.7%
2224	28.7%	33.1%	23.5%	4000	38.8%	41.1%	28.8%

Table A-9. Data for DNA efficiency attachment for Figure 3-10.

Sample	Efficiency (%)	Standard Deviation (%)
D* -12.4	5.1%	1.6%
C* -13	5.2%	1.9%
D^ -10.4	14.2%	1.6%
C^ -13	18.2%	1.9%

A.2 CHAPTER 4 DATA

Table A-10. Fluorescence data for Figure 4-8.

	100ng Probe		50ng Probe		25ng Probe	
Target Mass (ng)	Average (counts)	Standard Deviation (counts)	Average (counts)	Standard Deviation (counts)	Average (counts)	Standard Deviation (counts)
100	44617	740.05	24731	251.53	15036	285.08
75	44550	659.12	23384	152.11	14152	304.13
50	40148	336.02	22128	268.13	12801	221.00
30	26997	244.12	17199	216.05	11541	243.50
25	24024	307.75	16893	378.80	10337	218.17
20	20272	209.43	15616	157.16	10212	203.40
15	15844	408.35	12368	192.62	9072	122.34
10	13623	167.06	10717	173.35	7527	373.82
7.5	11770	216.34	8861	112.66	5865	151.11
5	11203	165.73	6516	86.06	4419	142.72
3	9430	218.43	5036	112.48	3568	614.30
2	9883	162.61	4277	87.82	2760	232.81
1	12358	171.76	10255	534.89	1642	76.13
0.75	11781	174.69	7273	96.58	1663	146.06
0.5	10930	157.41	6008	86.18	1560	35.70
0.1	8777	176.56	3500	103.70	1461	32.41
0	226	16.89	226	16.89	226	16.89

Table A-11. Additional fluorescence data for Figure 4-8.

	10ng Probe		5ng Probe		Probe only	
Target Mass (ng)	Average (counts)	Standard Deviation (counts)	Average (counts)	Standard Deviation (counts)	Average (counts)	Standard Deviation (counts)
100	18653	286.05	7271	507.36	5150	613.33
75	13996	844.08	6129	519.05	3128	419.53
50	10629	272.59	5279	386.11	2081	238.14
30	5063	217.26	3711	222.22	832	62.01
25	3416	177.93	3487	255.16	441	16.61
20	2503	176.75	2787	175.06	342	14.46
15	1851	58.72	2886	180.76	252	13.58
10	1181	80.74	1932	82.27	286	68.49
7.5	982	470.91	1874	139.23	260	14.06
5	394	28.90	1471	119.45	225	17.34
3	551	189.43	1123	168.76	196	6.82
2	410	26.21	1108	147.69	249	51.74
1	436	90.15	450	41.06	198	10.08
0.75	426	34.15	476	59.24	259	14.82
0.5	1002	22.07	398	29.11	225	9.36
0.1	586	19.85	314	24.16	187	6.50
0	226	16.89	226	16.89	226	16.89

Table A-12. Differential pulse voltammetry data for Figure 4-10.

Voltage	Differential pulse current				
	Water	Zinc (Zn)	Cadmium (Cd)	Zn/Cd	SYBR101 & QD
-1.13	0.0000580	0.0000760	0.0000730	0.0000690	0.0000530
-1.12	0.0000530	0.0000690	0.0000690	0.0000660	0.0000510
-1.11	0.0000500	0.0000620	0.0000660	0.0000640	0.0000480
-1.10	0.0000440	0.0000580	0.0000630	0.0000610	0.0000460
-1.09	0.0000430	0.0000510	0.0000590	0.0000600	0.0000440
-1.08	0.0000390	0.0000460	0.0000550	0.0000570	0.0000420
-1.07	0.0000380	0.0000420	0.0000520	0.0000550	0.0000400
-1.06	0.0000350	0.0000390	0.0000480	0.0000550	0.0000390
-1.05	0.0000330	0.0000370	0.0000450	0.0000510	0.0000380
-1.04	0.0000320	0.0000350	0.0000420	0.0000490	0.0000380
-1.03	0.0000310	0.0000330	0.0000390	0.0000470	0.0000370
-1.02	0.0000290	0.0000320	0.0000360	0.0000450	0.0000390
-1.01	0.0000290	0.0000300	0.0000340	0.0000430	0.0000400
-1.00	0.0000280	0.0000290	0.0000320	0.0000400	0.0000430
-0.99	0.0000290	0.0000280	0.0000310	0.0000400	0.0000440
-0.98	0.0000300	0.0000280	0.0000300	0.0000380	0.0000440
-0.97	0.0000260	0.0000270	0.0000290	0.0000370	0.0000450
-0.96	0.0000300	0.0000270	0.0000290	0.0000350	0.0000480
-0.95	0.0000300	0.0000260	0.0000280	0.0000340	0.0000530
-0.94	0.0000270	0.0000270	0.0000270	0.0000330	0.0000560
-0.93	0.0000280	0.0000270	0.0000270	0.0000330	0.0000620
-0.92	0.0000280	0.0000260	0.0000260	0.0000340	0.0000680
-0.91	0.0000260	0.0000250	0.0000280	0.0000390	0.0000740
-0.90	0.0000270	0.0000250	0.0000330	0.0000440	0.0000740
-0.89	0.0000270	0.0000250	0.0000400	0.0000510	0.0000730
-0.88	0.0000270	0.0000250	0.0000460	0.0000570	0.0000700
-0.87	0.0000260	0.0000240	0.0000540	0.0000570	0.0000630
-0.86	0.0000260	0.0000250	0.0000510	0.0000550	0.0000520
-0.85	0.0000250	0.0000250	0.0000480	0.0000490	0.0000420
-0.84	0.0000260	0.0000240	0.0000440	0.0000420	0.0000380
-0.83	0.0000270	0.0000230	0.0000400	0.0000360	0.0000330
-0.82	0.0000270	0.0000240	0.0000360	0.0000300	0.0000280
-0.81	0.0000270	0.0000220	0.0000320	0.0000260	0.0000280
-0.80	0.0000270	0.0000240	0.0000310	0.0000250	0.0000270
-0.77	0.0000270	0.0000240	0.0000270	0.0000190	0.0000270

Table A-12. Continued

-0.74	0.0000270	0.0000250	0.0000240	0.0000200	0.0000270
-0.71	0.0000260	0.0000240	0.0000220	0.0000190	0.0000270
-0.68	0.0000230	0.0000220	0.0000200	0.0000190	0.0000270
-0.65	0.0000210	0.0000210	0.0000170	0.0000180	0.0000270
-0.62	0.0000180	0.0000190	0.0000140	0.0000170	0.0000270
-0.59	0.0000150	0.0000160	0.0000130	0.0000160	0.0000270
-0.56	0.0000130	0.0000140	0.0000110	0.0000140	0.0000250
-0.53	0.0000110	0.0000110	0.0000100	0.0000110	0.0000240
-0.50	0.0000100	0.0000100	0.0000080	0.0000100	0.0000220
-0.47	0.0000040	0.0000080	0.0000070	0.0000080	0.0000210
-0.44	0.0000070	0.0000070	0.0000060	0.0000080	0.0000190
-0.41	0.0000050	0.0000060	0.0000050	0.0000050	0.0000170
-0.38	0.0000050	0.0000060	0.0000040	0.0000050	0.0000160
-0.35	0.0000060	0.0000050	0.0000040	0.0000040	0.0000140
-0.32	0.0000040	0.0000050	0.0000030	0.0000040	0.0000130
-0.29	0.0000030	0.0000040	0.0000030	0.0000040	0.0000120
-0.26	0.0000030	0.0000040	0.0000030	0.0000030	0.0000110
-0.23	0.0000030	0.0000030	0.0000020	0.0000040	0.0000100
-0.20	0.0000030	0.0000030	0.0000020	0.0000030	0.0000090
-0.17	0.0000030	0.0000030	0.0000030	0.0000020	0.0000090
-0.14	0.0000030	0.0000040	0.0000020	0.0000030	0.0000080
-0.11	0.0000040	0.0000040	0.0000020	0.0000030	0.0000080
-0.08	0.0000040	0.0000040	0.0000020	0.0000030	0.0000080
-0.05	0.0000030	0.0000030	0.0000030	0.0000040	0.0000070
-0.02	0.0000040	0.0000040	0.0000030	0.0000030	0.0000070
0.00	0.0000050	0.0000050	0.0000040	0.0000040	0.0000070

A.3 CHAPTER 5 DATA

Table A-13. Differential pulse voltammety data for Figure 5-7.

	Differential pulse current (dI)			
Voltage (V)	Blank	$5x10^7$ CFU/mL	$5x10^6$ CFU/mL	$5x10^5$ CFU/mL
1.49	0.00004563	0.00005740	0.00004233	0.00001347
1.47	0.00004277	0.00005393	0.00004167	0.00001343
1.45	0.00003980	0.00005037	0.00004100	0.00001337
1.43	0.00003663	0.00004693	0.00004033	0.00001327
1.41	0.00003337	0.00004367	0.00003933	0.00001320
1.39	0.00003007	0.00004083	0.00003800	0.00001317
1.37	0.00002660	0.00003823	0.00003733	0.00001310
1.35	0.00002307	0.00003617	0.00003667	0.00001303
1.33	0.00001967	0.00003437	0.00003567	0.00001307
1.31	0.00001640	0.00003287	0.00003533	0.00001300
1.29	0.00001330	0.00003167	0.00003467	0.00001293
1.27	0.00001053	0.00003080	0.00003467	0.00001290
1.25	0.00000820	0.00003017	0.00003433	0.00001283
1.23	0.00000627	0.00002967	0.00003333	0.00001280
1.21	0.00000477	0.00002933	0.00003333	0.00001273
1.19	0.00000360	0.00002900	0.00003300	0.00001273
1.17	0.00000273	0.00002877	0.00003300	0.00001270
1.15	0.00000223	0.00002867	0.00003333	0.00001267
1.13	0.00000203	0.00002857	0.00003333	0.00001263
1.11	0.00000200	0.00002850	0.00003333	0.00001260
1.09	0.00000227	0.00002857	0.00003367	0.00001257
1.07	0.00000270	0.00002863	0.00003400	0.00001260
1.05	0.00000330	0.00002873	0.00003400	0.00001267
1.03	0.00000413	0.00002890	0.00003433	0.00001260
1.01	0.00000530	0.00002910	0.00003533	0.00001263
0.99	0.00000677	0.00002920	0.00003533	0.00001260
0.97	0.00000850	0.00002957	0.00003600	0.00001260
0.95	0.00001070	0.00002997	0.00003533	0.00001263
0.93	0.00001313	0.00003030	0.00003633	0.00001270
0.91	0.00001577	0.00003070	0.00003700	0.00001270
0.89	0.00001850	0.00003123	0.00003700	0.00001273
0.87	0.00002137	0.00003160	0.00003767	0.00001273

Table A-13. Continued

0.85	0.00002423	0.00003207	0.00003833	0.00001273
0.83	0.00002707	0.00003257	0.00003867	0.00001280
0.81	0.00002993	0.00003300	0.00003933	0.00001283
0.79	0.00003263	0.00003340	0.00003967	0.00001277
0.77	0.00003513	0.00003363	0.00004000	0.00001277
0.75	0.00003743	0.00003393	0.00004033	0.00001277
0.73	0.00003953	0.00003400	0.00004067	0.00001277
0.71	0.00004140	0.00003397	0.00004100	0.00001277
0.69	0.00004313	0.00003383	0.00004133	0.00001277
0.67	0.00004457	0.00003343	0.00004133	0.00001277
0.64	0.00004557	0.00003297	0.00004167	0.00001277
0.62	0.00004623	0.00003243	0.00004167	0.00001273
0.60	0.00004670	0.00003187	0.00004133	0.00001270
0.58	0.00004670	0.00003137	0.00004200	0.00001270
0.56	0.00004623	0.00003110	0.00004233	0.00001270
0.54	0.00004557	0.00003103	0.00004200	0.00001273
0.52	0.00004457	0.00003113	0.00004233	0.00001277
0.50	0.00004313	0.00003160	0.00004200	0.00001273
0.48	0.00004140	0.00003243	0.00004200	0.00001277
0.46	0.00003953	0.00003363	0.00004167	0.00001280
0.45	0.00003850	0.00003450	0.00004133	0.00001283
0.44	0.00003743	0.00003540	0.00004133	0.00001287
0.43	0.00003630	0.00003633	0.00004133	0.00001290
0.42	0.00003513	0.00003720	0.00004100	0.00001297
0.41	0.00003387	0.00003797	0.00004067	0.00001307
0.40	0.00003263	0.00003850	0.00004033	0.00001317
0.39	0.00003130	0.00003890	0.00004033	0.00001327
0.38	0.00002993	0.00003907	0.00004000	0.00001337
0.37	0.00002850	0.00003900	0.00004000	0.00001350
0.36	0.00002707	0.00003863	0.00004000	0.00001363
0.35	0.00002567	0.00003803	0.00003967	0.00001373
0.34	0.00002423	0.00003737	0.00003967	0.00001383
0.33	0.00002290	0.00003663	0.00003967	0.00001383
0.32	0.00002133	0.00003603	0.00004000	0.00001390
0.31	0.00001970	0.00003547	0.00004033	0.00001397
0.30	0.00001803	0.00003500	0.00004067	0.00001410
0.29	0.00001663	0.00003457	0.00004167	0.00001417
0.28	0.00001540	0.00003417	0.00004233	0.00001420
0.27	0.00001427	0.00003390	0.00004300	0.00001417

Table A-13. Continued

0.26	0.00001320	0.00003370	0.00004333	0.00001417
0.25	0.00001230	0.00003353	0.00004367	0.00001413
0.23	0.00001073	0.00003310	0.00004433	0.00001410
0.21	0.00000937	0.00003263	0.00004367	0.00001407
0.19	0.00000817	0.00003210	0.00004233	0.00001390
0.17	0.00000710	0.00003170	0.00004200	0.00001373
0.15	0.00000633	0.00003130	0.00004167	0.00001363
0.13	0.00000567	0.00003093	0.00004200	0.00001353
0.11	0.00000510	0.00003067	0.00004133	0.00001353
0.09	0.00000460	0.00003047	0.00004167	0.00001333
0.07	0.00000420	0.00003030	0.00004167	0.00001347
0.05	0.00000397	0.00003033	0.00004167	0.00001343
0.03	0.00000363	0.00003027	0.00004167	0.00001343
0.01	0.00000333	0.00003027	0.00004200	0.00001343
-0.01	0.00000320	0.00003043	0.00004200	0.00001343
-0.03	0.00000297	0.00003047	0.00004200	0.00001343
-0.05	0.00000280	0.00003040	0.00004267	0.00001343
-0.07	0.00000273	0.00003037	0.00004300	0.00001350
-0.09	0.00000270	0.00003030	0.00004367	0.00001350
-0.11	0.00000270	0.00003013	0.00004400	0.00001353
-0.13	0.00000263	0.00002987	0.00004400	0.00001370
-0.15	0.00000263	0.00002960	0.00004400	0.00001380
-0.17	0.00000257	0.00002940	0.00004367	0.00001383
-0.19	0.00000260	0.00002910	0.00004367	0.00001383
-0.21	0.00000270	0.00002897	0.00004333	0.00001397
-0.23	0.00000290	0.00002880	0.00004300	0.00001400
-0.25	0.00000340	0.00002863	0.00004267	0.00001397
-0.27	0.00000530	0.00002833	0.00004267	0.00001403
-0.29	0.00001207	0.00002810	0.00004300	0.00001400
-0.31	0.00001650	0.00002800	0.00004267	0.00001397
-0.33	0.00001357	0.00002793	0.00004267	0.00001390
-0.35	0.00001140	0.00002770	0.00004267	0.00001393
-0.37	0.00000937	0.00002740	0.00004233	0.00001383
-0.39	0.00000763	0.00002723	0.00004300	0.00001373
-0.41	0.00000870	0.00002710	0.00004267	0.00001377
-0.43	0.00000770	0.00002683	0.00004300	0.00001380
-0.45	0.00000783	0.00002670	0.00004267	0.00001363
-0.47	0.00000793	0.00002667	0.00004267	0.00001370
-0.49	0.00000857	0.00002650	0.00004300	0.00001367

Table A-14. Additional differential pulse voltammety data for Figure 5-7.

	Differential pulse current (dI)			
Voltage (V)	$5x10^3$ CFU/mL	$5x10^2$ CFU/mL	$5x10^1$ CFU/mL	$5x10^0$ CFU/mL
1.49	0.00003900	0.00004733	0.00003833	0.00004233
1.47	0.00003867	0.00004600	0.00003700	0.00004100
1.45	0.00003800	0.00004500	0.00003700	0.00004000
1.43	0.00003733	0.00004400	0.00003667	0.00003900
1.41	0.00003633	0.00004233	0.00003567	0.00003767
1.39	0.00003467	0.00004133	0.00003533	0.00003667
1.37	0.00003333	0.00003933	0.00003433	0.00003567
1.35	0.00003233	0.00003800	0.00003333	0.00003433
1.33	0.00003200	0.00003667	0.00003300	0.00003367
1.31	0.00003100	0.00003567	0.00003167	0.00003333
1.29	0.00003100	0.00003433	0.00003167	0.00003300
1.27	0.00003033	0.00003400	0.00003100	0.00003233
1.25	0.00003000	0.00003333	0.00003067	0.00003200
1.23	0.00003000	0.00003233	0.00002967	0.00003200
1.21	0.00002900	0.00003233	0.00003000	0.00003200
1.19	0.00002900	0.00003233	0.00002967	0.00003133
1.17	0.00002933	0.00003267	0.00002933	0.00003167
1.15	0.00002933	0.00003167	0.00002967	0.00003200
1.13	0.00002900	0.00003167	0.00002933	0.00003167
1.11	0.00002900	0.00003200	0.00002967	0.00003167
1.09	0.00002933	0.00003133	0.00002967	0.00003167
1.07	0.00002967	0.00003167	0.00003033	0.00003200
1.05	0.00002933	0.00003167	0.00002967	0.00003200
1.03	0.00002967	0.00003200	0.00003000	0.00003233
1.01	0.00003000	0.00003233	0.00003033	0.00003300
0.99	0.00003033	0.00003267	0.00003067	0.00003300
0.97	0.00003067	0.00003233	0.00003033	0.00003300
0.95	0.00003100	0.00003267	0.00003133	0.00003333
0.93	0.00003167	0.00003300	0.00003167	0.00003333
0.91	0.00003200	0.00003333	0.00003100	0.00003433
0.89	0.00003267	0.00003433	0.00003167	0.00003433
0.87	0.00003267	0.00003500	0.00003333	0.00003433
0.85	0.00003333	0.00003567	0.00003300	0.00003533
0.83	0.00003367	0.00003600	0.00003300	0.00003567
0.81	0.00003367	0.00003667	0.00003300	0.00003567

Table A-14. Continued

0.79	0.00003400	0.00003700	0.00003367	0.00003667
0.77	0.00003433	0.00003767	0.00003400	0.00003700
0.75	0.00003500	0.00003833	0.00003433	0.00003733
0.73	0.00003533	0.00003900	0.00003467	0.00003700
0.71	0.00003567	0.00003933	0.00003500	0.00003767
0.69	0.00003533	0.00004000	0.00003500	0.00003800
0.67	0.00003500	0.00003967	0.00003500	0.00003767
0.64	0.00003567	0.00004000	0.00003500	0.00003767
0.62	0.00003600	0.00004000	0.00003500	0.00003800
0.60	0.00003567	0.00004000	0.00003500	0.00003767
0.58	0.00003600	0.00004000	0.00003533	0.00003767
0.56	0.00003567	0.00004000	0.00003500	0.00003733
0.54	0.00003533	0.00003967	0.00003467	0.00003767
0.52	0.00003533	0.00003867	0.00003500	0.00003700
0.50	0.00003567	0.00003833	0.00003467	0.00003633
0.48	0.00003500	0.00003900	0.00003467	0.00003600
0.46	0.00003467	0.00003933	0.00003367	0.00003600
0.45	0.00003467	0.00003933	0.00003367	0.00003567
0.44	0.00003467	0.00003933	0.00003367	0.00003567
0.43	0.00003467	0.00003967	0.00003367	0.00003567
0.42	0.00003467	0.00004033	0.00003333	0.00003633
0.41	0.00003467	0.00004067	0.00003300	0.00003700
0.40	0.00003533	0.00004167	0.00003300	0.00003800
0.39	0.00003600	0.00004267	0.00003333	0.00003900
0.38	0.00003667	0.00004367	0.00003400	0.00004000
0.37	0.00003733	0.00004467	0.00003467	0.00004067
0.36	0.00003800	0.00004533	0.00003500	0.00004133
0.35	0.00003900	0.00004633	0.00003533	0.00004167
0.34	0.00004000	0.00004667	0.00003567	0.00004233
0.33	0.00004067	0.00004733	0.00003667	0.00004267
0.32	0.00004100	0.00004767	0.00003733	0.00004300
0.31	0.00004133	0.00004767	0.00003800	0.00004300
0.30	0.00004167	0.00004733	0.00003833	0.00004267
0.29	0.00004200	0.00004667	0.00003833	0.00004233
0.28	0.00004167	0.00004600	0.00003867	0.00004167
0.27	0.00004133	0.00004533	0.00003867	0.00004133
0.26	0.00004067	0.00004467	0.00003900	0.00004067
0.25	0.00004000	0.00004400	0.00003833	0.00004000
0.23	0.00003933	0.00004267	0.00003733	0.00003867

Table A-14. Continued

0.21	0.00003867	0.00004200	0.00003633	0.00003833
0.19	0.00003767	0.00004167	0.00003600	0.00003700
0.17	0.00003733	0.00004233	0.00003567	0.00003700
0.15	0.00003667	0.00004200	0.00003567	0.00003667
0.13	0.00003600	0.00004133	0.00003467	0.00003633
0.11	0.00003567	0.00004133	0.00003500	0.00003667
0.09	0.00003567	0.00004100	0.00003533	0.00003633
0.07	0.00003600	0.00004133	0.00003467	0.00003633
0.05	0.00003600	0.00004100	0.00003467	0.00003667
0.03	0.00003600	0.00004100	0.00003467	0.00003633
0.01	0.00003633	0.00004100	0.00003433	0.00003633
-0.01	0.00003633	0.00004133	0.00003433	0.00003633
-0.03	0.00003667	0.00004167	0.00003433	0.00003567
-0.05	0.00003667	0.00004200	0.00003433	0.00003500
-0.07	0.00003733	0.00004200	0.00003467	0.00003533
-0.09	0.00003767	0.00004200	0.00003467	0.00003567
-0.11	0.00003700	0.00004200	0.00003500	0.00003533
-0.13	0.00003767	0.00004200	0.00003500	0.00003500
-0.15	0.00003767	0.00004200	0.00003467	0.00003433
-0.17	0.00003700	0.00004233	0.00003500	0.00003433
-0.19	0.00003667	0.00004167	0.00003433	0.00003400
-0.21	0.00003700	0.00004167	0.00003400	0.00003367
-0.23	0.00003667	0.00004200	0.00003467	0.00003367
-0.25	0.00003600	0.00004200	0.00003467	0.00003367
-0.27	0.00003667	0.00004200	0.00003500	0.00003267
-0.29	0.00003667	0.00004200	0.00003500	0.00003267
-0.31	0.00003667	0.00004200	0.00003467	0.00003300
-0.33	0.00003667	0.00004200	0.00003500	0.00003300
-0.35	0.00003667	0.00004200	0.00003433	0.00003267
-0.37	0.00003667	0.00004167	0.00003467	0.00003200
-0.39	0.00003700	0.00004167	0.00003500	0.00003233
-0.41	0.00003667	0.00004200	0.00003500	0.00003233
-0.43	0.00003667	0.00004233	0.00003533	0.00003233
-0.45	0.00003700	0.00004233	0.00003533	0.00003233
-0.47	0.00003733	0.00004233	0.00003500	0.00003233
-0.49	0.00003667	0.00004233	0.00003500	0.00003233

Table A-15. Differential pulse voltammetry data for Figure 5-8.

	Differential pulse current (dI)				
Voltage (V)	AuNP Standard	Blank	$5x10^7$ CFU/mL	$5x10^6$ CFU/mL	$5x10^5$ CFU/mL
1.49	0.00005067	0.00001033	0.00003033	0.00004200	0.00003600
1.47	0.00004900	0.00001533	0.00003033	0.00004167	0.00003633
1.45	0.00004600	0.00001533	0.00003067	0.00004133	0.00003600
1.43	0.00004367	0.00001500	0.00003167	0.00004133	0.00003600
1.41	0.00004033	0.00001467	0.00003133	0.00004067	0.00003533
1.39	0.00003700	0.00001433	0.00002933	0.00004000	0.00003500
1.37	0.00003333	0.00001433	0.00003200	0.00004000	0.00003500
1.35	0.00002967	0.00001367	0.00003133	0.00003967	0.00003433
1.33	0.00002567	0.00001367	0.00003067	0.00003933	0.00003367
1.31	0.00002200	0.00001300	0.00002867	0.00003900	0.00003367
1.29	0.00001833	0.00001267	0.00003167	0.00003867	0.00003267
1.27	0.00001567	0.00001300	0.00002900	0.00003767	0.00003200
1.25	0.00001233	0.00001333	0.00003000	0.00003700	0.00003133
1.23	0.00001033	0.00001367	0.00003067	0.00003633	0.00003067
1.21	0.00000867	0.00001400	0.00003067	0.00003533	0.00003000
1.19	0.00000700	0.00001467	0.00002967	0.00003433	0.00002967
1.17	0.00000633	0.00001367	0.00003133	0.00003367	0.00002900
1.15	0.00000567	0.00000900	0.00003067	0.00003333	0.00002900
1.13	0.00000533	0.00000733	0.00002767	0.00003267	0.00002800
1.11	0.00000533	0.00000733	0.00002633	0.00003200	0.00002767
1.09	0.00000600	0.00000667	0.00002600	0.00003133	0.00002700
1.07	0.00000667	0.00000667	0.00002700	0.00003033	0.00002733
1.05	0.00000733	0.00000733	0.00002700	0.00003033	0.00002733
1.03	0.00000833	0.00000633	0.00002600	0.00003033	0.00002700
1.01	0.00000933	0.00000533	0.00002500	0.00003033	0.00002667
0.99	0.00001033	0.00000533	0.00002467	0.00002967	0.00002633
0.97	0.00001167	0.00000533	0.00002500	0.00002933	0.00002600
0.95	0.00001300	0.00000533	0.00002433	0.00002900	0.00002533
0.93	0.00001467	0.00000600	0.00002433	0.00002867	0.00002567
0.91	0.00001633	0.00000533	0.00002433	0.00002800	0.00002600
0.89	0.00001867	0.00000567	0.00002400	0.00002800	0.00002600
0.87	0.00001967	0.00000533	0.00002367	0.00002867	0.00002633
0.85	0.00002067	0.00000533	0.00002333	0.00002833	0.00002633
0.83	0.00002200	0.00000533	0.00002267	0.00002867	0.00002600
0.81	0.00002400	0.00000500	0.00002200	0.00002900	0.00002567

Table A-15. Continued

0.79	0.00002500	0.00000500	0.00002133	0.00002867	0.00002567
0.77	0.00002667	0.00000533	0.00002067	0.00002900	0.00002567
0.75	0.00002733	0.00000533	0.00002000	0.00002833	0.00002567
0.73	0.00002833	0.00000533	0.00002000	0.00002867	0.00002567
0.71	0.00002867	0.00000533	0.00001933	0.00002867	0.00002600
0.69	0.00002867	0.00000500	0.00001900	0.00002833	0.00002600
0.67	0.00002867	0.00000500	0.00001900	0.00002867	0.00002600
0.65	0.00002800	0.00000500	0.00001867	0.00002900	0.00002667
0.63	0.00002700	0.00000533	0.00001833	0.00002933	0.00002700
0.61	0.00002600	0.00000600	0.00001833	0.00002967	0.00002700
0.59	0.00002400	0.00000500	0.00001833	0.00003000	0.00002700
0.57	0.00002200	0.00000467	0.00001800	0.00003000	0.00002700
0.55	0.00001933	0.00000467	0.00001800	0.00003067	0.00002767
0.53	0.00001700	0.00000500	0.00001833	0.00003100	0.00002800
0.51	0.00001567	0.00000500	0.00001800	0.00003100	0.00002867
0.49	0.00001433	0.00000500	0.00001800	0.00003100	0.00002933
0.47	0.00001333	0.00000500	0.00001800	0.00003100	0.00003000
0.45	0.00001333	0.00000500	0.00001800	0.00003033	0.00003000
0.43	0.00001433	0.00000567	0.00001800	0.00003000	0.00002933
0.41	0.00001600	0.00000633	0.00001833	0.00003067	0.00002900
0.39	0.00001833	0.00000600	0.00001833	0.00003067	0.00002900
0.37	0.00002067	0.00000600	0.00001833	0.00003000	0.00002900
0.35	0.00002233	0.00000600	0.00001867	0.00003000	0.00002833
0.33	0.00002267	0.00000567	0.00001900	0.00002967	0.00002800
0.31	0.00002100	0.00000567	0.00001867	0.00003000	0.00002800
0.29	0.00001733	0.00000600	0.00001900	0.00003033	0.00002800
0.27	0.00001367	0.00000600	0.00001933	0.00003033	0.00002800
0.25	0.00001100	0.00000600	0.00001933	0.00003033	0.00002800
0.23	0.00000967	0.00000567	0.00002000	0.00003000	0.00002767
0.21	0.00000967	0.00000600	0.00002033	0.00003000	0.00002733
0.19	0.00000933	0.00000567	0.00002100	0.00003000	0.00002800
0.17	0.00000867	0.00000567	0.00002100	0.00003000	0.00002733
0.15	0.00000833	0.00000600	0.00002167	0.00003000	0.00002767
0.13	0.00000833	0.00000633	0.00002167	0.00003000	0.00002800
0.11	0.00000867	0.00000533	0.00002233	0.00003000	0.00002767
0.09	0.00000867	0.00000567	0.00002267	0.00003000	0.00002700
0.07	0.00000833	0.00000633	0.00002200	0.00003000	0.00002700
0.05	0.00000867	0.00000633	0.00002233	0.00003033	0.00002733
0.03	0.00000900	0.00000633	0.00002300	0.00003000	0.00002733

Table A-16. Additional differential pulse voltammetry data for Figure 5-8.

	Differential pulse current (dI)			
Voltage (V)	$5x10^4$ CFU/mL	$5x10^3$ CFU/mL	$5x10^1$ CFU/mL	$5x10^0$ CFU/mL
1.49	0.00004933	0.00007033	0.00000005	0.00000040
1.47	0.00004900	0.00006933	0.00000006	0.00000040
1.45	0.00004867	0.00006833	0.00000007	0.00000037
1.43	0.00004833	0.00006700	0.00000006	0.00000037
1.41	0.00004733	0.00006533	0.00000006	0.00000040
1.39	0.00004667	0.00006400	0.00000005	0.00000037
1.37	0.00004600	0.00006233	0.00000003	0.00000030
1.35	0.00004567	0.00006067	0.00000004	0.00000037
1.33	0.00004433	0.00005933	0.00000004	0.00000033
1.31	0.00004300	0.00005733	0.00000003	0.00000033
1.29	0.00004200	0.00005467	0.00000004	0.00000033
1.27	0.00004100	0.00005233	0.00000003	0.00000037
1.25	0.00003933	0.00005000	0.00000003	0.00000037
1.23	0.00003800	0.00004800	0.00000004	0.00000033
1.21	0.00003700	0.00004633	0.00000004	0.00000033
1.19	0.00003533	0.00004500	0.00000004	0.00000040
1.17	0.00003467	0.00004233	0.00000004	0.00000037
1.15	0.00003333	0.00004100	0.00000004	0.00000040
1.13	0.00003233	0.00003967	0.00000004	0.00000040
1.11	0.00003133	0.00003767	0.00000004	0.00000027
1.09	0.00003033	0.00003633	0.00000004	0.00000033
1.07	0.00003033	0.00003600	0.00000003	0.00000033
1.05	0.00002967	0.00003567	0.00000003	0.00000037
1.03	0.00002933	0.00003500	0.00000003	0.00000033
1.01	0.00002967	0.00003367	0.00000003	0.00000023
0.99	0.00002933	0.00003400	0.00000003	0.00000023
0.97	0.00002933	0.00003367	0.00000002	0.00000023
0.95	0.00002933	0.00003367	0.00000002	0.00000027
0.93	0.00002967	0.00003367	0.00000003	0.00000027
0.91	0.00003000	0.00003333	0.00000003	0.00000033
0.89	0.00003000	0.00003367	0.00000003	0.00000030
0.87	0.00003000	0.00003367	0.00000002	0.00000030
0.85	0.00003033	0.00003400	0.00000002	0.00000027
0.83	0.00003000	0.00003367	0.00000002	0.00000027
0.81	0.00003000	0.00003367	0.00000002	0.00000030

Table A-16. Continued

0.79	0.00003033	0.00003400	0.00000002	0.00000030
0.77	0.00003033	0.00003400	0.00000002	0.00000027
0.75	0.00003100	0.00003400	0.00000002	0.00000023
0.73	0.00003033	0.00003400	0.00000002	0.00000027
0.71	0.00003100	0.00003433	0.00000002	0.00000023
0.69	0.00003100	0.00003433	0.00000002	0.00000023
0.67	0.00003133	0.00003467	0.00000002	0.00000017
0.65	0.00003167	0.00003500	0.00000003	0.00000013
0.63	0.00003167	0.00003567	0.00000003	0.00000000
0.61	0.00003200	0.00003667	0.00000003	0.00000000
0.59	0.00003200	0.00003767	0.00000004	0.00000000
0.57	0.00003233	0.00003900	0.00000004	-0.00000003
0.55	0.00003267	0.00004000	0.00000005	-0.00000007
0.53	0.00003367	0.00004067	0.00000006	0.00000000
0.51	0.00003400	0.00004133	0.00000005	0.00000000
0.49	0.00003400	0.00004200	0.00000005	-0.00000003
0.47	0.00003400	0.00004167	0.00000005	0.00000007
0.45	0.00003467	0.00004100	0.00000005	0.00000010
0.43	0.00003500	0.00004100	0.00000005	0.00000000
0.41	0.00003500	0.00004100	0.00000005	-0.00000007
0.39	0.00003467	0.00004067	0.00000004	0.00000007
0.37	0.00003467	0.00004033	0.00000004	0.00000000
0.35	0.00003533	0.00004067	0.00000003	0.00000003
0.33	0.00003500	0.00004033	0.00000003	0.00000003
0.31	0.00003500	0.00004000	0.00000003	0.00000003
0.29	0.00003467	0.00004000	0.00000003	-0.00000007
0.27	0.00003433	0.00003967	0.00000003	-0.00000010
0.25	0.00003500	0.00003933	0.00000003	-0.00000007
0.23	0.00003433	0.00003967	0.00000003	-0.00000003
0.21	0.00003400	0.00003933	0.00000003	0.00000000
0.19	0.00003400	0.00003933	0.00000003	0.00000003
0.17	0.00003433	0.00003900	0.00000003	-0.00000003
0.15	0.00003433	0.00003900	0.00000002	-0.00000003
0.13	0.00003433	0.00003900	0.00000002	-0.00000003
0.11	0.00003467	0.00003900	0.00000002	-0.00000003
0.09	0.00003467	0.00003900	0.00000002	-0.00000003
0.07	0.00003367	0.00003900	0.00000002	-0.00000003
0.05	0.00003433	0.00003900	0.00000003	0.00000000
0.03	0.00003500	0.00003967	0.00000002	0.00000000

Table A-17. Differential pulse voltammetry data for Figure 5-9.

	Differential pulse current (dI)			
Voltage (V)	$5x10^7$ CFU/mL	$5x10^6$ CFU/mL	$5x10^5$ CFU/mL	$5x10^4$ CFU/mL
1.47	0.00001629	0.00001143	0.00001143	-0.00000029
1.45	0.00001614	0.00001129	0.00001129	0.00000000
1.43	0.00001557	0.00001086	0.00001100	0.00000043
1.41	0.00001486	0.00001043	0.00001086	0.00000071
1.39	0.00001400	0.00001000	0.00001057	0.00000071
1.37	0.00001314	0.00000943	0.00001029	0.00000071
1.35	0.00001257	0.00000900	0.00001000	0.00000057
1.33	0.00001214	0.00000871	0.00001000	0.00000043
1.31	0.00001186	0.00000829	0.00000986	0.00000014
1.29	0.00001143	0.00000814	0.00000971	-0.00000029
1.27	0.00001114	0.00000786	0.00000943	0.00000000
1.25	0.00001100	0.00000786	0.00000929	-0.00000029
1.23	0.00001029	0.00000786	0.00000971	-0.00000029
1.21	0.00001000	0.00000786	0.00001000	-0.00000029
1.19	0.00000971	0.00000786	0.00001014	-0.00000043
1.17	0.00000986	0.00000771	0.00001043	-0.00000029
1.15	0.00000971	0.00000786	0.00001029	-0.00000014
1.13	0.00000957	0.00000786	0.00001014	0.00000000
1.11	0.00000943	0.00000757	0.00001000	-0.00000014
1.09	0.00000943	0.00000743	0.00001000	-0.00000029
1.07	0.00000986	0.00000743	0.00001014	0.00000000
1.05	0.00000986	0.00000757	0.00001014	0.00000014
1.03	0.00001000	0.00000786	0.00001014	0.00000014
1.01	0.00001014	0.00000800	0.00001014	0.00000000
0.99	0.00001014	0.00000800	0.00001000	-0.00000029
0.97	0.00001043	0.00000786	0.00001014	-0.00000014
0.95	0.00001029	0.00000786	0.00001029	-0.00000014
0.93	0.00001057	0.00000786	0.00001043	0.00000014
0.91	0.00001086	0.00000786	0.00001043	-0.00000014
0.89	0.00001114	0.00000814	0.00001043	0.00000000
0.87	0.00001157	0.00000843	0.00001029	-0.00000014
0.85	0.00001200	0.00000871	0.00001043	0.00000029
0.83	0.00001229	0.00000900	0.00001014	0.00000043
0.81	0.00001257	0.00000900	0.00001043	0.00000043
0.79	0.00001257	0.00000929	0.00001014	0.00000043

Table A-17. Continued

0.77	0.00001271	0.00000929	0.00001043	0.00000043
0.75	0.00001300	0.00000957	0.00001057	0.00000043
0.73	0.00001329	0.00000957	0.00001071	0.00000029
0.71	0.00001357	0.00000971	0.00001071	0.00000000
0.69	0.00001400	0.00001000	0.00001071	0.00000000
0.67	0.00001414	0.00001000	0.00001057	0.00000014
0.65	0.00001414	0.00001000	0.00001057	0.00000043
0.63	0.00001400	0.00001000	0.00001057	0.00000029
0.61	0.00001414	0.00000986	0.00001071	0.00000014
0.59	0.00001443	0.00001000	0.00001043	0.00000000
0.57	0.00001471	0.00001000	0.00001029	0.00000014
0.55	0.00001443	0.00001000	0.00001029	0.00000000
0.53	0.00001429	0.00001000	0.00001043	0.00000000
0.51	0.00001386	0.00001014	0.00001057	-0.00000029
0.49	0.00001371	0.00001029	0.00001071	-0.00000029
0.47	0.00001371	0.00001029	0.00001057	0.00000014
0.45	0.00001386	0.00001014	0.00001057	0.00000029
0.43	0.00001357	0.00000971	0.00001043	0.00000043
0.41	0.00001343	0.00000971	0.00001071	0.00000029
0.39	0.00001357	0.00000943	0.00001086	0.00000043
0.37	0.00001371	0.00000943	0.00001114	0.00000029
0.35	0.00001414	0.00000957	0.00001100	0.00000029
0.33	0.00001429	0.00001000	0.00001086	0.00000057
0.31	0.00001457	0.00001029	0.00001114	0.00000029
0.29	0.00001457	0.00001043	0.00001114	0.00000014
0.27	0.00001514	0.00001043	0.00001143	-0.00000029
0.25	0.00001543	0.00001057	0.00001143	-0.00000029
0.23	0.00001571	0.00001071	0.00001157	-0.00000014
0.21	0.00001557	0.00001114	0.00001186	0.00000000
0.19	0.00001543	0.00001100	0.00001200	-0.00000029
0.17	0.00001514	0.00001100	0.00001186	0.00000000
0.15	0.00001471	0.00001057	0.00001186	0.00000000
0.13	0.00001443	0.00001029	0.00001171	0.00000014
0.11	0.00001414	0.00001014	0.00001157	0.00000000
0.09	0.00001386	0.00001000	0.00001114	-0.00000014
0.07	0.00001371	0.00001000	0.00001114	0.00000014
0.05	0.00001386	0.00001000	0.00001114	0.00000000
0.03	0.00001400	0.00000986	0.00001129	-0.00000014
0.01	0.00001414	0.00000986	0.00001129	-0.00000043

Table A-17. Continued

-0.01	0.00001457	0.00000971	0.00001100	-0.00000029
-0.03	0.00001486	0.00000986	0.00001100	0.00000000
-0.05	0.00001514	0.00001029	0.00001129	0.00000029
-0.07	0.00001529	0.00001043	0.00001129	0.00000029
-0.09	0.00001543	0.00001086	0.00001143	0.00000029
-0.11	0.00001571	0.00001057	0.00001129	0.00000043
-0.13	0.00001571	0.00001086	0.00001143	0.00000029
-0.15	0.00001586	0.00001071	0.00001157	0.00000043
-0.17	0.00001571	0.00001086	0.00001186	0.00000014
-0.19	0.00001557	0.00001086	0.00001171	0.00000029
-0.21	0.00001543	0.00001057	0.00001157	0.00000014
-0.23	0.00001529	0.00001057	0.00001157	-0.00000029
-0.25	0.00001500	0.00001043	0.00001143	-0.00000014
-0.27	0.00001514	0.00001043	0.00001157	0.00000000
-0.29	0.00001500	0.00001029	0.00001157	0.00000043
-0.31	0.00001514	0.00001029	0.00001157	0.00000029
-0.33	0.00001500	0.00001043	0.00001143	0.00000014
-0.35	0.00001486	0.00001043	0.00001129	0.00000014
-0.37	0.00001471	0.00001029	0.00001114	-0.00000014
-0.39	0.00001457	0.00001029	0.00001129	0.00000014
-0.41	0.00001457	0.00001014	0.00001129	0.00000000
-0.43	0.00001457	0.00001014	0.00001129	-0.00000029
-0.45	0.00001457	0.00001014	0.00001157	0.00000000
-0.47	0.00001457	0.00001043	0.00001171	-0.00000043

Table A-18.Additional differential pulse voltammetry data for Figure 5-9.

	Differential pulse current (dI)		
Voltage (V)	$5x10^3$ CFU/mL	$5x10^1$ CFU/mL	$5x10^0$ CFU/mL
1.47	0.00000714	0.00000614	0.00000229
1.45	0.00000700	0.00000629	0.00000243
1.43	0.00000671	0.00000614	0.00000257
1.41	0.00000671	0.00000614	0.00000214
1.39	0.00000671	0.00000600	0.00000200
1.37	0.00000657	0.00000600	0.00000214
1.35	0.00000629	0.00000614	0.00000229
1.33	0.00000600	0.00000614	0.00000243
1.31	0.00000600	0.00000614	0.00000214
1.29	0.00000600	0.00000571	0.00000186
1.27	0.00000586	0.00000557	0.00000186
1.25	0.00000586	0.00000557	0.00000186
1.23	0.00000586	0.00000557	0.00000200
1.21	0.00000600	0.00000543	0.00000200
1.19	0.00000586	0.00000557	0.00000200
1.17	0.00000571	0.00000557	0.00000214
1.15	0.00000571	0.00000571	0.00000214
1.13	0.00000557	0.00000571	0.00000214
1.11	0.00000557	0.00000543	0.00000214
1.09	0.00000557	0.00000529	0.00000200
1.07	0.00000543	0.00000500	0.00000186
1.05	0.00000571	0.00000529	0.00000186
1.03	0.00000586	0.00000557	0.00000171
1.01	0.00000571	0.00000557	0.00000157
0.99	0.00000600	0.00000571	0.00000143
0.97	0.00000586	0.00000557	0.00000129
0.95	0.00000571	0.00000571	0.00000143
0.93	0.00000571	0.00000557	0.00000171
0.91	0.00000571	0.00000543	0.00000171
0.89	0.00000571	0.00000557	0.00000200
0.87	0.00000600	0.00000571	0.00000200
0.85	0.00000600	0.00000586	0.00000200
0.83	0.00000600	0.00000600	0.00000200
0.81	0.00000614	0.00000600	0.00000200
0.79	0.00000629	0.00000586	0.00000200

Table A-18. Continued

0.77	0.00000629	0.00000586	0.00000200
0.75	0.00000629	0.00000586	0.00000200
0.73	0.00000643	0.00000586	0.00000200
0.71	0.00000629	0.00000586	0.00000200
0.69	0.00000643	0.00000586	0.00000200
0.67	0.00000657	0.00000571	0.00000200
0.65	0.00000657	0.00000557	0.00000200
0.63	0.00000657	0.00000571	0.00000200
0.61	0.00000657	0.00000571	0.00000200
0.59	0.00000643	0.00000571	0.00000200
0.57	0.00000643	0.00000586	0.00000200
0.55	0.00000657	0.00000586	0.00000214
0.53	0.00000700	0.00000571	0.00000243
0.51	0.00000686	0.00000571	0.00000243
0.49	0.00000671	0.00000586	0.00000243
0.47	0.00000643	0.00000586	0.00000200
0.45	0.00000614	0.00000614	0.00000186
0.43	0.00000629	0.00000614	0.00000200
0.41	0.00000629	0.00000614	0.00000214
0.39	0.00000657	0.00000600	0.00000214
0.37	0.00000657	0.00000614	0.00000214
0.35	0.00000671	0.00000614	0.00000200
0.33	0.00000686	0.00000629	0.00000171
0.31	0.00000686	0.00000643	0.00000186
0.29	0.00000686	0.00000643	0.00000200
0.27	0.00000686	0.00000643	0.00000214
0.25	0.00000671	0.00000657	0.00000243
0.23	0.00000671	0.00000657	0.00000243
0.21	0.00000686	0.00000657	0.00000257
0.19	0.00000714	0.00000671	0.00000243
0.17	0.00000700	0.00000671	0.00000229
0.15	0.00000686	0.00000657	0.00000214
0.13	0.00000671	0.00000643	0.00000186
0.11	0.00000686	0.00000657	0.00000186
0.09	0.00000657	0.00000643	0.00000186
0.07	0.00000643	0.00000629	0.00000200
0.05	0.00000657	0.00000629	0.00000214
0.03	0.00000671	0.00000629	0.00000214
0.01	0.00000686	0.00000629	0.00000214

Table A-18. Continued

-0.01	0.00000686	0.00000629	0.00000214
-0.03	0.00000686	0.00000614	0.00000214
-0.05	0.00000686	0.00000614	0.00000229
-0.07	0.00000686	0.00000643	0.00000243
-0.09	0.00000700	0.00000643	0.00000257
-0.11	0.00000729	0.00000657	0.00000229
-0.13	0.00000757	0.00000671	0.00000214
-0.15	0.00000786	0.00000643	0.00000229
-0.17	0.00000800	0.00000657	0.00000229
-0.19	0.00000786	0.00000629	0.00000243
-0.21	0.00000771	0.00000629	0.00000243
-0.23	0.00000757	0.00000643	0.00000243
-0.25	0.00000729	0.00000657	0.00000271
-0.27	0.00000757	0.00000671	0.00000271
-0.29	0.00000757	0.00000643	0.00000271
-0.31	0.00000743	0.00000643	0.00000271
-0.33	0.00000729	0.00000629	0.00000257
-0.35	0.00000700	0.00000629	0.00000257
-0.37	0.00000700	0.00000629	0.00000243
-0.39	0.00000714	0.00000629	0.00000243
-0.41	0.00000743	0.00000629	0.00000243
-0.43	0.00000743	0.00000629	0.00000229
-0.45	0.00000743	0.00000629	0.00000243
-0.47	0.00000714	0.00000600	0.00000257

Table A-19. Fluorescence data for Figure 5-10.

Sample	Fluorescence (RFU)	Standard Deviation
Control	424	109
$5x10^8$ CFU/mL	188	55
$5x10^7$ CFU/mL	204	20
$5x10^6$ CFU/mL	185	15
$5x10^5$ CFU/mL	183	23
$5x10^4$ CFU/mL	255	98
$5x10^3$ CFU/mL	310	192
$5x10^2$ CFU/mL	173	7
$5x10^1$ CFU/mL	169	1

Table A-20. Fluorescence data for Figure 5-11.

Concentration	Method	Fluorescence (RFU)	Standard Deviation
Control	C-linker	9965	391
$5x10^{8}$ CFU/mL	C-linker	11347	276
$5x10^{7}$ CFU/mL	C-linker	11950	389
$5x10^{6}$ CFU/mL	C-linker	11206	311
$5x10^{5}$ CFU/mL	C-linker	11006	428
$5x10^{4}$ CFU/mL	C-linker	10684	442
$5x10^{3}$ CFU/mL	C-linker	10394	320
$5x10^{2}$ CFU/mL	C-linker	10147	356
$5x10^{1}$ CFU/mL	C-linker	10003	1223
Control	AB-thiol	5031	195
$5x10^{8}$ CFU/mL	AB-thiol	7616	4240
$5x10^{7}$ CFU/mL	AB-thiol	5521	2239
$5x10^{6}$ CFU/mL	AB-thiol	6590	1061
$5x10^{5}$ CFU/mL	AB-thiol	6028	1456
$5x10^{4}$ CFU/mL	AB-thiol	5711	384
$5x10^{3}$ CFU/mL	AB-thiol	5867	642
$5x10^{2}$ CFU/mL	AB-thiol	5735	788
$5x10^{1}$ CFU/mL	AB-thiol	4809	482

REFERENCES

REFERENCES

1. Abu-Ali, G.S., et al., *Genomic diversity of pathogenic Escherichia coli of the EHEC 2 clonal complex.* BMC Genomics, 2009. **10**: p. 296.

2. Leclerc, H., et al., *Advances in the bacteriology of the coliform group: their suitability as markers of microbial water safety.* Annual Review of Microbiology, 2001. **55**: p. 201-34.

3. Eaton, A.D., *Standard methods for the examiniation of water and wastewater*, W.E. Federation, Editor. 1992, American Public Health Association.

4. March, S.B. and S. Ratnam, *Sorbitol-MacConkey medium for detection of Escherichia coli O157:H7 associated with hemorrhagic colitis.* Journal of Clinical Microbiology, 1986. **23**(5): p. 869-72.

5. Federal, R., *Quality standards for foods with no identity standards; bottled water*, F.a.D. Administration, Editor. 1993. p. 52042-52050.

6. Yakub, G.P., et al., *Evaluation of Colilert and Enterolert defined substrate methodology for wastewater applications.* Water Environment Research, 2002. **74**(2): p. 131-5.

7. Federal, R., *Guidelines establishing test procedures for the analysis of pollutants; analytical methods for the biological pollutants in wastewater and sewage sludge; final rule.* 2007. **72**(157): p. 14220-14233.

8. Rompre, A., et al., *Detection and enumeration of coliforms in drinking water: current methods and emerging approaches.* Journal of Micobiological Methods, 2002. **49**: p. 31-54.

9. Fode-Vaughan, K.A., et al., *Direct PCR detection of Escherichia coli O157:H7.* Letters in Applied Microbiology, 2003. **37**(3): p. 239-43.

10. Torres-Chavolla, E. and E.C. Alocilja, *Nanoparticle based DNA biosensor for tuberculosis detection using thermophilic helicase-dependent isothermal amplification.* Biosensors & Bioelectronics, 2011. **26**(11): p. 4614-8.

11. Hill, H.D. and C.A. Mirkin, *The bio-barcode assay for the detection of protein and nucleic acid targets using DTT-induced ligand exchange.* Nature Protocols, 2006. **1**(1): p. 324-36.

12. Anderson, M.J., et al., *One step alkaline synthesis of biocompatible gold nanoparticles using dextrin as capping agent.* Journal of Nanoparticle Research, 2011. **13**(7): p. 2843-2851.

13. Anderson, M.J., D. Zhang, and E.C. Alocilja, *Spectral and electrical nanoparticle-based molecular detection of Bacillus anthracis using copolymer mass amplification.* Ieee Transactions on Nanotechnology, 2011. **10**(1): p. 44-49.

14. Goluch, E.D., et al., *A bio-barcode assay for on-chip attomolar-sensitivity protein detection.* Lab Chip, 2006. **6**(10): p. 1293-9.

15. Hill, H.D., R.A. Vega, and C.A. Mirkin, *Nonenzymatic detection of bacterial genomic DNA using the bio-barcode assay.* Analytical Chemistry, 2007. **79**(23): p. 9218-23.

16. Nam, J.M., S.I. Stoeva, and C.A. Mirkin, *Bio-bar-code-based DNA detection with PCR-like sensitivity.* Journal of the American Chemical Society, 2004. **126**(19): p. 5932-3.

17. Dirks, R.M. and N.A. Pierce, *Triggered amplification by hybridization chain reaction.* Proceedings of the National Academy of Sciences of the United States of America, 2004. **101**(43): p. 15275-8.

18. Goluch, E.D., et al., *A bio-barcode assay for on-chip attomolar-sensitivity protein detection.* Lab on a Chip, 2006. **6**(10): p. 1293-9.

19. Sujakhu, K. and U.T. Shrestha, *Micrbial (Coliform and Vibrio cholerae) analysis of drinking water collected from outbreak region of Bhaktapur municipality*. 2011.

20. Woodall, C.J., *Waterborne diseases - Whar are the primary killers?* Desalination, 2008. **252**: p. 199-204.

21. Gleick, P.H., *Dirty water: Estimated deaths from water-related diseases 2000-2020*. 2002, Pacific Insitute for Studies in Development, Environment, and Security. p. 1-12.

22. Envirometnal_Protection_Agency, *Drinking Water, National Primary Drinking Water Regualtion, Total Coliforms (Including Fecal Coliforms and E. Coli); Final Rule*, E.P. Agency, Editor. 1989. p. 26.

23. Beutin, L., et al., *Prevalence and some properties of verotoxin (Shiga-like toxin)-producing Escherichia coli in seven different species of healthy domestic animals.* J Clin Microbiol, 1993. **31**(9): p. 2483-8.

24. McIntire, R.J. *California Firm Recalls Ground Beef Products Due to Possible E. coli O157:H7 Contamination*. 2011 [cited 2011 Feb. 02 2011]; Available from: http://www.fsis.usda.gov/News_&_Events/Recall_008-2011_Release/index.asp.

25. Ready_Pac_Foods (2010) *Ready Pac Foods, Inc. Announces Voluntary Product Recall because of Possible Health Risk*. **Volume**,

26. FDA, *FDA Warns Consumers Not to Eat Nestle Toll House Prepackaged, Refrigerated Cookie Dough*, B.o.C.E.H.F. Protection, Editor. 2009.

27. EPA, *Economic Analysis for the Proposed Revised Total Coliform Rule.* 2010.

28. Federal, R., *Rules and regulations*, E.P. Agency, Editor. 1989. p. 27544-27568.

29. Kilian, M. and P. Bulow, *Rapid diagnosis of Enterobacteriaceae. I. Detection of bacterial glycosidases.* Acta Pathologica et Microbiologica Scandinavica, 1976. **84B**(5): p. 245-51.

30. Tryland, I. and L. Fiksdal, *Enzyme characteristics of beta-D-galactosidase- and beta-D-glucuronidase-positive bacteria and their interference in rapid methods for detection of waterborne coliforms and Escherichia coli.* Applied and Environmental Microbiology, 1998. **64**(3): p. 1018-23.

31. Navarro, A., et al., *Antibody responses to Escherichia coli O157 and other lipopolysaccharides in healthy children and adults.* Clin Diagn Lab Immunol, 2003. **10**(5): p. 797-801.

32. Zhang, D., et al., *Nanoparticle-based Bio-barcoded DNA Sensor for the Rapid Detection of pagA Gene of Bacillus Anthracis.* Ieee Transactions on Nanotechnology, Accepted 2011.

33. Pal, S. and E.C. Alocilja, *Electrically active magnetic nanoparticles as novel concentrator and electrochemical redox transducer in Bacillus anthracis DNA detection.* Biosensors & Bioelectronics, 2010. **26**(4): p. 1624-30.

34. Setterington, E.B. and E.C. Alocilja, *Rapid electrochemical detection of polyaniline-labeled Escherichia coli O157:H7.* Biosensors & Bioelectronics, 2011. **26**(5): p. 2208-14.

35. Olsvik, O., et al., *Use of automated sequencing of polymerase chain reaction-generated amplicons to identify three types of cholera toxin subunit B in Vibrio cholerae O1 strains.* Journal of Clinical Microbiology, 1993. **31**(1): p. 22-5.

36. Bellin, T., et al., *Rapid detection of enterohemorrhagic Escherichia coli by real-time PCR with fluorescent hybridization probes.* Journal of Clinical Microbiology 2001. **39**(1): p. 370-4.

37. Desmarchelier, P.M., et al., *A PCR specific for Escherichia coli O157 based on the rfb locus encoding O157 lipopolysaccharide.* Journal of Clinical Microbiology, 1998. **36**(6): p. 1801-4.

38. Prager, R., et al., *Subtyping of pathogenic Escherichia coli strains using flagellar (H)-antigens: serotyping versus fliC polymorphisms.* International Journal of Medical Microbiology, 2003. **292**(7-8): p. 477-86.

39. Bej, A.K., S.C. McCarty, and R.M. Atlas, *Detection of coliform bacteria and Escherichia coli by multiplex polymerase chain reaction: comparison with defined substrate and plating methods for water quality monitoring.* Applied and Environmental Microbiology, 1991. **57**(8): p. 2429-32.

40. Wieler, L.H., et al., *Shiga toxin-producing Escherichia coli strains from bovines: association of adhesion with carriage of eae and other genes.* Journal of Clinical Microbiology, 1996. **34**(12): p. 2980-4.

41. Spierings, G., et al., *Polymerase chain reaction for the specific detection of Escherichia coli/Shigella.* Research in Microbiology, 1993. **144**(7): p. 557-64.

42. Wahlberg, J., et al., *General colorimetric method for DNA diagnostics allowing direct solid-phase genomic sequencing of the positive samples.* Proceedings of the National Academy of Sciences of the United States of America, 1990. **87**(17): p. 6569-73.

43. Juck, D., et al., *Nested PCR protocol for the rapid detection of Escherichia coli in potable water.* Canadian Journal of Microbiology, 1996. **42**(8): p. 862-6.

44. Iqbal, S., et al., *Efficiency of the polymerase chain reaction amplification of the uid gene for detection of Escherichia coli in contaminated water.* Letters in Applied Microbiology, 1997. **24**(6): p. 498-502.

45. Blanco, C., P. Ritzenthaler, and M. Mata-Gilsinger, *Cloning and endonuclease restriction analysis of uidA and uidR genes in Escherichia coli K-12: Determiniation of transcription direction for the uidA gene.* Journal of Bacteriology, 1981. **149**(2): p. 587-594.

46. Fricker, E.J. and C.R. Fricker, *Application of the polymerase chain reaction to the identification of Escherichia coli and coliforms in water.* Letters in Applied Microbiology, 1994. **19**(1): p. 44-6.

47. Geiss, G.K., et al., *Direct multiplexed measurement of gene expression with color-coded probe pairs.* Nature Biotechnology, 2008. **26**(3): p. 317-25.

48. Sassolas, A., B.D. Leca-Bouvier, and L.J. Blum, *DNA biosensors and microarrays.* Chemical Reviews, 2008. **108**(1): p. 109-39.

49. Murakami, A., et al., *Highly sensitive detection of DNA using enzyme-linked DNA-probe. 1. Colorimetric and fluorometric detection.* Nucleic Acids Research, 1989. **17**(14): p. 5587-95.

50. Vaknin, A. and H.C. Berg, *Single-cell FRET imaging of phosphatase activity in the Escherichia coli chemotaxis system.* Proceedings of the National Academy of Sciences of the United States of America, 2004. **101**(49): p. 17072-7.

51. Tang, Y.Z., K.Y. Gin, and T.H. Lim, *High-temperature fluorescent in situ hybridization for detecting Escherichia coli in seawater samples, using rRNA-targeted oligonucleotide probes and flow cytometry.* Applied and Environmental Microbiology, 2005. **71**(12): p. 8157-64.

52. Quinones, B., et al., *Identification of Eschericia coli O157 by using a novel colorimetric detection method with DNA microarrays.* Foodborne Pathogens and Disease, 2011. **8**(6): p. 705-711.

53. Fritz, J., et al., *Translating biomolecular recognition into nanomechanics.* Science, 2000. **288**(5464): p. 316-8.

54. Metzgar, D., et al., *Evaluation and validation of a real-time PCR assay for detection and quantitation of human adenovirus 14 from clinical samples.* PLoS One, 2009. **4**(9): p. e7081.

55. Walker, G.T., et al., *Strand displacement amplification--an isothermal, in vitro DNA amplification technique.* Nucleic Acids Research, 1992. **20**(7): p. 1691-6.

56. Walker, G.T., et al., *Isothermal in vitro amplification of DNA by a restriction enzyme/DNA polymerase system.* Proceedings of the National Academy of Sciences of the United States of America, 1992. **89**(1): p. 392-6.

57. Bergmann, J.S. and G.L. Woods, *Clinical evaluation of the BDProbeTec strand displacement amplification assay for rapid diagnosis of tuberculosis.* Journal of Clinical Microbiology, 1998. **36**(9): p. 2766-8.

58. Demidov, V.V., *Rolling-circle amplification in DNA diagnostics: the power of simplicity.* Expert Review of Molecular Diagnostics, 2002. **2**(6): p. 542-8.

59. Thomas, D.C., G.A. Nardone, and S.K. Randall, *Amplification of padlock probes for DNA diagnostics by cascade rolling circle amplification or the polymerase chain reaction.* Archives of Pathology & Laboratory Medicine, 1999. **123**(12): p. 1170-6.

60. Notomi, T., et al., *Loop-mediated isothermal amplification of DNA.* Nucleic Acids Research, 2000. **28**(12): p. E63.

61. Song, W., C. Lau, and J. Lu, *Quantum dot-based isothermal chain elongation for fluorescence detection of specific DNA sequences via template-dependent surface-hybridization.* The Analyst, 2012. **137**(7): p. 1611-7.

62. Dore, K., M. Leclerc, and D. Boudreau, *Investigation of a fluorescence signal amplification mechanism used for the direct molecular detection of nucleic acids.* Journal of Fluorescence, 2006. **16**(2): p. 259-65.

63. Tsongalis, G.J., *Branched DNA technology in molecular diagnostics.* American Journal of Clinical Pathology, 2006. **126**(3): p. 448-53.

64. Sato, K., K. Hosokawa, and M. Maeda, *Colorimetric biosensors based on DNA-nanoparticle conjugates.* Analytical Sciences, 2007. **23**(1): p. 17-20.

65. Zhao, W., M.A. Brook, and Y. Li, *Design of gold nanoparticle-based colorimetric biosensing assays.* Chembiochem, 2008. **9**(15): p. 2363-71.

66. Nam, J.M., K.J. Jang, and J.T. Groves, *Detection of proteins using a colorimetric bio-barcode assay.* Nature Protocols, 2007. **2**(6): p. 1438-44.

67. Elghanian, R., et al., *Selective colorimetric detection of polynucleotides based on the distance-dependent optical properties of gold nanoparticles.* Science, 1997. **277**(5329): p. 1078-81.

68. Nam, J.M., C.S. Thaxton, and C.A. Mirkin, *Nanoparticle-based bio-bar codes for the ultrasensitive detection of proteins.* Science, 2003. **301**(5641): p. 1884-6.

69. Thaxton, C.S., et al., *A bio-bar-code assay based upon dithiothreitol-induced oligonucleotide release.* Analytical Chemistry, 2005. **77**(24): p. 8174-8.

70. Stoeva, S.I., et al., *Multiplexed detection of protein cancer markers with biobarcoded nanoparticle probes.* Journal of the American Chemical Society, 2006. **128**(26): p. 8378-9.

71. Stoeva, S.I., et al., *Multiplexed DNA detection with biobarcoded nanoparticle probes.* Angewandte Chemie (International ed), 2006. **45**(20): p. 3303-6.

72. Oh, B.K., et al., *A fluorophore-based bio-barcode amplification assay for proteins.* Small, 2006. **2**(1): p. 103-8.

73. Borucki, M.K., et al., *Suspension microarray with dendrimer signal amplification allows direct and high-throughput subtyping of Listeria monocytogenes from genomic DNA.* Journal of Clinical Microbiology, 2005. **43**(7): p. 3255-9.

74. Turkevich, J., P.C. Stevenson, and J. Hillier, *A study if the nucleation and growth processes in the synthesis of colloidal gold.* Discussion of the Faraday Society, 1951. **11**: p. 55-75.

75. Brust, M., et al., *Synthesis and reactions of functionalized gold nanoparticles.* Journal of the Chemical Society - Chemical Communications, 1995: p. 1655-1656.

76. Brust, M., et al., *Synthesis of thiol-derivatized gold nanoparticles in a 2-phase liquid-liquid system.* Journal of the Chemical Society - Chemical Communications, 1994: p. 801-801.

77. Sanyal, A. and M. Sastry, *Gold nanosheets via reduction of aqueous chloroaurate ions by anthracene anions bound to a liquid-liquid interface.* Chemical Communications (Cambridge, England), 2003(11): p. 1236-7.

78. Ahmad, A., et al., *Extracellular biosynthesis of monodisperse gold nanoparticles by a novel extremophilic Actinomycete, Thermomonospora sp.* Langmuir, 2003. **19**: p. 3550-3553.

79. Ma, Z. and H. Han, *One-step synthesis of cystine-coated gold nanoparticles in aqueous solution.* Colloids and Surfaces A: Physicochemical and Engineering Aspects, 2008. **317**(1-3): p. 229-233.

80. de la Fuente, J.M. and S. Penades, *Glyconanoparticles: types, synthesis and applications in glycoscience, biomedicine and material science.* Biochim Biophys Acta, 2006. **1760**(4): p. 636-51.

81. Huang, Y.J., D. Li, and J.H. Li, *Beta-cyclodextrin controlled assembling nanostructures from gold nanoparticles to gold nanowires.* Chemical Physics Letters, 2004. **389**(1-3): p. 14-18.

82. Li, Z., et al., *Multiple thiol-anchor capped DNA-gold nanoparticle conjugates.* Nucleic Acids Research, 2002. **30**(7): p. 1558-1562.

83. Rechberger, W., et al., *Optical properties of two interacting gold nanoparticles.* Optics Communications, 2003. **220**(1-3): p. 137-141.

84. Kneipp, J., et al., *In vivo molecular probing of cellular compartments with gold nanoparticles and nanoaggregates.* Nano Letters, 2006. **6**(10): p. 2225-31.

85. Dudak, F.C., *Rapid and label-free bacteria detection by surface plasmon resonance (SPR) biosensors.* Biotechnology Journal, 2009(4): p. 1003-1011.

86. Pal, S., E.C. Alocilja, and F.P. Downes, *Nanowire labeled direct-charge transfer biosensor for detecting Bacillus species.* Biosensors & Bioelectronics, 2007. **22**(9-10): p. 2329-36.

87. Xiliang, L., et al., *Application of nanoparticles in electrochemical sensors and biosensors.* Electroanalysis, 2006. **18**(4): p. 319-326.

88. Chah, S., M.R. Hammond, and R.N. Zare, *Gold nanoparticles as a colorimetric sensor for protein conformational changes.* Chemistry & Biology 2005. **12**(3): p. 323-8.

89. Slocik, J.M., M.O. Stone, and R.R. Naik, *Synthesis of gold nanoparticles using multifunctional peptides.* Small, 2005. **1**(11): p. 1048-52.

90. Zhou, M., et al., *Minute synthesis of extremely stable gold nanoparticles.* Nanotechnology, 2009. **20**(50): p. 505606.

91. Turkevich, J., P.C. Stevenson, and J. Hillier, *A study of the nucleation and growth processes in the synthesis of colloidal gold.* Discussions of the Faraday Society, 1951(11): p. 55-57.

92. Das, S.K., A.R. Das, and A.K. Guha, *Gold nanoparticles: Microbial synthesis and application in water hygiene management.* Langmuir, 2009. **25**(14): p. 8192-8199.

93. Aslan, K., J.R. Lakowicz, and C.D. Geddes, *Nanogold plasmon resonance-based glucose sensing. 2. Wavelength-ratiometric resonance light scattering.* Analytical Chemistry, 2005. **77**(7): p. 2007-14.

94. de la Fuente, J.M. and S. Penades, *Glyconanoparticles: types, synthesis and applications in glycoscience, biomedicine and material science.* Biochimica et Biophysica Acta, 2006. **1760**(4): p. 636-51.

95. Newman, J.D. and G.J. Blanchard, *Formation of gold nanoparticles using amine reducing agents.* Langmuir, 2006. **22**(13): p. 5882-7.

96. Li, X., et al., *Enhancement of cell recognition in vitro by dual-ligand cancer targeting gold nanoparticles.* Biomaterials, 2011. **32**(10): p. 2540-5.

97. Porta, F., et al., *Gold-ligand interaction studies of water-soluble aminoalcohol capped gold nanoparticles by NMR.* Langmuir, 2008. **24**(14): p. 7061-4.

98. Polte, J., et al., *Mechanism of gold nanoparticle formation in the classical citrate synthesis method derived from coupled in situ XANES and SAXS evaluation.* Journal of the American Chemical Society, 2010. **132**(4): p. 1296-301.

99. Ishkanian, A., et al., *A tiling resolution DNA microarray with complete coverage of the human genome.* Nature Genetics 2004. **36**: p. 299-303.

100. Taton, T.A., C.A. Mirkin, and R.L. Letsinger, *Scanometric DNA array detection with nanoparticle probes.* Science, 2000. **289**(8): p. 1757-1760.

101. Thaxton, C.S., D.G. Georganopoulou, and C.A. Mirkin, *Gold nanoparticle probes for the detection of nucleic acid targets.* Clinica Chimica Acta, 2006. **363**(1): p. 120-126.

102. Zhang, D., et al., *Nanoparticle-based bio-barcoded DNA sensor for the rapid detection of pagA gene of Bacillus anthracis.* Ieee Transactions on Nanotechnology, 2011.

103. Zhang, D., D.J. Carr, and E.C. Alocilja, *Fluorescent bio-barcode DNA assay for the detection of Salmonella enterica serovar Enteritidis.* Biosensors & Bioelectronics, 2009. **24**(5): p. 1377-1381.

104. Dragan, A.I., et al., *Characterization of PicoGreen interaction with dsDNA and the origin of its fluorescence enhancement upon binding.* Biophysical journal, 2010. **99**(9): p. 3010-9.

105. Hayashi, T., et al., *Complete genome sequence of enterohemorrhagic Escherichia coli O157:H7 and genomic comparison with a laboratory strain K-12.* DNA Research, 2001. **8**(1): p. 11-22.